Master's thesis

NTNU
Norwegian University of Science and Technology
Faculty of Natural Sciences
Department of Chemistry

Hans-Petter Larsen

Synthesis of a self-healing graphene/ polyurethane nanocomposite using the Diels-Alder reaction

Master's thesis in Chemistry
Supervisor: Solon Economopoulos
May 2021

NTNU
Kunnskap for en bedre verden

Hans-Petter Larsen

Synthesis of a self-healing graphene/ polyurethane nanocomposite using the Diels-Alder reaction

Master's thesis in Chemistry
Supervisor: Solon Economopoulos
May 2021

Norwegian University of Science and Technology
Faculty of Natural Sciences
Department of Chemistry

NTNU
Kunnskap for en bedre verden

Abstract

In today's society, there is a shift towards green chemistry and finding more environmentally friendly solutions to various challenges. Electronic devices, industrial equipment and other polymer-based products are often cheaper to replace than to repair due to low mechanical properties and cheap materials. The aim for this thesis is to synthesize a thermally stable graphene-crosslinked polyurethane nanocomposite with self-healing properties. In order to achieve self-healing, the Diels-Alder/retro Diels-Alder reaction between two suitable functional groups will be explored. Polyurethane and graphene will be functionalized with a complimentary pendant group to achieve this, namely maleimide and furan.

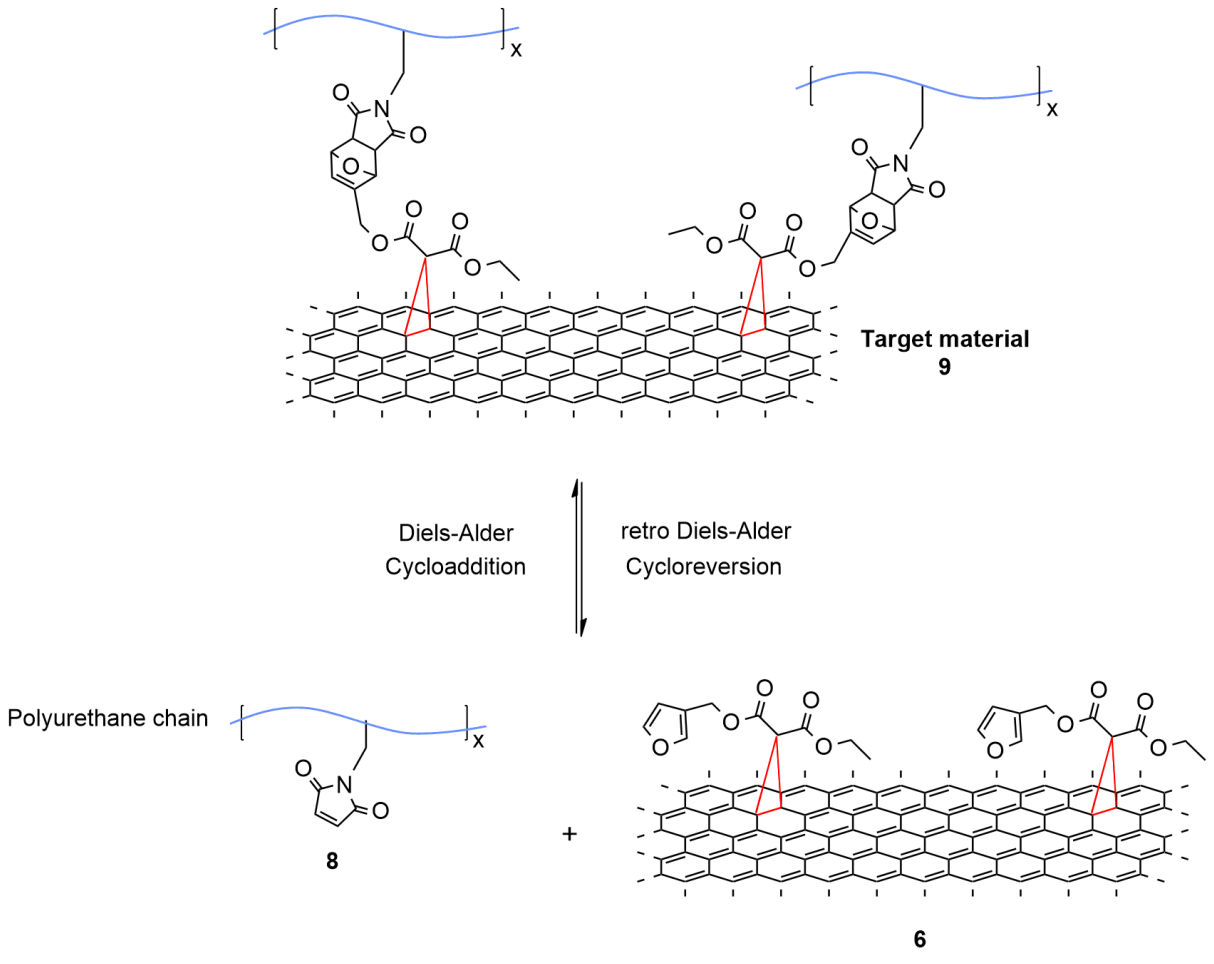

The synthesis route consisted of eight steps, separated into the synthesis of the two main components; maleimide polyurethane **8** and furan functionalized graphene hybrid **6**. The maleimide compound **3** was prepared through a three step synthesis, resulting in a maleimide model compound equipped with two hydroxyl group needed for polyurethane polyaddition with MDI and PTMG. Further, a pyridine catalysed esterification between Ethyl

3-chloro-3-oxopropionate and Furan-3-methanol resulted in a novel ethyl malonate derivative bearing the furan pendant. Exfoliated graphene was prepared through solvent-exfoliation of graphite in N-methyl pyrrolidone using tip sonication. Microwave assisted Bingel reaction, allowed for [2+1] cycloaddition of the ethyl malonate onto the graphene, thus decorating the graphene with the furan pendant group.

The two main components were mixed together, with varying graphene hybrid concentration, resulting in 4 graphene-crosslinked polyurethane nanocomposites **9A-D**. The nanocomposites were drop casted onto Silicon wafers for film forming. Each film was first damaged, and subsequently heated to temperatures high enough to initiate the retro Diels-Alder reaction, allowing new covalent bonds to form thus healing the damaged areas. Imaging through scanning electron microscope confirmed self-healing properties of thin films exhibiting a trend of improved healing proportional to the graphene hybrid's concentration.

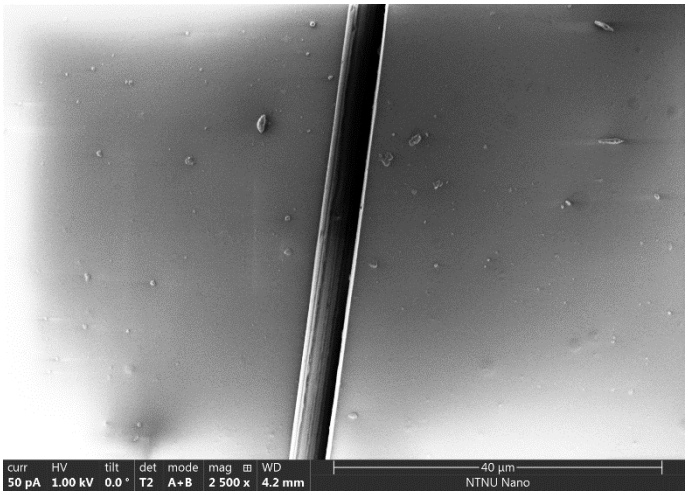

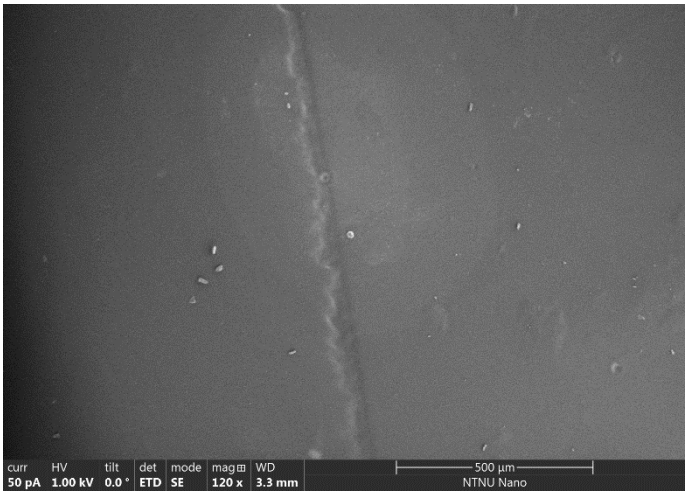

Sammendrag

I dagens samfunn er det et stadig økende fokus på grønn kjemi for å finne mer miljøvennlige løsninger til fremtidens utfordringer. Elektroniske apparater, industrielt utstyr og andre polymerbaserte produkter er ofte billigere å erstatte enn å reparere på grunn av dårlige mekaniske kvaliteter samt at disse materialene har lave produksjonskostnader. Målet for denne masteroppgaven er å syntetisere en termisk stabil grafén-kryssbundet polyuretan nanokomposittmed selvlegende egenskaper. Diels-Alder / retro Diels-Alder-reaksjonen mellom to egnede funksjonelle grupper ble utforsket for å oppnå disse egenskapene. Polyuretan og grafén ble funksjonalisert med hver sin funksjonelle gruppe for å oppnå dette, nemlig maleimid og furan.

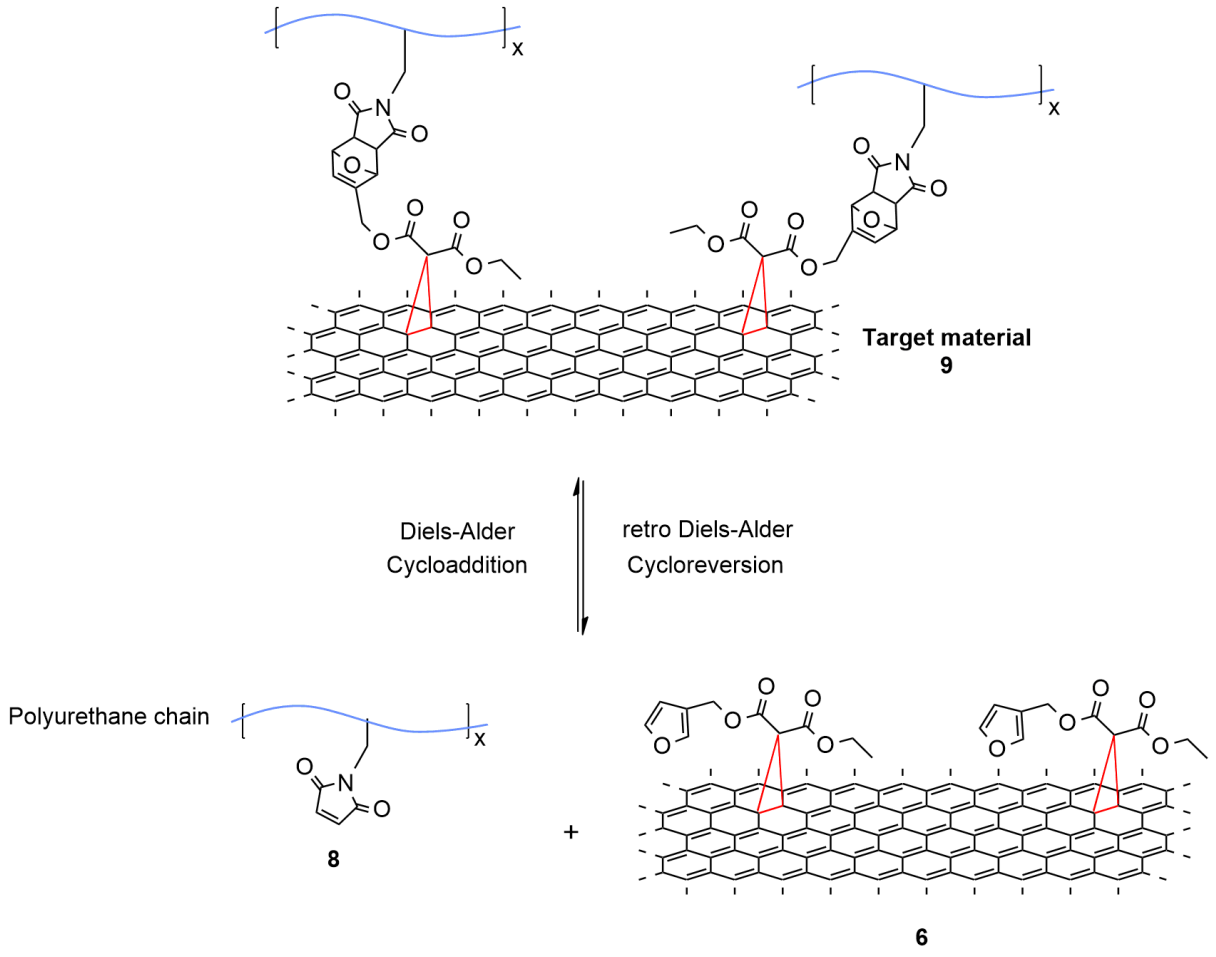

Synteseveien besto av 8 trinn, og syntesen ble atskilt i to hovedkomponenter; syntese av maleimide-polyuretan **8** og syntesen av furan-funksjonalisert grafén-hybrid **6**. Maleimide-monomeren **3** ble fremstilt gjennom en tretrinnssyntese som resulterende i en maleimide-forbindelse utstyrt med to hydroksylgrupper som var nødvendige for polyaddisjon med MDI og PTMG som resulterte i maleimide-polyuretan **8**. Gjennom en pyridin-katalysert

esterifisering mellom etyl-3-klor-3-oksopropionat og Furan-3-metanol ble et nytt etylmalonat-derivat med furan syntetisert. Videre ble grafén produsert gjennom løsemiddelassistert eksfoliering av grafitt i N-metylpyrrolidon ved bruk av ultralydprobe. Bingelreaksjonen tillot for [2 + 1] sykloaddisjon av etylmalonatet og grafén, som resulterte i furan-funksjonalisert grafén **6**.

De to hovedkomponentene ble blandet sammen med varierende konsentrasjoner av grafén-hybrid, noe som resulterte i 4 grafén-kryssbundne polyuretan-nanokompositter **9A-D**. Nanokompositten ble deretter dryppet på Si wafere for støping av polymerfilmer. Små kutt ble påført filmene før de deretter oppvarmet til temperaturer som var høye nok til å igangsette retro Diels-Alder-reaksjonen slik at nye kovalente bindinger kunne dannes, og dermed reparere de skadede områdene. Elektronmikroskop (SEM) ble benyttet for å studere polymerfilmene. I tillegg ble det observert en tendens av at polymerfilmene sin egenskap til å reparere seg selv var proporsjonal med konsentrasjonen av grafén hybrid i nanokompositten.

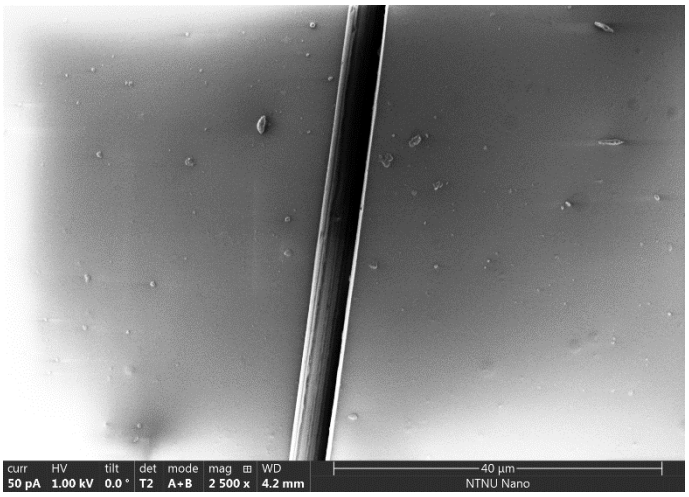

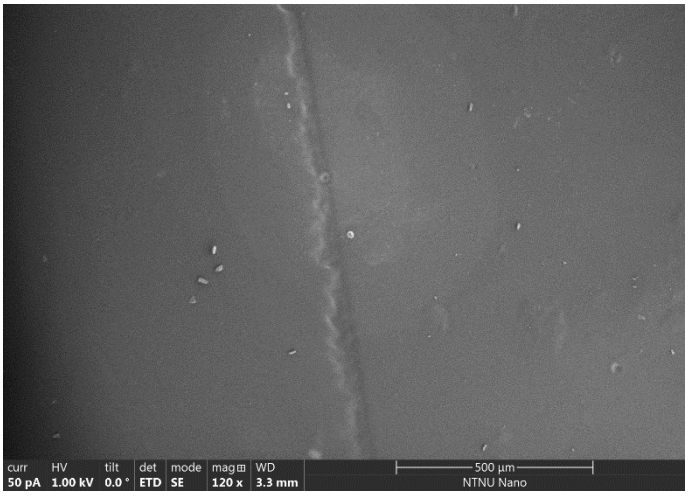

Acknowledgments

First, I would like to extend my sincere gratitude to supervisor, Solon Economopoulos for providing me with such an interesting and diverse project including several topics. I am grateful for the valuable support, constructive advices and guidance you have shown me during this project.

I would also like to thank the "Solon group" with Maria Psarrou and Cristina Perinu for giving me invaluable feedback, guidance and support through this project. Working next to you, exchanging knowledge has been encouraging. The same thanks goes to David Moe Almenningen for his down-to-earth attitude while helping me, his contribution with great music, and for accepting me to the "Solar Cell Lab".

Thanks to the technical staff at IKJ, including Susana Villa Gonzales for providing MS results, and Roger Aarvik for his express delivery of chemicals and equipment to the lab.

I would also like to thank my family and friends. My mother and father for supporting me through these years, and for believing in me. My friends for all the encouragement along the way and their interest in my work.

Thanks to NKS-FOK for financial support to attend OKV2020 at Skeikampen.

Thanks to The Research Council of Norway, (RCN) through the ACT programme (Accelerating CCS Technologies, Horizon2020 Project No 294766) for financial support.

Thanks to the Nano-Fabrication Facility, NorFab for letting me work in your facilities to perform microRaman and SEM analysis for my project NL1023.

Finally, I would like to thank my girlfriend and best friend, Veronika Killingberg, for always supporting me. Cheering me on with your genuine show of interest for my project. You are my hero! I could not have done this without you by my side.

Thank you.

Abbreviations

AFM	Atomic force microscopy
APO	3-Amino-1,2-propanediol
a.u.	Arbitrary units
CASE	Coatings, adhesives, sealants and elastomers
CNT	Carbon nanotube
COSY	^{1}H-^{1}H Correlation spectroscopy
CBr_4	Tetrabromomethane
$CDCl_3$	Deuterated chloroform
DA	Diels Alder
DABCO	1,4 Diazabicyclo[2.2.2]octane
DBU	1,8-Diazabicyclo[5.4.0]undec-7-ene
DCM	Dichloromethane
DMAc	Dimethylacetamide
DMF	Dimethylformamide
DMSO	Dimethyl sulfoxide
Et_3N	Triethylamine
Et_2O	Diethyl ether
EtOAc	Ethyl Acetate
EtOH	Ethanol
GO	Graphene Oxide
GPC	Gel permeation chromatography
HMBC	Heteronuclear multiple-bond correlation spectroscopy
HRMS	High resolution mass spectroscopy
HSQC	Heteronuclear single-quantum correlation spectroscopy
IR	Infrared spectroscopy
KOH	Potassium hydroxide
MDI	4,4´-Methylenebis(phenyl isocyanate)
MeOH	Methanol
M_n	Number average molecular weight
M_w	Weight average molecular weight
MW	Microwave
NMP	N-Methyl-2-pyrrolidone
NCO	Isocyanate
PDI	Polydispersity Index

ppm	Parts per million
PTMG	Poly(tetrahydrofuran)
PU	Polyurethane
RCF	Relative centrifugal force
rDA	Retro Diels Alder
RID	Refractive index detector
rpm	Revolutions per minute
RT	Room temperature
SEM	Scanning electron microscope
TEA	Triethylamine
THF	Tetrahydrofuran
TLC	Thin layer chromatography
TOF	Time of flight

Numbered Compounds

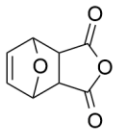

1

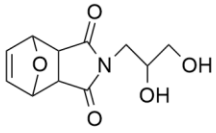

2

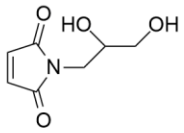

3

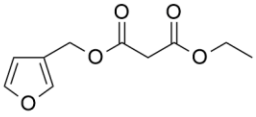

4

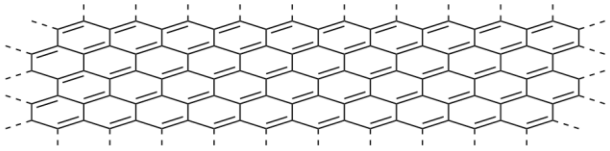

5

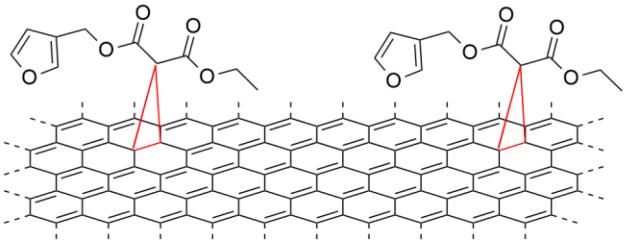

6

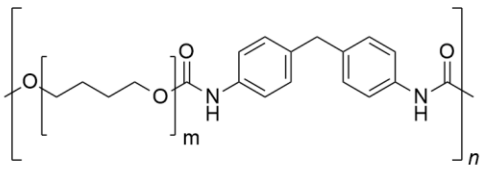

7

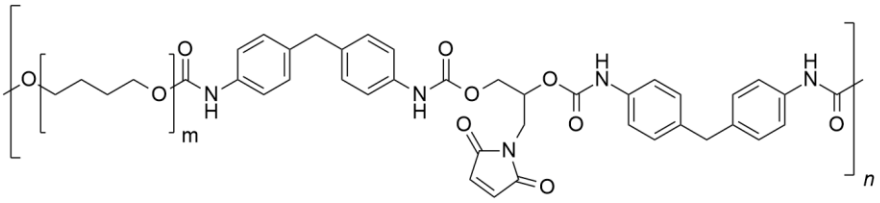

8

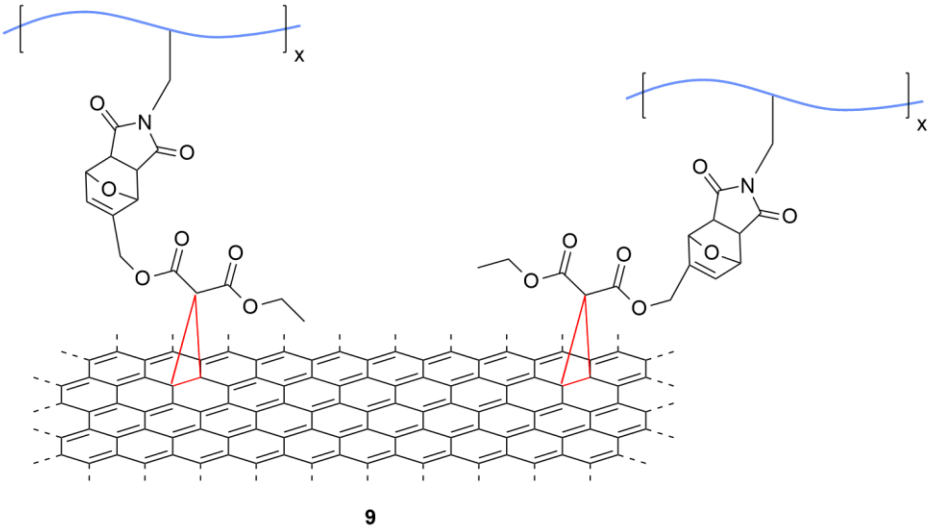

9

Table of contents

1 Polymer Chemistry 1

1.1 Polymerization Reactions 4

1.1.1 Chain-Growth polymerization 5

1.1.2 Step-Growth Polymerization 7

1.2 Self-healing polymers 8

1.2.1 Dynamic covalent bonding, Diels-Alder 10

1.2.3 Dynamic covalent bonding, Imine bond 12

1.2.4 Dynamic covalent bonding, Boronic acid 13

1.2.5 Reversible physical interactions, H-bonding 14

1.2.6 Reversible physical interactions, Pi-stacking 15

1.3 Polyurethane 16

1.3.1 Polyols 18

1.3.2 Isocyanates 19

2 Graphene 20

2.1 Preparation of graphene 22

2.1.1 Reduced graphene oxide 23

2.1.2 Liquid phase exfoliation (LPE) 24

2.1.3 Chemical vapor deposition 26

2.2 Functionalization of graphene 27

2.2.1 [2+1] Cycloadditions 28

2.3 Micro-Raman spectroscopy of Graphene 31

3 Aim of thesis 34

4 Results and discussion 35

4.1 Synthesis strategy 35

4.2 Synthesis of Maleimide pendant, Compound **3** 38

4.2.1 Diels-Alder protection of maleic anhydride 38

4.2.2 Direct condensation of compound **1** 41

4.2.3 Retro Diels-Alder de-protection of compound **2** 44

4.3 Synthesis of compound **4** 47

4.3.1 Pyridine catalyzed esterification between acyl chloride and an alcohol 47

4.4 Preparation and synthesis of compound **6** 49

4.4.1 Solvent assisted exfoliation of graphite powder 49

4.4.2 [2+1] Cycloaddition of compound **4** 51

4.5 Polyurethane Synthesis 54

4.5.1 Polyaddition of isocyanate and diol 55

4.5.2 Polyaddition of PTMG and maleimide (**3**) with MDI 57
4.6 Preparation and casting of nanohybrid polymer film 60
5 Conclusion and further work 67
6 Experimental 69
6.1 General 69
6.2 Synthesis of maleimide pendant 70
6.2.1 Synthesis of compound **1** 71
6.2.2 Synthesis of compound **2** 72
6.2.3 Synthesis of compound **3** 73
6.3 Synthesis of malonate derivative 74
6.3.1 Synthesis of compound **4** 74
6.4 Exfoliation of graphene 75
6.5 Microwave-assisted Bingel reaction of exfoliated graphene 76
6.6 MicroRaman characterization 77
6.7 Polyurethane synthesis 78
6.7.1 Preliminary tests of Polyurethane synthesis 78
6.7.2 Synthesis of maleimide functionalized polyurethane **8** 79
6.8 Graphene-crosslinked Polyurethane, compound **9A-D** 81
6.9 Scanning Electron Microscope analysis 82
References 83
Appendices 95
A Spectroscopic data - Compound **1** 96
B Spectroscopic data - Compound **2** 101
C Spectroscopic data - Compound **3** 108
D Spectroscopic data - Compound **4** 115
E Spectroscopic data - Exfoliated Graphene **5** 122
F Spectroscopic data - Bingel Graphene **6** 124
G Spectroscopic data - Compound **7** 125
H Spectroscopic data - Compound **8** 127
I Parameters for graphene exfoliation and microwave assisted Bingel reaction 131

1 Polymer Chemistry

The existence of polymers were first proposed in 1920 by the German chemist, Hermann Staudinger.[1] He classified them as a broad class of compounds were chains of identical molecules were bound together by strong bonds to make bigger macromolecules. As a result, for his discoveries, he was awarded the 1953 Nobel Prize in Chemistry.[2] Today, polymer materials have a great impact on our daily life, and can be found in every-day items. Most common applications of polymers are clothing, automobile parts, paints, adhesives, hospital equipment, 3D-printing, self-healing polymers, and much more.[3] Conventional polymers mainly consisting of long molecular chains have been used in modern technology and industries because of their good mechanical, thermal and electronic properties. Polymers have been widely regarded as single-use materials mostly due to their low cost, but also due to their degradation over time from wear and tear.

The prefix poly indicates several molecules, and furthermore, a single molecule or building block gives the prefix mono-, thus giving the name monomer. Poly (Phenylethene), more known as polystyrene, is one of the most frequently used polymers on the market. Its polymeric form and monomer is shown in Figure 1.

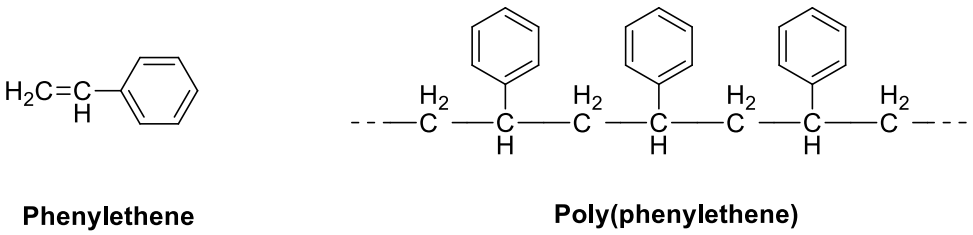

Figure 1. Phenylethene as monomer (left) and its polymeric state (right), Poly(Phenylethene).[4]

Because of their size, bigger molecules such as polymers have different physical properties than smaller molecules. Flexibility, hardness and solvent resistance are important, and polymers holds much higher melting points due to their stronger intermolecular forces due to their size.[5] Sometimes when polymer chains fold or pack in a repetitive order, they achieve regions of crystallinity, thus facilitating an even higher melting point. T_m, melt transition temperature is the point at which a crystalline structure melts, and for temperatures higher than T_m, the polymer has a more amorphous state. On the other hand, it is at the glass transition temperature, T_g, where hard and amorphous polymers transition from hard and rigid to a more rubbery and pliable state.[6]

The properties of a polymer can vary dramatically by changing the density of polymer network. Polymer networks can be made through polymerization, or by linking together linear polymer chains using covalent bonds. This is more known as *crosslinking* of pre-existing polymer chains.[5] Multi-functional monomers are needed to synthesize network polymers without crosslinking linear chains. Monomers with two reactive ends will polymerize into linear chains, while monomers with three or more reactive groups tend to form a network.

Polymers are divided into homopolymers and heteropolymers.[5] *Homopolymers* are polymers consisting of one species of monomer in their polymeric chain or network. A typical homopolymer is represented by $[A]_n$, where A is the structural unit such as Phenylethene (see Figure 1) and *n* is the number of repeating units of A.

Heteropolymers, also known as co-polymers, are polymers derived from two or more different monomers.[5] Co-polymers are quite useful since they hold the properties of the monomers, which makes up the co-polymer. An example of this is polystyrene which is quite brittle on its own as a homopolymer. Whereas, when copolymerized with buta-1,3-diene, the co-polymer blend has noticeable more strength and resilience than the polystyrene homopolymer. Styrene is polymerized first, followed by buta-1,3-diene polymerizing onto the polystyrene chain ends. This specific polymer structure is named *block polymer* (see Figure 2) as two different repeating monomers stack together in blocks. Additionally, Acrylonitrile can add to the double bonds of buta-1,3-diene to form small side chains to the block co-polymer. This new polymer belongs to the class of *graft co-polymers* and commercially is also known as ABS, consisting of acrylonitrile, buta-1,3-diene and styrene.[7] Linear polyurethane belongs to the class of alternating co-polymer because isocyanate and diol must alternate every other molecule.[8] The two monomers have specific reactive groups to further progress the polymerization. Lastly, *random co-polymers* are heteropolymers where the monomers are arranged statistically along the polymer chain.

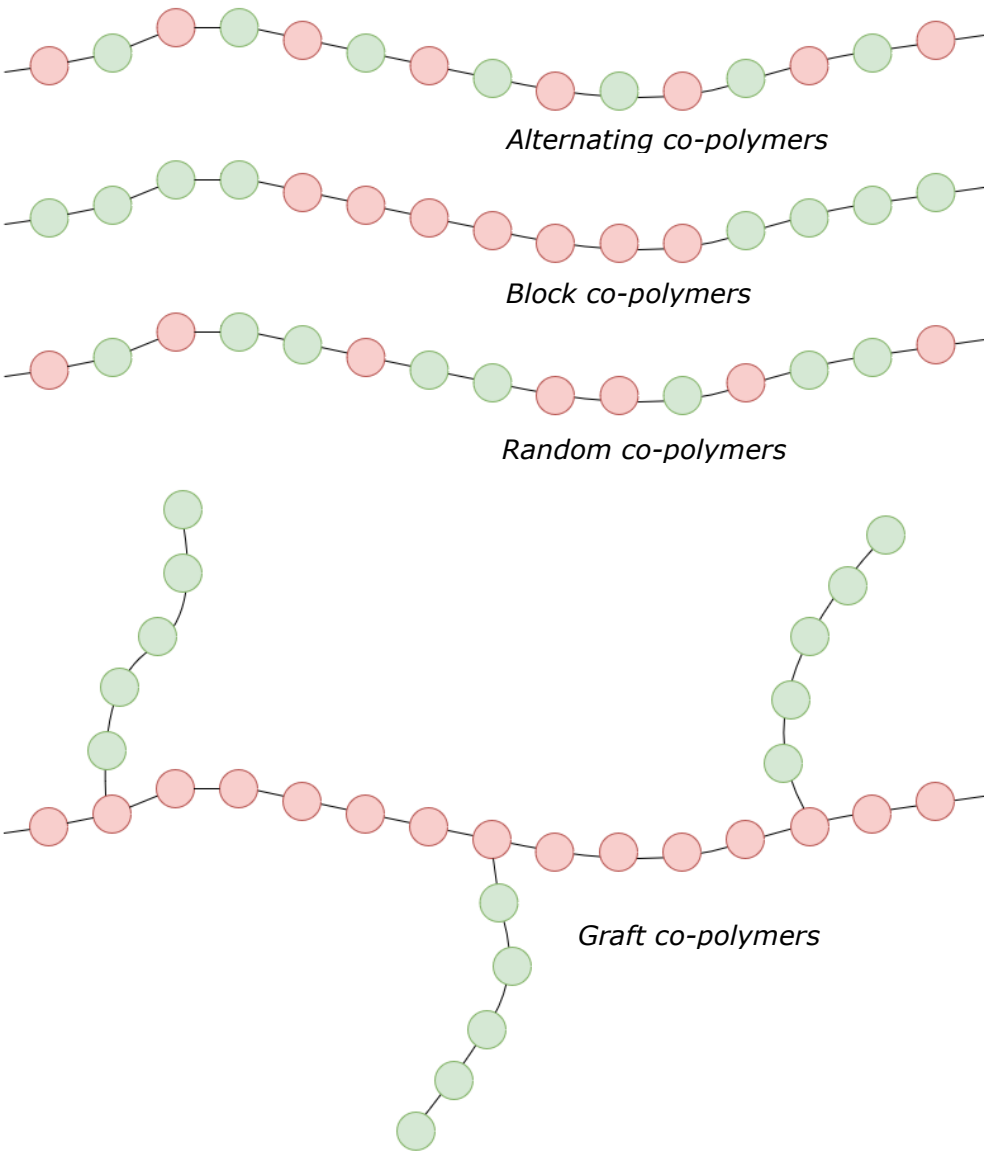

Figure 2. Illustration of the different types of co-polymers; Alternating, block, random and graft co-polymers.[5]

1.1 Polymerization Reactions

To synthesize a polymer, monomers must have the possibility to link to each other through a reaction to make a repeating unit. Monomers also need to have a functionality of two to make linear polymer chains, and a functionality of three or more to make network polymers.[5] There is a huge scope of ways to produce polymers, and each year new methods are developed. Because of this, the most established ways of polymerization are quickly introduced in this chapter with a focus towards the method most important to this thesis.

In the early 1900s, Carothers suggested that polymers could be categorized into two mechanisms of polymerization, condensation and addition polymerizations.[9] Condensation polymerization was described to be a method where the polymer product had fewer atoms compared to its building blocks, meaning, small molecules such as H_2O are released in the process as byproducts. Addition polymerizations, on the other hand, were described as polymerizations that gave the same structural formula than its monomer similar to a homopolymer. Both terms for polymerization were later changed because both types could have the characteristic features overlapping each other.

New terminology of polymerization is more focused on the underlying polymerization mechanism, and two new main branches of polymerization were established. *Step-growth polymerization* describes a step-wise chain growth from reaction between two molecules, which includes the previously condensation polymerization.[5] On the other hand, polymer chains that grow by reaction between a monomer and a reactive end-group, are termed *chain-growth polymerization* reactions. These methods are most common for synthesis of homopolymers, but is also widely used for heteropolymers. Chain-growth polymerization will be closer introduced in section 1.1.1, and step-growth polymerization, which is most important for this thesis will be introduced in section 1.1.2.

1.1.1 Chain-Growth polymerization

Chain growth polymerizations is a fast polymerization method that involves one type of reactive monomer.[5] Most common monomers that polymerize via chain-growth polymerization are vinyl monomers, olefins, dienes, acetylenes and various epoxides. The latter one via epoxide ring opening. An initiator is needed, and the type of initiator decides which type of chain-growth polymerization happens. Cationic polymerization, for example, uses an acid as initiator and the reactive site on the chain is a carbocation. For anionic polymerization, the initiator is a nucleophile and the reactive site a carbanion. For radical polymerization, the initiator is a radical and the reactive site a carbon radical. To get a better understanding this type of polymerization, an example of radical polymerization of a general vinyl polymer, CH_2=CHX (where X is a substituent group) is shown in Scheme 1.

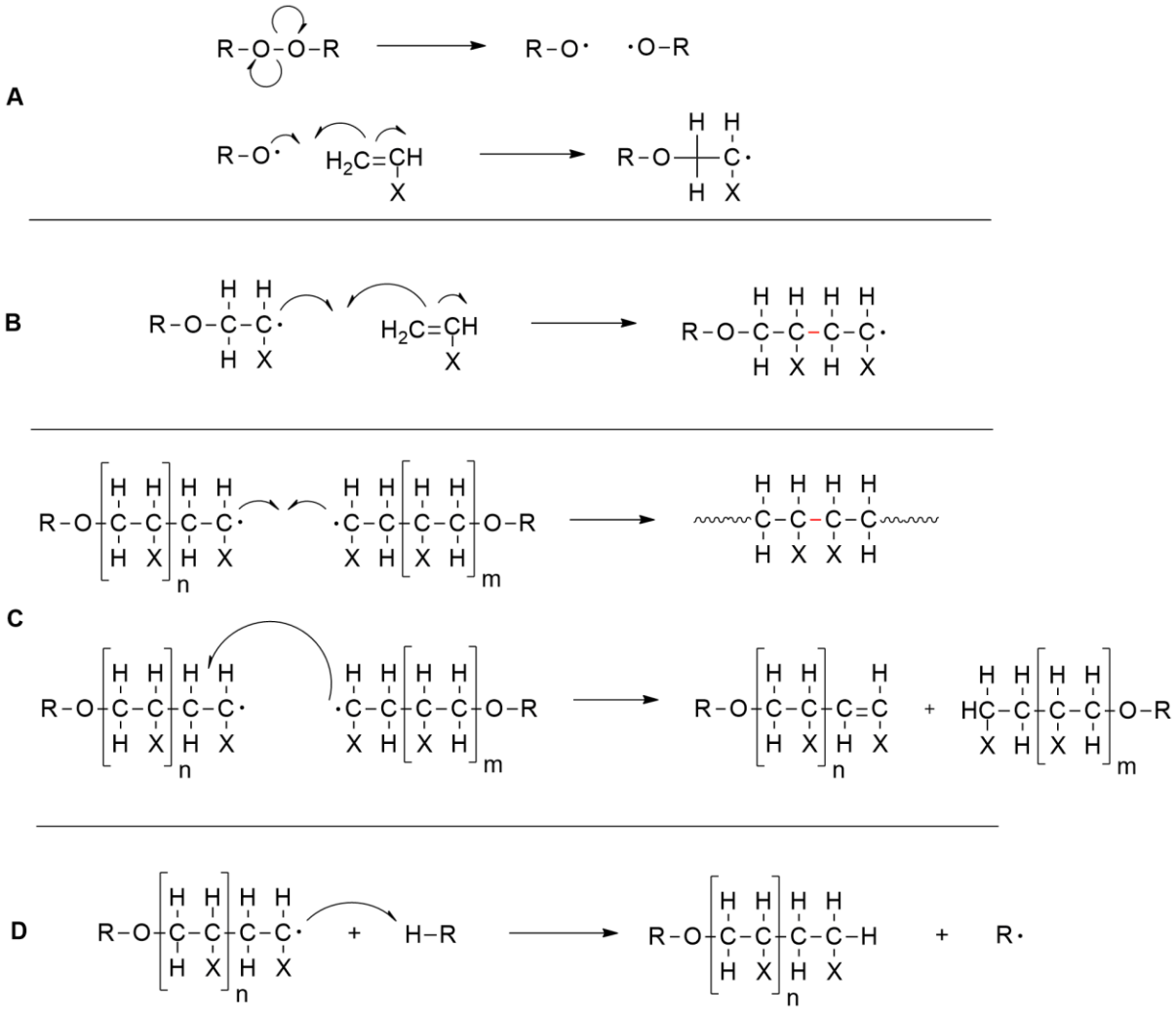

Scheme 1. (A) Initiation. (B) Propagation. (C) Termination by recombination or disproportionation. (D) Termination by chain transfer of the free radical.

There are four stages to chain-growth polymerization (see Scheme 1); (A) Initiation, (B) propagation, (C) termination and (D) chain transfer. The first stage involves the creation of a free-radical active center and happens normally in two steps. First, free radicals are formed from an initiator (i.e. peroxides (–O-O-) and azo (–N=N-) linkages), and secondly is the addition of one of these radicals to a monomer. The most common method for radical formation from an initiator is through *homolytic scission* of a single bond, often facilitated by application of heat.[5] After an active center is created, the free radical will attack the π-bond of a monomer, initiating the free-radical polymerization. Initiation most commonly happens at the methylene (CH_2) carbon because it is less sterically hindered than the substituent (CHX) carbon.

The propagation involves the growth of the polymer. This happens from rapid addition of new monomers, where the active centre moves to every monomer added. Addition of new monomers can either happen in a Head-to-tail or tail-to-tail orientation, with the former being the most dominating. Head-to-tail is where the substituent group is situated every other carbon along the polymer chain, and this type of sequence is more favoured because it is less sterically hindered.

Termination of chain growth polymerization happens as the active centre is either destroyed or moved to a new polymer chain. One way of termination is bimolecular reaction of two propagating chains to form one bigger polymer molecule via *recombination*. The other known process is through *disproportionation*, where the radical centre of one chain takes a hydrogen from the end of another chain. The electron from the broken C-H bond pairs together with the radical from the active centre to form a terminal π-bond of the polymer chain that lost a hydrogen.

Chain transfer reaction is the fourth and last stage of chain-growth polymerization. Here, the active centre is transferred from the active chain to a new species in the polymerization system. This happens most often by abstraction of a hydrogen (similar to disproportionation) from another molecule. This leads to a homolytic scission of the C-H bond in the new species, which yields a new active centre for further propagation.

1.1.2 Step-Growth Polymerization

From its name, this polymerization happens stepwise where pairs of mutually reactive functional groups react successive to form a polymer chain or network.[5,10] This type of polymerization can happen either with or without the elimination of small byproducts such as H_2O, HCl, HBr, etc. An example of step-growth reaction is the condensation of carboxylic acids and alcohols.[11] As both monomers are bi-functional, they will yield a linear alternating Copolymer. This reaction exhaust one H_2O molecule to form an ester linkage, and is called a polycondensation to form a polyester. Another example of polycondensation is the condensation between carboxylic acids and diamines to give polymers connected through amide linkages, thus yielding polyamides. One familiar polyamide is Nylon 6,6 from hexamethylene diamine and adipic acid.[12] Polymers are often named according to the type of linkage that is formed from the two reactive monomers as shown in Figure 3.

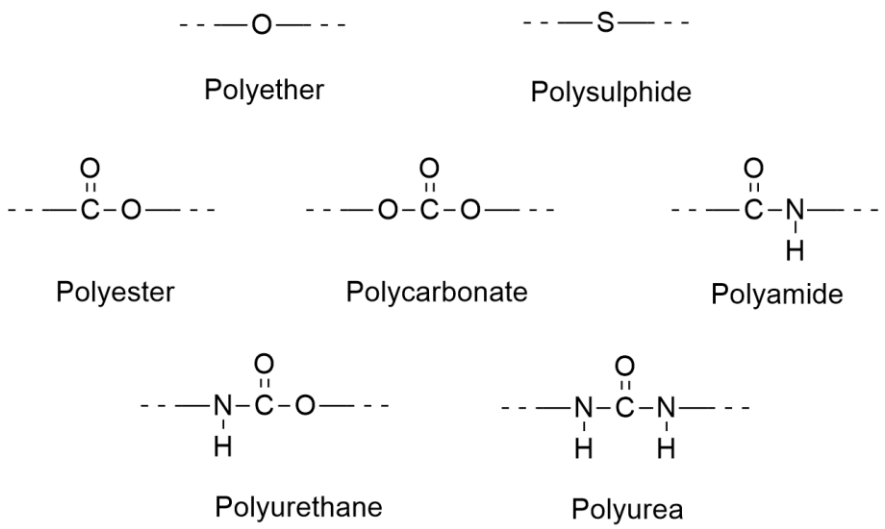

Figure 3. Common classes of polymers made through step-growth polymerization.[5]

Relevant for this thesis is the step-growth polymerization of polyols and isocyanates to form polyurethane. This type of step-growth polymerization is a polyaddition and does not split out small molecules such as H_2O.[5,8] The polyaddition to produce polyurethane is further discussed in chapter 1.3.

1.2 Self-healing polymers

When polymers are subject to mechanical damage, small cracks start at a molecular level and often go unnoticed until the damage is visible on a macroscopic level.[13] At this point, the material has failed and often needs replacement. The idea of self-healing polymers is to stop the problem at ground-zero on molecular level.

In many cases, an external trigger is needed to initiate the self-healing process in a material.[14] These triggers can be heat, light, change in pH, and microwaves and solvent assisted self-healing. Healable materials may also mend together by simple contact of the pieces broken apart by mechanical stress. Self-healing initiated by thermal stimulus is the most common method due to its easy preparation and cost. Heating also increases the mobility of polymer chains, thus facilitating self-healing of most polymer composites. On the other hand, heating may also cause some interference with parts of the polymer less important to the self-healing through deterioration and degradation of said part. A less invasive and alternative way to repair damaged polymers is by light radiation.[15] Infrared (IR) sensitive materials may absorb the radiation to transfer heat to thermal sensitive parts for self-healing.

Earlier reports show that additives such as graphene oxide (GO), reduced graphene oxide (rGO) and functionalized graphene nanosheets (FGNS) has been imbedded into polymer composites to increase the mechanical strength of self-healing polymers.[14,16,17] Due to graphene's microwave absorption capabilities, its implementation into polymers is also facilitated via the use of microwaves to initiate self-healing.[18,19] Graphene's extended conjugation transforms the graphene into an electric dipole leading to the transformation of microwaves into heat in the form of dipole distortion. In the same way as for IR, this heat can be used as a less invasive stimulus to initiate self-healing.

The development of polymer materials with the built-in ability to self-heal is constantly changing, introducing new ways of self-healing through dynamic covalent bonds and supramolecular physical interactions. In the following sections, some of these methods will be studied after an introduction in classification and terminology of self-healing materials.

There are several ways of categorizing self-healing polymers, one of these being able to divide into extrinsic and intrinsic self-healing polymers.[20] **Extrinsic** self-healing methods involves systems of capsules, fibers or vasculatures, which contain external healing-agents such as monomers, catalysts or crosslinkers.[21-23] These reactive containers are embedded into the polymer matrix. Upon crack or damage, the healing agent is released from the ruptured containers to heal the materials by a designed polymerization/chemical reaction. Capillary forces drive out the released healing agent and mix with other healing agents or

crosslink with the matrix, which it is imbedded in. The effectiveness of the healing is correlated to the size of the particles and increases with the capsule size. Uniform distribution throughout the polymeric matrix is needed, mechanical strength of the capsules, and miscibility of the capsules. One also have to design the encapsulation medium. This is often done with urea-formaldehyde or polyurethane-resins, which are prepared in-situ and by interfacial encapsulation in an oil-in-water emulsion.[24] The biggest drawback is the exhaustion of the healing agent, giving only a single use or heal per damaged area.

The design of **intrinsic** self-healing materials involves the incorporation of dynamic covalent bonds as crosslinkers in self-healing networks.[25] These reversible linkages are later used through the reformation or bond exchange of covalent bonds to re-attach fractured materials. The damage can also be mended by physical crosslinking through supramolecular (or non-covalent) interactions.[26] This is a repeatable process and can be designed a lot more freely than extrinsic methods and will be the focus of this thesis. Self-healing materials are also categorized into **autonomic** and **non-autonomic** self-healing.[20,27] Non-autonomic self-healing materials require an external stimulus such as temperature, light or pH to be able to initiate its self-healing property.[23] On the other hand, autonomic self-healing materials need no external conditions to initiate self-healing.[27] As briefly mentioned above, self-healing materials are quite often divided after their ability to achieve self-healing through strong covalent bonds or through supramolecular non-covalent interactions such as hydrogen bonding and pi-stacking.[20,23] The target polymer in this thesis, is a non-autonomic intrinsic self-healing polymer, which achieve self-healing through dynamic covalent bonds.

1.2.1 Dynamic covalent bonding, Diels-Alder

The Diels-Alder (DA) reaction is one of the most commonly utilized reactions in the design of self-healing materials.[17,28-31] The reaction is a thermoreversible [4+2] cycloaddition between an electron rich diene and an electron deficient dienophile to form a DA adduct. The reason for its popularity within self-healing materials comes from the reagent free conditions, its region- and stereo-controlled transformation, and the easily controlled click chemistry this mechanism provide. Through cycloaddition, strong dynamic covalent bonds are formed without any formation of byproducts at mild conditions. For its uses in self-healing materials, furan and maleimide are generally used as diene and dienophile respectively.[32] Retro Diels-Alder (rDA) is the cycloreversion of the DA adduct, re-generating the corresponding diene and dienophile.[33] The cycloreversion is promoted by higher temperatures around 150-160°C, providing good control over the reaction pathway.[32] A representation of the DA reaction mechanism between furan and maleimide can be seen in Scheme 2.

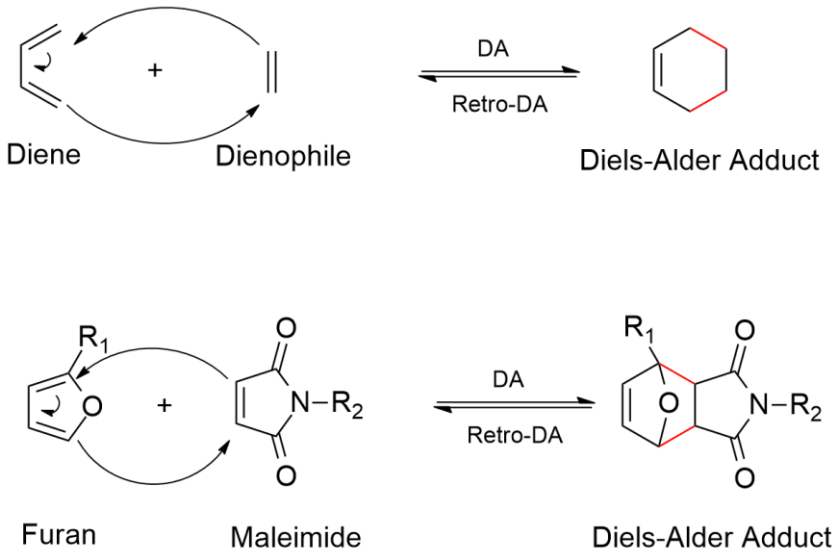

Scheme 2. Diels-Alder mechanism. Formed covalent bonds are marked red.

The diene must consist of two pi-bonds in a conjugated system and hold a *s-cis* conformation,[34] while the dienophile consists of one pi-bond. In the [4+2] cycloaddition, these three pi-bonds are broken to form two new sigma bonds marked red in Scheme 2, and one new pi-bond.[34,35] The formed sigma bonds are the covalent bonds that binds together furan and maleimide, thus crosslinking the substituents in which the diene and dienophile are functionalized onto. The rate of the DA reaction is affected by these substituents.[36,37] Having electron withdrawing groups near the dienophile, increases the rate of reaction (i.e. the carbonyls in maleimide increases the rate of the DA reaction). On the other hand, if the diene carries electron donor groups, the rate of reaction is increased.

1.2.2 Dynamic covalent bonding, Disulfide

The ability to make self-healing polymers utilizing disulfide linkages comes from their reversible nature to both form and break via different reaction pathways.[32] The disulfide S-S bond can be broken into two thiol groups using phosphines as reducing agents. However, it may also be cleaved by thiol-disulfide exchange reaction in the presence of other thiol groups, or by cleaving of the disulfide bridge into two thiyl radicals through photo-irradiation, mechanical stress or thermal scission.[38] Reversibly, the thiols and thiyls formed can be recombined through the opposite reactions such as oxidation of thiols, recombination of cleaved thiyl radicals or through thiol-disulfide exchange reaction.[39] Disulfide bridges may also by rearranged through disulfide metathesis, which can be catalyzed by either tertiary amines, phosphines or photo irradiation.[38] All these different methods enabling the dynamic disulfide linkage has been used in the development and synthesis of disulfide-containing self-healing polymers as shown in Scheme 3.

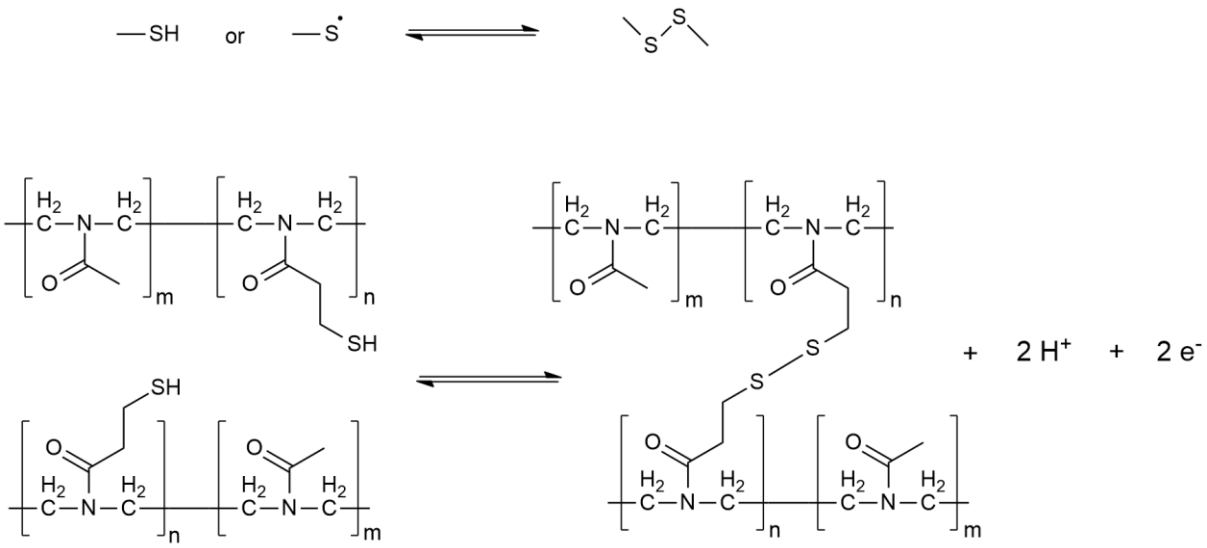

Scheme 3. (Top) Formation and breaking of disulfide bridges by redox chemistry and thermal scission/recombination of thiyl radicals. (Bottom) Oxidation of thiols into disulfide and reduction back into thiol moieties.[40]

1.2.3 Dynamic covalent bonding, Imine bond

Utilizing the reversible imine bond is another way of designing self-healing materials using dynamic covalent bonds. When carbonyls and primary amines react through condensation, they form imines as shown in Scheme 4 below and the nature of their carbon-nitrogen double bond makes them Schiff bases. This is a non-autonomic self-healing method as it requires a change in pH to both break bonds and form new covalent bonds to achieve self-healing. This pH dependent dynamic reversibility was further explored by Lehn *et al*.[41] The imine linkage is formed fastest when subject to a neutral pH. However, this reaction is dynamic as the reaction is reversible when the imine is hydrolyzed back to carbonyl compounds (often aldehydes) and a primary amine in acidic conditions. Because of the pH dependent nature of the imine bond, it has been designed to be used as an injectable self-healing hydrogel functioning as an anti-tumor drug carrier.[42,43] The drug is designed for steady *in situ* release at pH-specific areas, leading to less harm to the patient from the anti-tumor drug, and a more direct delivery of the anti-tumor drug.[42] The anti-tumor drug can be situated at either the carbonyl or primary amine compound.

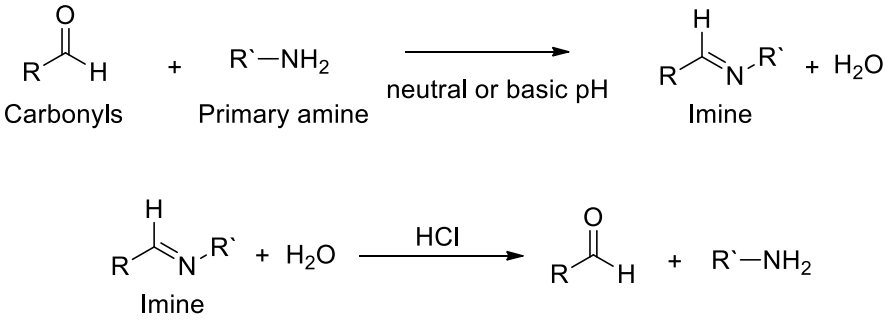

Scheme 4. Basic scheme of self-healing through imine bond[40]

1.2.4 Dynamic covalent bonding, Boronic acid

Boronate ester also function as a useful cross-linker among the dynamic materials with the possibility of reversible covalent bonding.[44-46] This reaction is governed by the solution pH and pK_a of the Boronic acid. With a pH above the Boronic acid pKa the equilibrium favors bond formation through a condensation reaction between Boronic acid and cis-1,2 or cis-1,3 diols to form Boronate ester.[44] This reaction is reversible as pH below the Boronic acid pKa favors the equilibrium to go towards free Boronic acid and diol, giving a bond breaking of the Boronate ester bonds.[43] Because of this, the reaction rate of the esterification is inversely proportional to the pH giving a lower reaction rate as the pH goes up. The pH needed for the reaction changes with different Boronic acids, as different substituent groups can tune the boronic acid pK_a. This reversible reaction is carried out in an aqueous solution under mild conditions at room temperature and the reaction needs no catalyst.[44] Scheme 5 below shows the general reaction for formation and breaking of Boronate ester. Similar to the dynamic imine bond, boronic acid has been studied for anti-tumor drug delivery as reported by Adams *et al*.[47] The antitumor drug was used as an enzyme inhibitor and consisted of a dipeptide containing a boronic acid that binds to the hydroxyl groups, which can be found in the active site of serine proteases.[47]

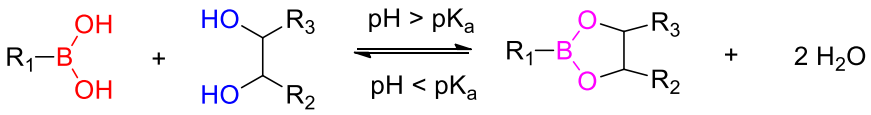

Scheme 5. Boronate ester bond formation is favored for solution pH values above the pK_a of boronic acid, and reversed when the solution pH is lower than the pK_a.[45]

1.2.5 Reversible physical interactions, H-bonding

Self-healing abilities may also be obtained through non-covalent physical interactions such as hydrogen bonding,[48] pi stacking,[26] ionic interactions,[32] metal complexes,[49] and host-guest interactions.[32] These supramolecular interactions are easily disrupted when subject to temperature, pH and mechanical stress, and their unique reversibility let them revert to their original interactions.[50] This dynamic reversibility allows these methods to be utilized when designing self-healing materials.

For hydrogen bonding both a suitable hydrogen donor and acceptor are needed, which can be embedded into the polymer structure as side chains as a graft co-polymer. 2-ureido-4-pyrimidone (**UPy**) which has several organic groups that fits as both donor and acceptor is frequently used.[51] Secondary amides are a widely used hydrogen donor, while imines and carbonyl groups function as hydrogen acceptors.[51] In the example shown in Figure 4, Mollet et al.[52] attached UPy to a poly ethylene glycol (**PEG**) polymer. A mixture of monofunctional and difunctional **UPy PEG** has been reported to self-heal into a hydrogel in water. By varying the ratios of monofunctional **UPy PEG** and crosslinking-capable difunctional **UPy PEG**, the self-healing ability, the mechanical and structural properties of the end polymer could be tweaked.[53] Self-healing polymers that utilize hydrogen bonding generally possess weak mechanical properties and classify as soft polymers.[32] This weakness has been improved by introducing hard domains into the polymer matrix such as polystyrene, thus improving mechanical strength and toughness, and giving rise to the polymer glass transition state, T_g.[51]

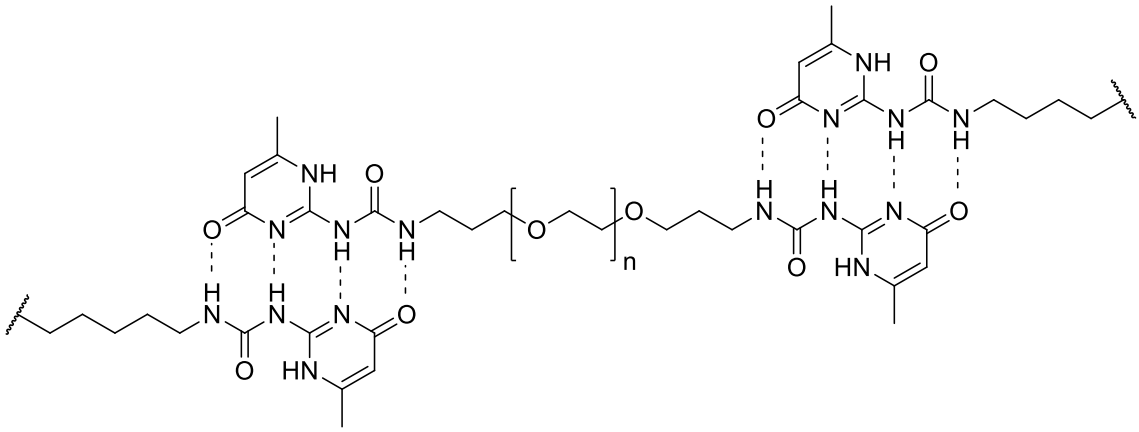

Figure 4. Hydrogen bonding between difunctional **UPy PEG**.[52]

1.2.6 Reversible physical interactions, Pi-stacking

Pi-stacking of aromatic units and groups can also provide self-healing abilities, and similarly to hydrogen bonding, they also utilize a donor and acceptor relationship.[26,32] The aromatic Pi-electron rich regions in the molecule can act as donors, while the Pi-electron deficient areas acts as electron acceptors to achieve self-healing.[32] Pyrene moieties are commonly used as the pi-electron donor while diimide moieties are often used as Pi-electron acceptors.[54] The two moieties will go into a chain folded complex through pi-pi stacking interactions between pyrene and diimide.[50] As exhibited by Greenland and coworkers,[55] a pyrenyl end-capped telechelic polyurethane can function as a cross-linking agent for the poly diimide chains (Figure 5). The interactions between the pi-electron donor and acceptor are easily disrupted by thermal response, and they are quickly reoriented back into a chain folded pi-pi stack.[32] This thermal reversibility gives the chain folded polymer its self-healing ability. A telechelic polymer is capable to enter further polymerization or other reactions due to its reactive end groups.

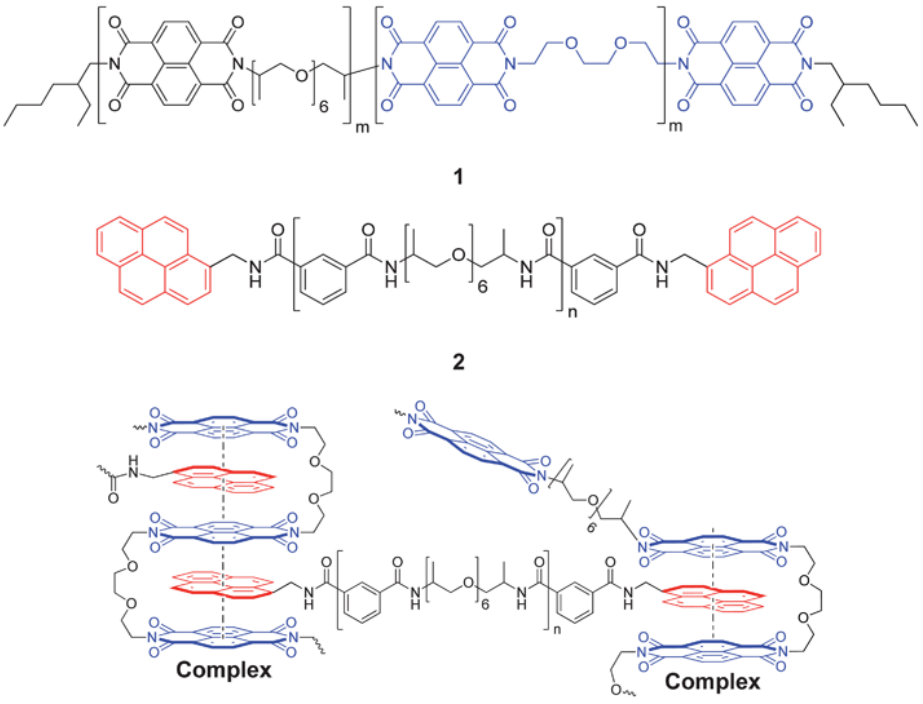

Figure 5. Chain-folding polydiimide **1** and pyrenyl end-capped polymer **2** folded into a pi-electron stacking interaction.[54](Reproduced with permission)

1.3 Polyurethane

Polyurethane (PUs) are among the most versatile materials in the polymer industry. Its possibility to range from soft elastomers to hard rigid construction materials makes it south after.[56] The ease of changing Polyurethanes' chemical, mechanical properties has led to a significant rise in interest for industrial research, but also biological communities.[56] These changes can be made by varying the quantity and type of polyol and isocyanate monomer used, changing the ratios between soft or hard domains, or by implementing other additives or nanomaterials such as graphene.[16] Since polyurethane is such modifiable, it may be tailored into a vast range of uses. This material has seen its use in construction industry, medical science, automobiles, coatings, adhesives, sealants, paints, textile, wood composite and apparel.[56-58] Polyurethane was first developed pre-world war II in 1937 by Dr. Otto Bayer and his co-workers in Leverkusen, Germany.[59] They called it "Das di-Isocganat-Poluadditionsverfahren".

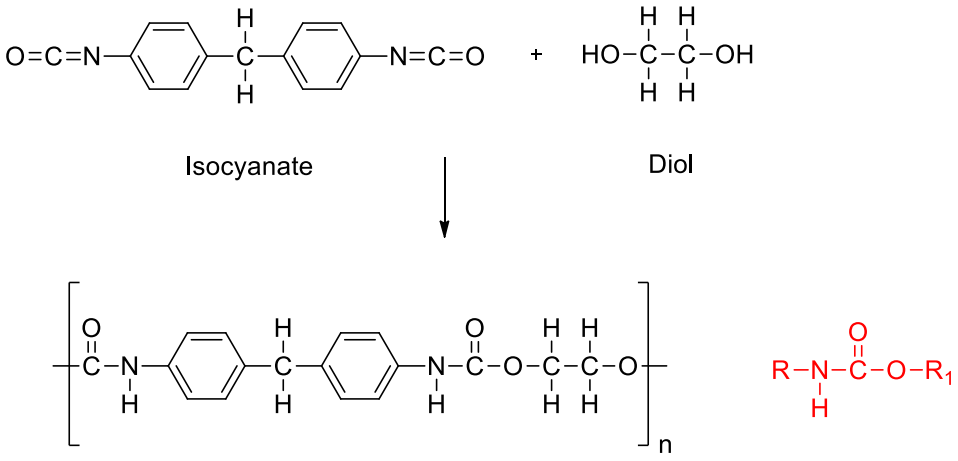

Scheme 6. The general formation of the urethane link and the specific urethane bond (red).

The easy incorporation of additives and functionality to alter polyurethanes characteristic features makes it a suitable polymer for various application such as self-healing materials. A linear Polyurethane with self-healing abilities has earlier been synthesized by Feng et al.[60] consisting of a furan decorated chain and Bismaleimide (BMI) carrying two maleimide pendant groups to cross-link the PU chains through the Diels-Alder reaction. A composite of reduced graphene oxide (rGO) and polyurethane was synthesized by Li et al.,[28] with polyurethane being functionalized with both furan and maleimide, and rGO being decorated with furan pendants for cross-linking of the polyurethane. This composite was synthesised for applications in healable flexible electronics.

Catalysis also plays an important role in the synthesis of polyurethane. By using catalysts, the polymerizations are more energetically favourable and can be reacted under milder conditions.[61] Using catalysts in polyurethane synthesis promotes the isocyanate-polyol reaction to form the urethane linkage. Tertiary amines are the most commonly used organic base catalysts used in PU synthesis, and two possible mechanisms for urethane formation is proposed.[61-63] The first is proposed by Baker et al.[62] where the tertiary amine and isocyanate forms an amine-isocyanate complex before the subsequently reacting with the polyol monomer. The second amine-catalysed mechanism proposed by Farka et al.[63] suggest that the amine interacts with a proton source i.e. hydroxyl in the polyol, making the oxygen more electronegative and reactive. This leads to the reaction with isocyanate to form the urethane linkage. Both mechanisms for amine catalysed urethane formation can be seen in Scheme 7.

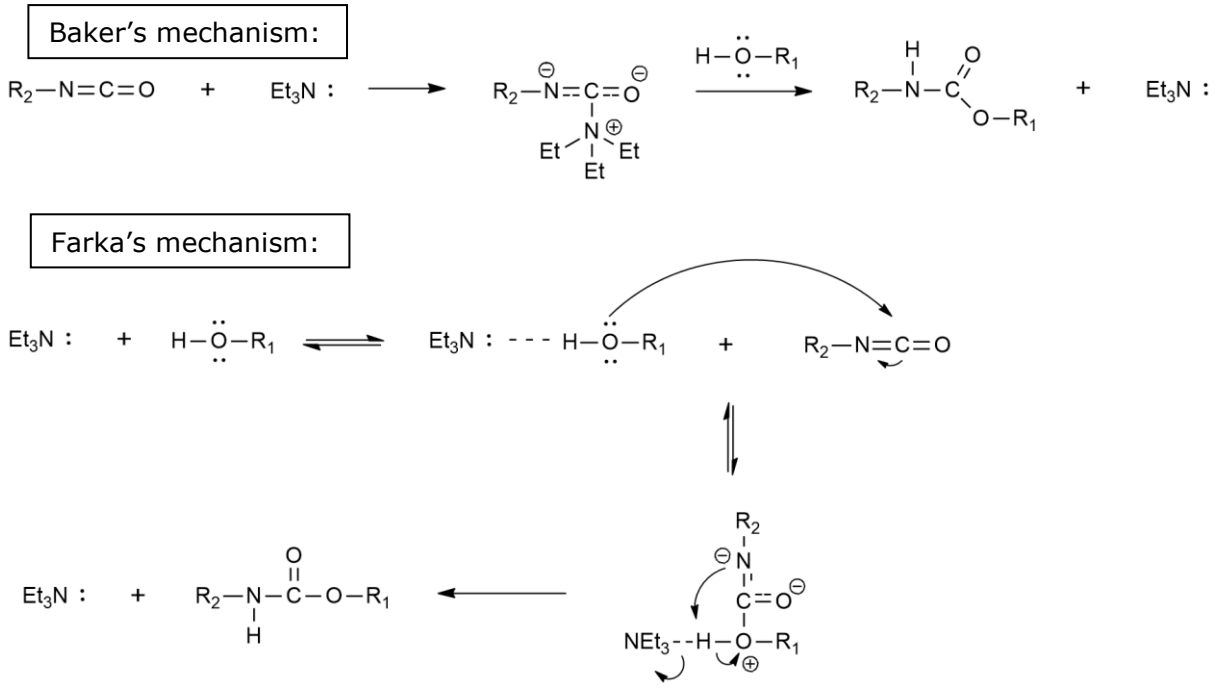

Scheme 7. Amine catalysed urethane formation as proposed by Baker et al.[62] (top) and Farka et al.[63] (bottom).

1.3.1 Polyols

Polyols is one of the main components to polyurethane synthesis and contributes with flexible long segments in the polymer chain.[56] Polyols are end-capped with hydroxyl functional groups, but also contain other functional groups such as ester, ether, amide, acrylic, metal, metalloid, with the first two being the most used. One way to obtain Polyether-based polyols is through ring-opening polymerization of epoxides in the presence of a proton-donating compound.[64,65] This reaction is commonly called alkoxylation.[66] The most common epoxides for polymerization is ethylene oxide, propylene oxide or butylene oxide (See Scheme 8). Earlier studies show catalyst bases used for this alkoxylation are trimethylamine, DABCO, *t*-BuOK, NaOH, KOH or CH_3OK.[67]

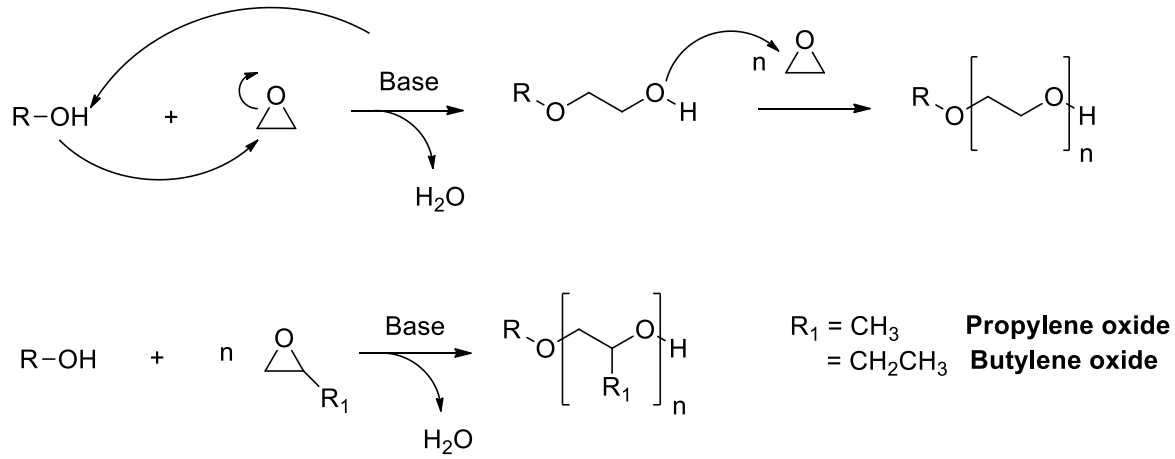

Scheme 8. Alkoxylation of epoxides into polyether polyols[65]

Polyester polyols are also highly used in Polyurethane production and was first studied by Carothers in 1929.[9,68] This was accomplished through a step-growth polymerization between aliphatic dicarboxylic acids and diols.[67] Today, the most common synthetic routes to obtain polyester polyols are polycondensation reaction, transesterification and ring opening polymerization. Because of their higher cost, lower functionality, higher rigidity, polyester polyols are less developed than polyether polyols.

Polyols with lower molecular weight will give a higher concentration of urethane links in the polymer chain, resulting in a more rigid and hard polyurethane.[56] The shorter chains react more easily with –NCO groups, thus giving a higher molecular weight polymer. Polyols with higher molecular weight will give the opposite effect to polymer formation. Less concentration of urethane links giving a more flexible polymer chain. Functionality of polyols are also important to the rigidness of the polymer. Short polyols with a functionality greater than three allows a more rigid and crosslinked polymer. Longer chained polyols with a functionality of two gives softer and long chained polymers.

1.3.2 Isocyanates

Isocyanates is the second main component in polyurethane synthesis and contributes with the reactivity of the polyurethane and its curing properties.[69] Isocyanates are either aromatic, aliphatic or cycloaliphatic. They are often di-functional with two –NCO groups per molecule or poly-functional with three or greater –NCO groups.

Isocyanates have a high reactivity, which is dependent on the nature of the isocyanate structure or by use of a catalyst (i.e. tertiary amines) to increase the rate of the reaction.[62,63] This happens through polarization of the isocyanate group giving a rise in polar interactions. The reactivity is also controlled by the positive nature of the carbon atom in the R-N=C=O group sequence. The carbon is eligible to a nucleophilic attack, and the nitrogen and oxygen atoms are open for electrophilic attacks.

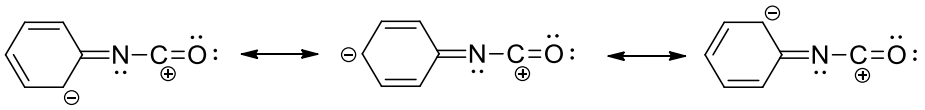

Scheme 9. Resonance stabilization in the aromatic ring.[56]

As earlier mentioned, the reactivity also follows the other structural properties of the isocyanates. Aromatic isocyanates are noticeably more reactive than their aliphatic and cycloaliphatic counterparts, as the –NCO carbon atoms charge is affected by the resonance stabilization of the aromatic ring (Scheme 9).[56] The reactivity of the isocyanates is also affected by its substituents.[56] Electron withdrawing substituents in the ortho or para will increase the reactivity, and electron donating substituents will contribute with the opposite effect. Having a second electron withdrawing isocyanate will increase the reactivity of the first one within the same molecule.

2 Graphene

Graphene is a two-dimensional structure arranged in a hexagonal lattice, and is a naturally occurring allotrope of carbon. The formal IUPAC definition describes graphene as "a single carbon layer of the graphite structure, describing its nature by analogy to a polycyclic aromatic hydrocarbon of quasi infinite size."[70] The same article stated that the term graphene should only be used when reactions, structural relations or other properties of individual layers are discussed.[70]

Geim and Novoselov isolated single layer graphene for the first time in 2004,[71] though Boehm *et al.*[72] first mentioned its existence back in 1994. Their method of discovery was through the "Scotch Tape method" by mechanical exfoliation of graphite. By using common adhesive tape, they could remove layer by layer of graphite until they were left with a few layer graphite product. By the end, they had isolated high-quality single layer graphene. The surge in interest for this material rose over the next few years culminating by the Nobel Prize in Physics awarded in 2010, only 6 years after the first report. Since then, the research and development of graphene-based materials has increased every year. Features such as strong mechanical properties, optical transparency,[73] and both thermal and electrical conductivity are key properties,[74] which makes this material popular.

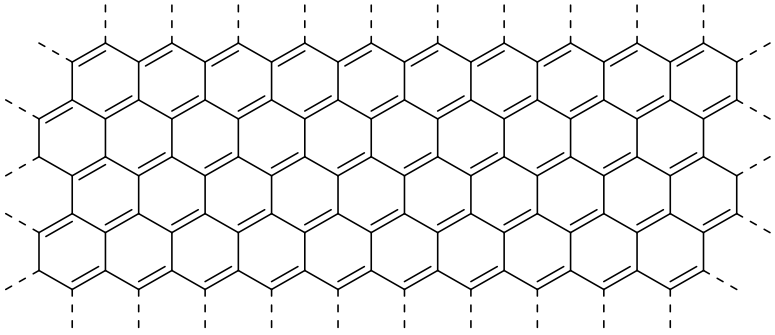

Figure 6. The honeycomb lattice structure of graphene.

The hexagon two-dimensional honeycomb lattice originates from sp2 hybridized atomic orbitals. These carbon atomic orbitals are 2s, $2p_x$ and $2p_y$ which hybridizes into sp^2 orbitals to form covalent sigma bonds with neighboring carbon atoms. The three sp2 orbitals is what makes each carbon in the graphene lattice three-valent, thus allowing the hexagonal structure. The fourth and last 2pz orbital allows for the formation for an out of plane pi-bond between every other carbon atom. The 2pz atomic orbital is perpendicular in respect of the carbon lattice made from the three other orbitals. This allows for a perfect conjugated structure since each carbon only can contribute with one spare 2p orbital to form double bonds. In conclusion, the atomic orbitals of each graphene carbon allows three sigma bonds and one pi bond. This tight and covalently bonded crystalline structure

measuring 1.42 Å between each carbon atoms allows for graphene's great mechanical strength, and the conjugated structure gives graphene its conductive properties. Graphene also holds a high specific surface area at 2630 m^2 g^{-1} and great thermal conductivity at 5000 W m^{-1} K^{-1}. It also has a high optical transmittance at 97.7%, which means it only absorbs 2.3% of visible light.[73] With these properties in mind, graphene may be highly useful for a vast number of applications, both by replacing existing materials and strengthen already well-known products. Furthermore, graphene has been used in application such as flexible electronics, energy storage, carbon capture, photovoltaic systems, coatings, sensors,[75] high-frequency transistors, clothing and much more.

2.1 Preparation of graphene

The recent interest in graphene applications and synthesis has also brought several methods to synthesis this one atom thick material, or exfoliate it from multi-layered graphite. In this section, these methods are reviewed and elaborated. The synthesis of single-layered graphene is divided into two main branches, bottom-up synthesis and top-down synthesis. Bottom up graphene production is done by assembly to form a single graphene sheet atom by atom. This method is slower than top-down production, and is prone to error in the form of loss of uniformity. Bottom-up methods includes classic organic synthesis, epitaxial growth, or chemical deposition vapor (CVD). For the latter two a carbon source is needed and typical precursor gases like CH_4, C_2H_6 and C_3H_8 are utilized.

Table 1. Different methods of producing or isolating graphene.

Graphene production	
Top-down methods	**Bottom-up methods**
Micromechanical exfoliation	Organic synthesis
Solvent-assisted exfoliation	Epitaxial growth
Reduced graphene oxide	Chemical vapor deposition

Top down approaches for graphene production focus mostly on extracting it from graphite. Graphite is formed when rock containing high amounts of carbon, such as coal, is exposed to high pressure and temperatures. This causes the high carbon rock to stratify and form into perfect graphene sheets millions of layers thick. If the pressure increases further, diamonds form. One of the most convenient top-down graphene production processes includes the splitting of graphite layers apart, yielding the individual graphene sheets, a process commonly referred to as exfoliation. Initially, this was performed *via* the scotch tape method developed by Geim and Novoselov in 2004. Additionally, it can be completed through liquid phase exfoliation of graphite assisted by ultra-sonication. Lastly, the oxidation of graphite into graphite oxide, followed by exfoliation into graphene oxide (GO) and subsequent reduction to partially restore its conductive properties as reduced graphene oxide or rGO is also an extremely popular production method.[76]

2.1.1 Reduced graphene oxide

Graphene oxide (GO) is an oxidized graphene compound, which is prepared by treating graphite with oxidizing mixtures consisting of concentrated acids[77] or ozone.[78] It is one of the earliest forms of produced carbon Nano structures, and was formerly called graphitic acid.[77] Back in 1859, it was first prepared by Brodie by oxidizing graphite with concentrated nitric acid with potassium chlorate.[77] By oxidizing graphite into GO, carboxyl, epoxy, and hydroxyl groups are functionalized into the normally homogenous honeycomb lattice of graphite. The formation of these functional groups through oxidation leads to exfoliation of graphitic layers. An illustration of GO can be viewed in Figure 7 The Hummers method was developed to yield GO by treating graphite with a water-free mixture of concentrated sulfuric acid, sodium nitrate and potassium permanganate. The procedure were carried out in under 2 hours, using low temperatures, resulting in GO in a carbon to oxygen ratio of 2.25.[77] Effectiveness of the oxidation is governed by the carbon to oxygen ratio of the GO product, and well reacted oxidations were judged to be within 2.1-2.9 carbon to oxygen atomic ratio.[77] From the Figure 7, a disruption in the conjugation of the system is visible.

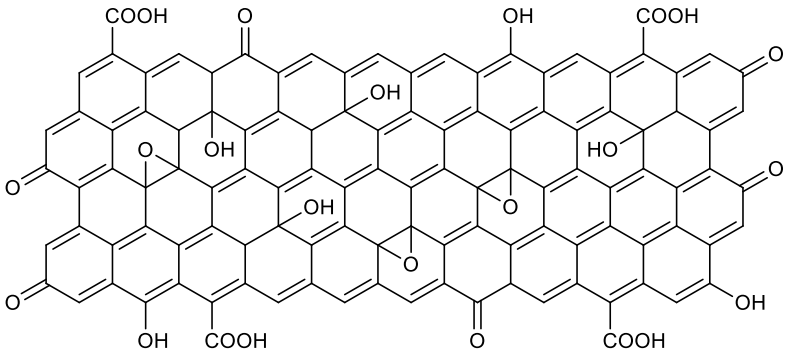

Figure 7. GO with oxygen containing functional groups.[79]

2.1.2 Liquid phase exfoliation (LPE)

LPE is a method designed to exfoliate powdered graphite into graphene without causing severe defect formation by oxidation.[80] This method relies on the physics and chemistry of interfaces in solid-liquid systems. The exfoliation of graphene uses special solvents and surfactants that does not lead to either defect formation or oxidation of the graphite. Normally, graphene can only be dispersed in concentrations as low as <0.01 mg mL^{-1}, which gives dispersion of graphene in solvents a disadvantage compared to GO that's disperse-able in concentration up to 1 mg mL^{-1} in organic solvents and 7 mg mL^{-1} in water. Khan and coworkers was able to increase the concentration of graphene up to approximately 1 mg mL^{-1} by applying mild sonication to the graphite powder in NMP. Transmission electron microscopy (TEM) analysis showed that a sample sonicated for 100h had 90% of graphene flakes had <5 layers. Furthermore, Raman spectroscopy could determine that minimal defects had formed in the basal-plane of the exfoliated graphene.

On a macroscopic level, the graphene seems soluble in the exfoliation solvent, as the dispersion is uniform and stable. Nevertheless, graphene sheets and aggregates are insoluble in solvents, making graphene the dispersed phase with the exfoliating solvent as the continuous phase in a colloidal system. A representation of solvent-assisted exfoliation of graphene using NMP is shown in Scheme 10 The weak bonds between each layer in graphite is comparable to Van Der Waals forces.[70] Kinetic energy from the sonication breaks apart the graphite, assisting the solvent to permeate the graphite.[81] The exfoliated graphene sheets are stabilized through interactions with the continuous phase, although over time, exfoliated graphene will aggregate, as the interactions between the separated graphene flakes will exceed the permeation of the solvent.

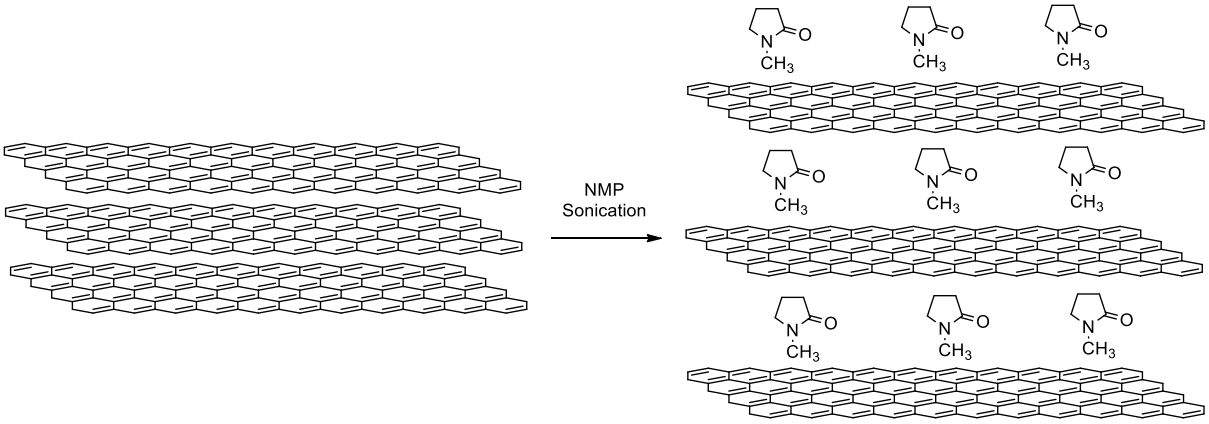

Scheme 10. Graphite (left) is exfoliated into individual graphene sheets (right) using NMP as the dispersion solvent.

To increase the concentration of graphene in organic solvents through solvent-assisted exfoliation of graphene, two methods of sonication can be utilized, bath sonication or tip sonication. Both sonication methods are represented and described in Figure 8. Subsequently, the exfoliated graphene in continuous phase is centrifuged after sonication to collect the supernatant, which were successfully exfoliated. Khan et al. explored rotation rates from 500 rpm to 4000 rpm, and through Raman spectroscopy, they were able to report that defect formation increased with rotation rate. Further, they were able to see the same increase in defect formation as sonication times increased. The reported defects comes from changes in the topography in the basal-plane and introduction of new graphene flake edges as graphite is exfoliated. Defects formation of graphene is analyzed by Raman spectroscopy, which is further introduced in section 2.3

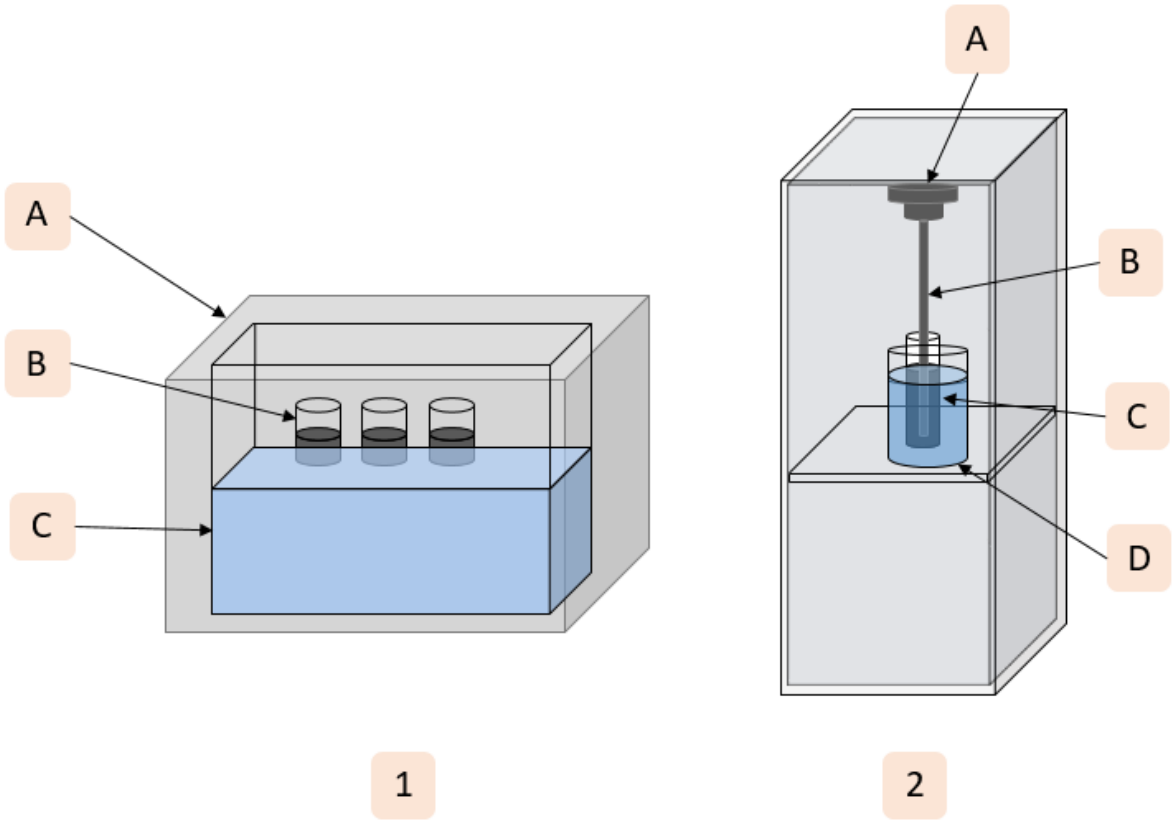

Figure 8. Representation of bath sonication [1] and tip sonication [2]. [1] Ultrasonic generator (A); Sample vials with powdered graphite in exfoliating solvent (B); Water bath (C). [2] Tip sonicator (A); Titanium probe (B); Ice bath (C); Graphite in NMP submerged so height of liquid matches the height of the ice bath (D).

2.1.3 Chemical vapor deposition

Chemical vapor deposition (CVD) is reported to be the most promising method of synthesizing pristine single layer graphene in larger scale.[82] When producing graphene using CVD, the decomposition of the carbon sources is used to synthesize graphene films. These carbon precursors can be in both solid, liquid and gas phase. One example of solid carbon source in graphene synthesis was done by Sun *et al*.[83] using poly (methyl methacrylate), PMMA. A temperature of 800°C was applied to decompose PMMA, thus "growing" high quality graphene on copper surfaces. The quality of the graphene was confirmed by Raman spectroscopy showing no to little disorder in the sp^2 hybridization network. Polystyrene has also been utilized as a solid phase precursor in CVD, but requiring lower temperature to decompose since it holds weaker C-H bonds than PMMA.[84] A lower temperature in the CVD method contribute to a more convenient production.

Gan *et al*.[85] also utilized Hexacholorbenzene (HCB), in a modified CVD method, only requiring 360°C to decompose. This method required the chlorine atoms to be removed from HCB, but this was enabled by the copper metal foils used in the process as $CuCl_2$ molecules formed. Other precursors used for solid carbon CVD are solid polyethylene and polystyrene-based waste as reported by Sharma *et al*.[86] Next, Ruan *et al*.[87] was able to use food, food waste and insects to obtain high quality graphene comparable to other carbon sources.

Hydrocarbon gases such as methane, acetylene and ethylene are commonly used as carbon sources when producing graphene from gas phase, with methane (CH_4) as the most common source. Several researcher groups' report of high quality mono-layered graphene using CH_4 as a carbon sources processed at around 1000°C.[88,89] This was done on both nickel and copper films deposited over complete Si/SiO_2 wafers.[90] CH_4 has also been used in plasma enhanced CVD (PE-CVD), where CH_4 also doubled as a hydrogen gas source as well as the carbon source.[91] Utilizing PE-CVD, the graphene growth process was possible at a noticeably lower temperature, allowing for an easier process. Chan *et al*.,[92] was able to successfully grow a mono-layered graphene film onto a copper foil at 600°C, which is comparably lower than without plasma enhanced CVD.

2.2 Functionalization of graphene

With its numerous ways of applications, graphene is a versatile material, but not without its drawbacks. For graphene to be applicable in semiconductor technology, it needs a wide energy gap of at least 0.5 eV.[93] However, graphene has a zero band-gap energy by nature, which makes it less effective as a semiconductor. Graphene also holds poor solubility abilities in organic and aqueous solvents.[94,95] A workaround to circumvent these challenges are chemical functionalization of graphene. Electronic, structural and chemical properties of graphene can be altered to make it more suitable for specific purposes and uses. One example is functionalization with a nitrophenyl group, which resulted in a graphene material with lower resistance towards electron transfer.[96] Furthermore, graphene can be decorated with functional groups targeted towards specific applications (i.e. functionalizing graphene with dienes or dienophiles to covalently bind it to other compounds, such as polymer composites). In section 2.2.1, several methods of functionalizing graphene via cycloaddition will be introduced.

2.2.1 [2+1] Cycloadditions

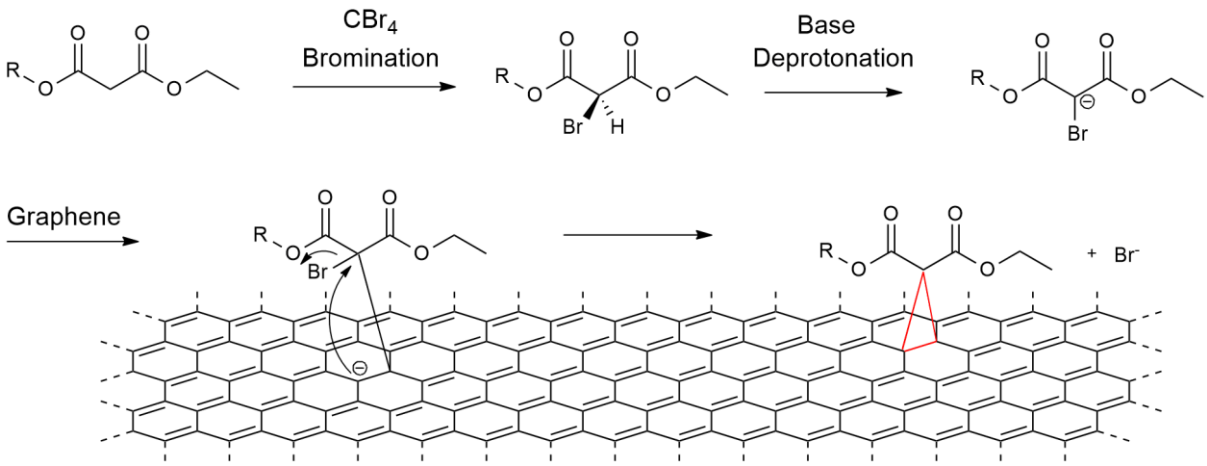

Scheme 11. Reaction mechanism of nucleophilic [2+1] cycloaddition of as proposed by Biglova *et al.*[97] Carbon tetrabromide (CBr_4) is used as a brominating agent, followed by base deprotonation of the other α-proton, resulting in a stabilized α-halocarbanion that reacts with graphene through cycloaddition.[98]

[2+1] cycloaddition is the most commonly utilized [2+n] cycloaddition method to functionalize carbon Nano structures such as Graphene.[97] This can occur in several various ways, including addition of carbenes,[94] nitrenes,[99] stabilized carbanions,[100] etc. From these, the Bingel reaction, which is an addition of a stabilized carbanion shown in Scheme 11, is reported to be the most efficient way to perform this type of functionalization.[97] From Scheme 11, a malonate derivative is brominated by CBr_4, followed by deprotonation of the other α-proton with 1,8-diazabicyclo[5.4.0]-undec-7-ene (DBU).[98] A nucleophilic stabilized α-halocarbanion is formed, which can react through addition to suitable electrophiles such as graphene.[100] As a result, the anionic centre generated in the graphene matrix will lead to an intramolecular displacement of the halide.[98] The mechanism is regarded as an addition/elimination reaction.

Earlier, functionalization with carbenes on carbon materials has been explored with examples showing addition of carbenes to the sidewalls of carbon nanotubes. Carbenes such as dicholorcarbenes derived from chloroform ($CHCl_3$), are nucleophilic giving them increased affinity to the electrophilic nature of the sp^2-hybridized network of graphene. This type of functionalization has further been explored using graphene obtained from reduction of GO. The graphene used were GO obtained from the Staudenmaier's method, reduced with hydrazine monohydrate.[101] The functionalization were processed using a conventional method for production of dicholorcarbenes. Graphene suspended in CHCl3,

sodium hydroxide (NaOH), and phase transfer catalyst (PTC) were processed at reflux conditions, resulting in cycloaddition of dicholorcarbenes to the graphene lattice. The result is dihalogenated cyclopropanes at the edges of the graphene flakes as seen in Scheme 12.[94]

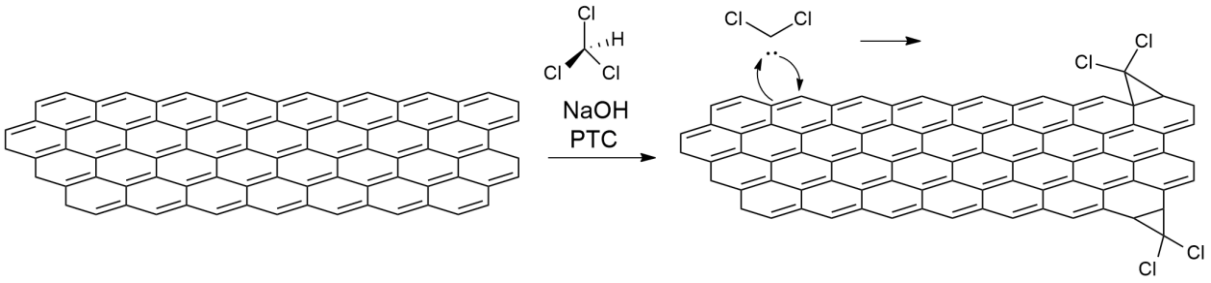

Scheme 12. Addition of dicholorcarbenes to the edges of graphene.[94]

Nitrene chemistry is another route to covalent functionalization of graphene through [2+1] cycloaddition.[99] Nitrenes are generated by removing N_2 from azidotrimethylsilane (ATS), nitrene can either react with graphene via electrophilic [2+1] cycloaddition reaction (Scheme 13C-E), or by a biradical pathway after intersystem crossing (Scheme 13D-E).[99] The cycloaddition of nitrenes are electrophilic compared to the Bingel cycloaddition, which is nucleophilic. After removal of N_2 from ATS, the nitrene nitrogen is neutral and electron deficient, making it an electrophile.

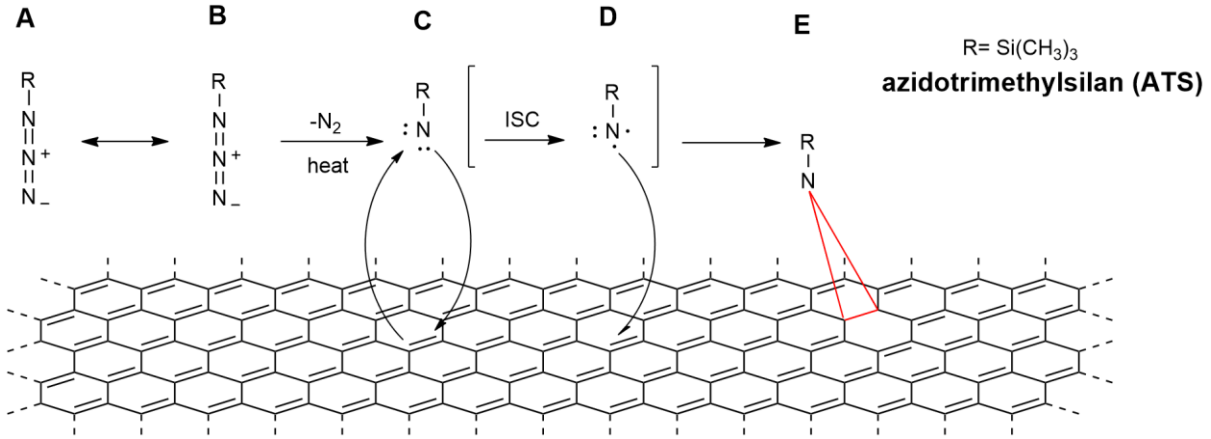

Scheme 13. (A & B) Resonance forms of ATS (C to E) electrophilic [2+1] cycloaddition reaction (D to E) biradical pathway onto graphene after intersystem crossing (ISC).[99]

Functionalization of graphene is also subject to other types of cycloaddition, such as 1,3-dipolar cycloaddition of azomethine ylides to graphene.[102] Similar to the other cycloadditions, this method has been successfully used in the functionalization of fullerene C_{60} and carbon nano tubes (CNTs).[103] The azomethine ylides are generated by condensation of an α-amino acid and an aldehyde. The aldehyde is able to hold other organic functional groups wanted in the functionalization of fullerenes, CNTs and graphene. The functionalization in focus was completed by suspending single-walled CNTs in DMF with excess of aldehyde and a modified glycine as the amino acid.[100] This resulted in functionalization by 1,3-dipolar cycloaddition to the single-walled CNT. An example of this cycloaddition to graphene can be seen in Scheme 14.

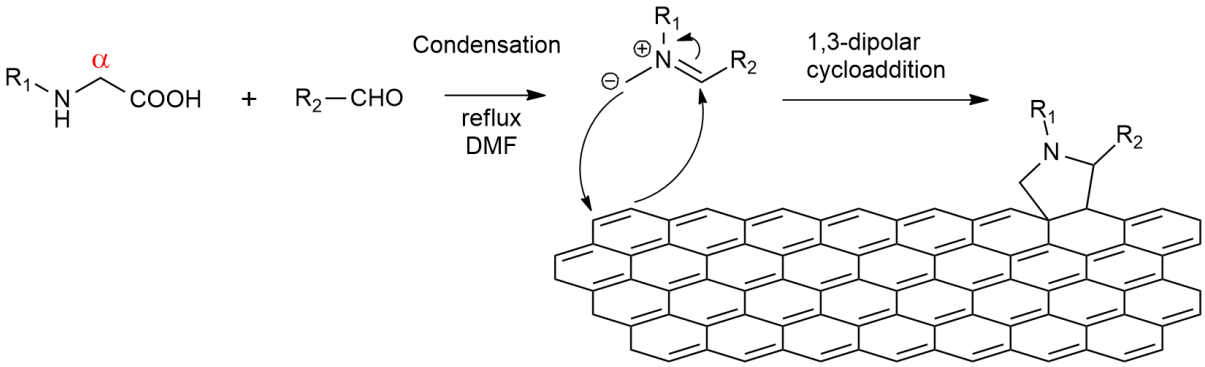

Scheme 14. Condensation of an α-amino acid (modified glycine) and an aldehyde, followed by 1,3-dipolar cycloaddition of the resulting azomethine ylide to graphene.[102]

2.3 Micro-Raman spectroscopy of Graphene

Raman spectroscopy is a fast and practical tool in analysis of sp^2 hybridized carbon structures such as graphene.[104] A monochromatic laser (532 nm) is used to irradiate a sample with photons, causing the irradiated molecule to vibrate. This is a result from an exchange of energy from the photons to vibrational energy in the analyzed molecule, and this effect is called Raman scattering.[105,106] This vibrational energy contribute with disorder-induced features in sp^2 hybridized carbon structures, which have high symmetry. These types of structures are highly sensitive to symmetry-breaking effects, making Raman spectroscopy an informative method to characterize defects in graphene. Rama scattering leading to disorder and symmetry breaking results in an observable spectrum giving information about vibrational modes of the irradiated material. Raman spectroscopy is widely used in the analysis of sp2 carbon networks such as amorphous carbon, CNTs, carbon nanohorns, graphene and diamond-like carbon.[107-109] The spectra acquired from Raman scattering showcase a series of bands that represent the different features of the analyzed material.

Raman spectrum of crystalline graphite exhibits two strong bands centered at 1580 and 2670 cm^{-1}, commonly referred as G and G' respectively.[106] As disorder is introduced to crystalline graphite, new peaks centered around 1350 and 1640 cm^{-1} emerges, referred as D and D' respectively. A source of disorder introduced to the graphitic lattice can be through the liquid exfoliation process to produce graphene. A Raman spectra acquired in this master project is shown in Figure 9 with band assignments G, G', D and D'.

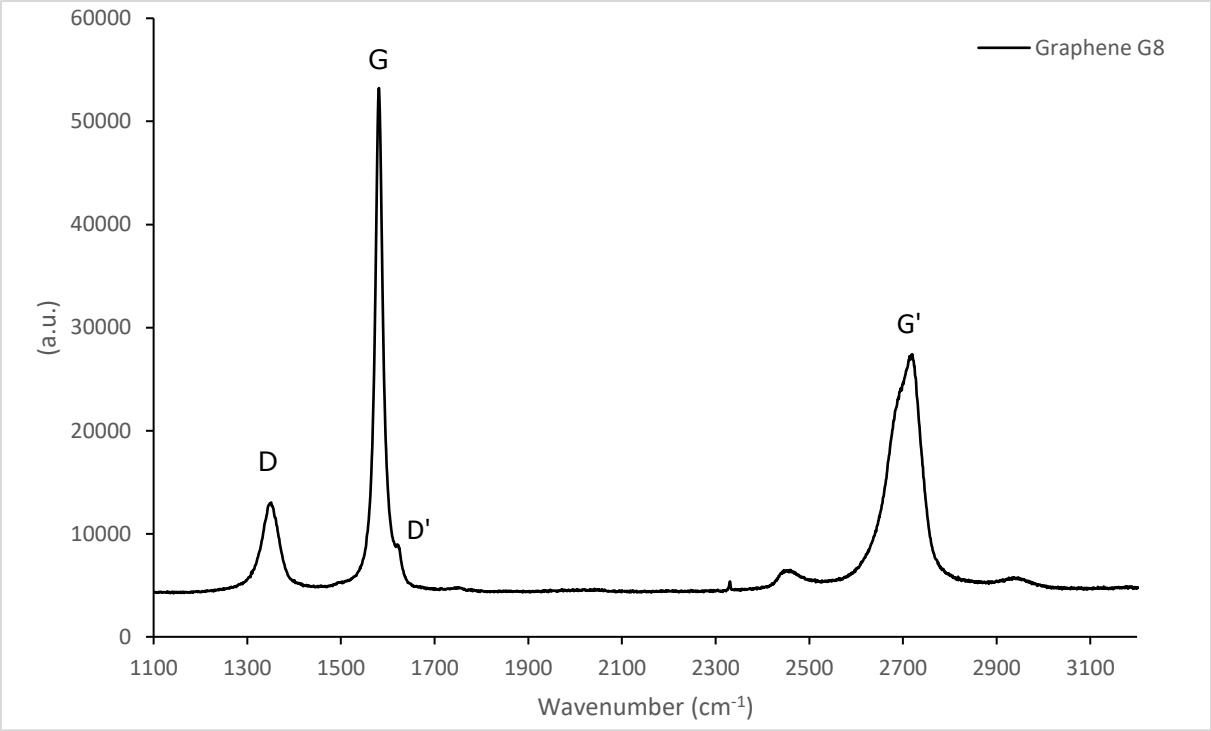

Figure 9. Raman spectra of exfoliated graphene prepared in this master project. G' band is visible at ~2670 cm^{-1}, a D' band at ~1620 cm^{-1} is slightly visible at the right shoulder of the strong G band at ~1580 cm^{-1}, and the D band at ~1350 cm^{-1}.[110]

The G band of graphite and graphene originate from first-order Raman scattering by in-plane doubly degenerate vibrational modes corresponding to C-C stretching in the graphitic lattice.[104] The G' band is the second-order Raman scattering by in-plane transverse optical phonons. A lot of valuable information can be derived from the shape of the G' peak as seen in Figure 10. Graphite shows a slightly more prominent peak shifted more to the right and with a noticeably higher wavenumber than few-layer graphene. As the number of graphene layers decrease, the band shifts to the left and to a lower wavenumber. 1-layer graphene shows a sharp symmetric peak.

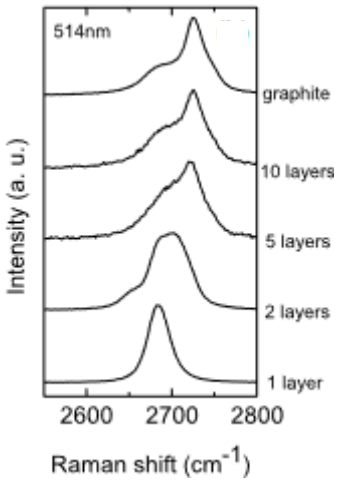

Figure 10. Evolution of G' band shape from Raman spectra at 514 nm performed by Ferrari *et al*.,[107] which is comparable to the wavelength 532 nm used in this thesis.

Further, the D and D' bands at ~1350 and ~1620 cm^{-1} respectively, are visible in Raman spectroscopy as defect formation or impurities are introduced. These bands are proportional to the disruption of the sp^2 hybridized graphene surface. From intensity of the disorder-induced D band and the first-order graphite G band, a ratio (I_D/I_G) can be derived. This is simply calculated by dividing the intensity of the D band by the intensity of the G band, and provides a parameter that can be used to describe the disorder of the irradiated material.

3 Aim of thesis

The aim of this master thesis has been to synthesize a self-healing polymer using polyurethane as the main backbone for the polymer, while using graphene as a cross-linking agent. To achieve self-healing, the thermoreversible Diels-Alder reaction has been utilized. Polyurethane being functionalized with a maleimide group as the dienophile, while graphene was functionalized with furan as the diene. The focus of this thesis has been to make this self-healing nano hybrid as a proof of concept. The main challenges were to synthesize a novel graphene hybrid bearing the diene moiety and promote its dispersibility in the polyurethane matrix in order avoid the inherent material's thermodynamic tendency to aggregate and achieve the desirable healing effect.

4 Results and discussion

This chapter discusses the different synthesis to reach the target material which is a self-healing polymer composite comprised of a graphene-crosslinked polyurethane. The chapter is divided into six sub chapters: synthesis strategy, synthesis of maleimide **3**, synthesis of malonate **4**, exfoliation and Bingel reaction to make compound **6**, polymerization of maleimide-PU, and the casting of the final target material **9A-9D**.

4.1 Synthesis strategy

Two key building blocks were planned for the synthesis for the target composites **9A-9D**: maleimide functionalized polyurethane (**8**) and furan functionalized graphene (**6**). Compound **8** as a linear polyurethane crosslinked by **6** through non-autonomic dynamic covalent bonding, using thermoreversible Diels-Alder. From this hypothesis, the plan were to functionalize each key molecule with the diene and dienophile for the Diels-Alder reaction. From several previously reported articles, furan and maleimide have been widely used for self-healing polymers.[30,111-115]

One functional pendant was selected with a single hydroxyl group, which is required to attach the malonate moiety through esterification with Ethyl 3-chloro-3-oxopropionate. Furan-3-methanol was chosen to afford the malonate product **4** in order to be covalently attached to graphene through [2+1] cycloaddition. When functionalizing polyurethane, on the other hand, a diol with a pendant group bearing the dienophile was chosen. A maleimide with two hydroxyl group was chosen as a logical pathway since this molecule has been reported earlier by Yu *et al*.[114] and Gramlich *et al*.[115]

Opposite pendants were investigated (i.e. a graphene hybrid with a dienophile and a polyurethane bearing the diene), but not pursued. Maleimide with one hydroxyl group for esterification with malonate came at a much higher cost than furan. Furthermore, using a furan with two hydroxyl groups would make it part of the polyurethane chain rather than a side chain, thus making it more sterically hindered for Diels-Alder.

An overview of the chosen strategy is presented in Scheme 15.

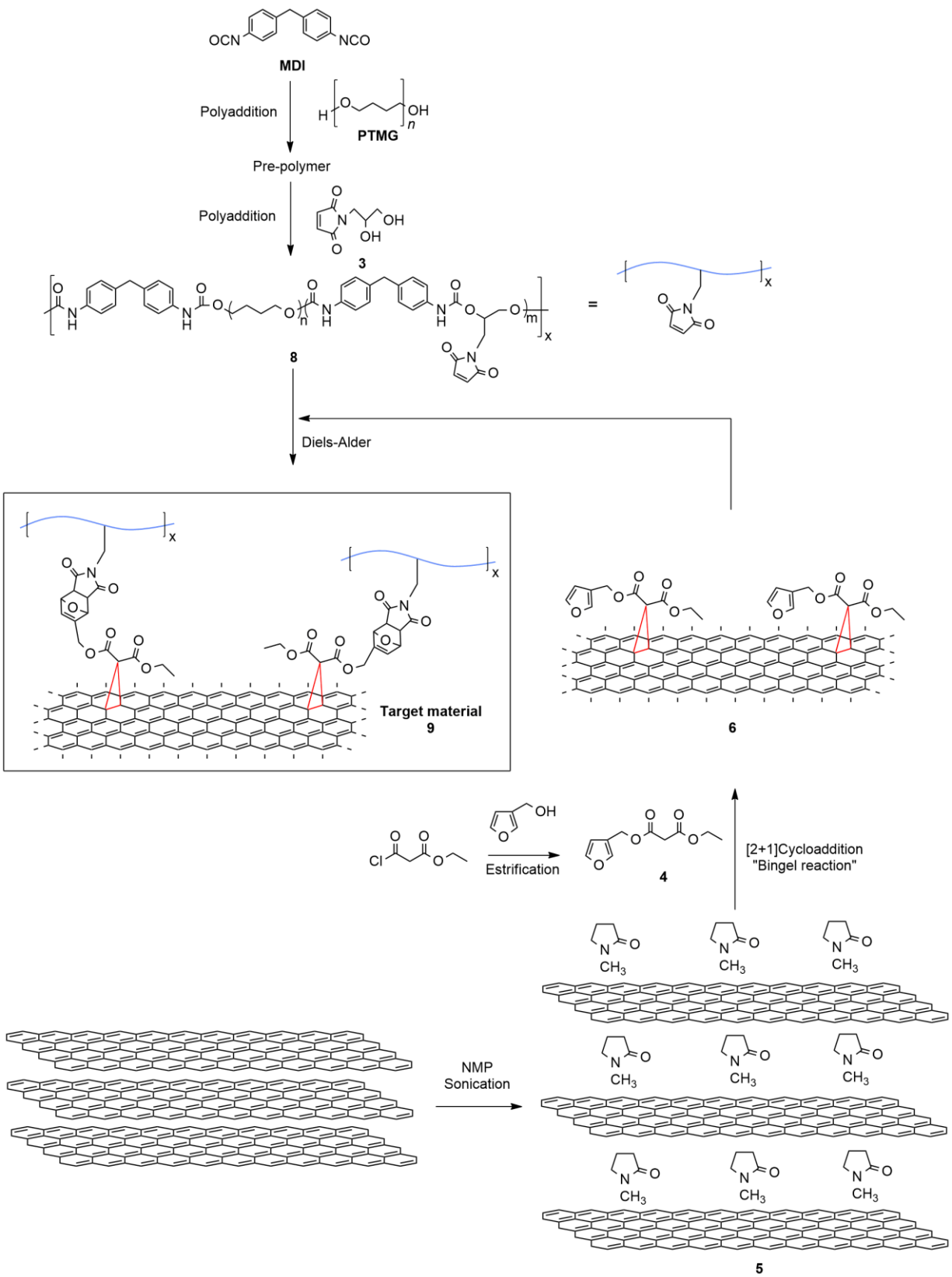

Scheme 15. Main strategy for synthesis of target material **9**.

Earlier, maleimide and furan have been reacted to a Diels-Alder adduct before attaching them to other polymers (i.e. polyurethane).[116] This could be a viable synthetic route, although, by using a Diels-Alder adduct of maleimide and furan, the three hydroxyl groups would give less control of further reactions. It would be necessary to explore other ways of attaching either the diene or the dienophile to graphene instead of using the MW assisted Bingel reaction. By synthesizing the two main parts separately, more control over the synthetic pathway were achieved. It also allowed controlling of the amounts of polyurethane and graphene used in the synthesis of the target material.

Scheme 16. shows two routes for the synthesis of maleimide (**3**): a three-step synthesis with a furan protection group, and a direct route with nucleophilic attack of APO onto maleic anhydride. However, Route **B** is subject to an unwanted Michael addition, further discussed in section 4.2.1, so route **A** was chosen as the safest synthetic route.

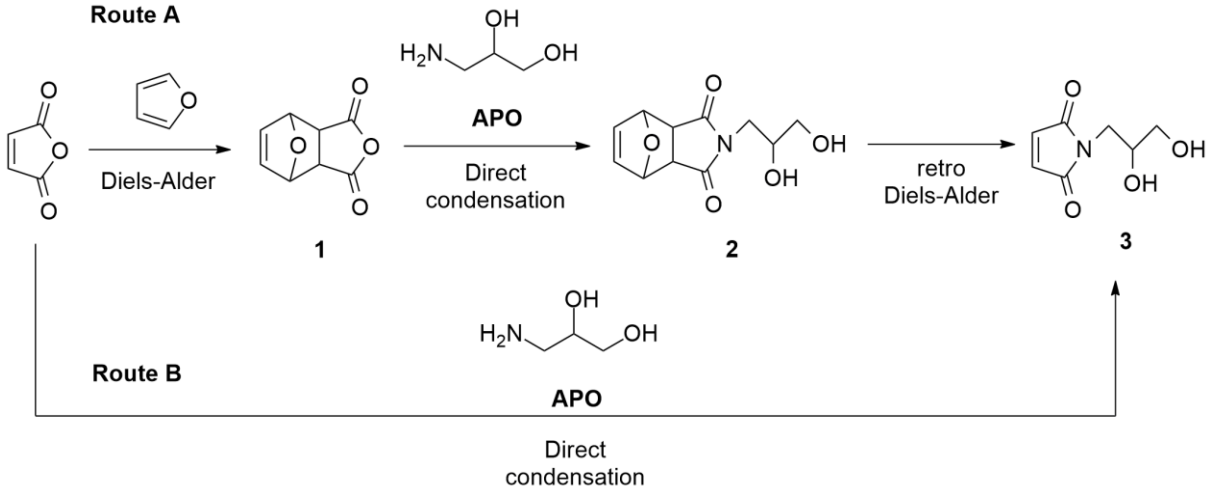

Scheme 16. Proposed synthetic routes to compound **3**.

4.2 Synthesis of Maleimide pendant, Compound **3**

4.2.1 Diels-Alder protection of maleic anhydride

Following route A from Scheme 16., the first step of preparing compound **3**, was the Diels-Alder protection of maleic anhydride. This protection was the first part of a 3-step synthesis to make the cyclic imide with a diol functionality needed for polyurethane synthesis. Mechanism for this Diels-Alder protection is shown in Scheme 17 below.

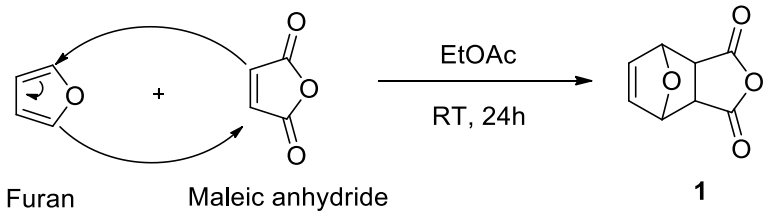

Scheme 17. Diels-Alder mechanism for protection of maleic anhydride.

The necessity of this protection comes from unwanted Michael addition to maleic anhydride when introducing a nucleophile, in this case the primary amine, *APO*. When a nucleophilic agent is reacted with a α,β–unsaturated carbonyl compound, two nucleophilic attacks occur. Either direct nucleophilic attack by 1,2-addition to the carbonyl carbon, or nucleophilic attack on the carbon-carbon double bond through 1,4-addition.[117] By adding furan as a protective group, Michael addition to the α,β -unsaturated pi-bond of the maleic anhydride is prevented.[118] By using this protective group, the selectivity of the nucleophilic attack of the amino group is shifted to direct 1,2-addition to the carbonyl carbon.[119] The mechanism for Michael addition is shown in Scheme 18 below, and the direct 1,2-addition is shown in Scheme 19 in section 4.2.2.

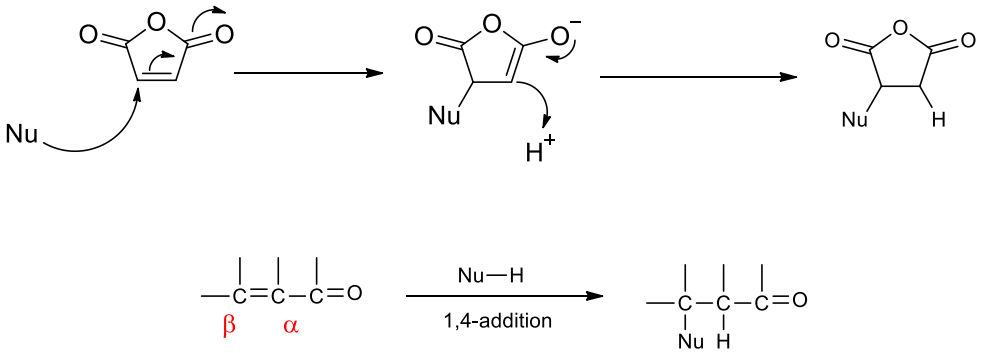

Scheme 18. Mechanism for the unwanted Michael 1,4-addition.[117,120]

The presence of electron withdrawing groups such as the two carbonyl groups also favors the Michael addition over the 1,2-addition, thus making the protection of the carbon-carbon double bond even more important.[117]

Table 2. Protection of carbon-carbon double bond of maleic anhydride. All reactions were conducted with EtOAc as reaction solvent.

Run	MA [g]	Furan [g]	Rx temp. [°C]	Rx time [h]	Yield [%]
1	3.00	2.09	RT	24	31
2	5.39	3.74	RT	24	-
3	6.39	4.44	RT	24	33
4	22.3	15.5	RT	24	15[a]
5	7.43	5.16	RT	24	34[b]
6	7.05	4.89	RT	24	30
7	6.46	4.48	RT	24	-
8	7.97	5.53	RT	24	37[c]
9	9.12	6.33	RT	24	**58**[c]
10	11.8	8.19	RT	24	42[c]

a) Purified by recrystallization with EtOAc

b) Cooled in freezer overnight to yield white crystals

c) Heat (60 °C) applied at the start of the reaction

The synthetic pathway for compound **1** were conducted based on the synthetic parameters suggested by Yu *et al*.[114] and Gramlich *et al*.[115], with yields at 78.5% and 87.6 % respectively. The initial runs turned a steady yield around 30-35%, with a couple of failed runs. By applying some heat to the reaction upon the furan addition, the yields were significantly increased, with the highest one recorded at 58%. Some runs turned out unreacted as maleic anhydride precipitated overnight. More reaction solvent was added in an attempt to process the reaction further. Given this was the first step, using low-cost reagents, these reactions were not optimized any further.

Ten experiments were completed at a 3.0 g – 22.3 g scale, with yields ranging from 15-58%. In most cases, crystallization of compound **1** happened overnight in room temperature. The runs, which did not turn out pure, were purified by recrystallization with EtOAc.

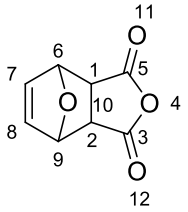

Figure 11. The structure of compound **1** and peak assignment numbering.

Table 3. Assignment of ^{1}H- and ^{13}C-NMR shifts, and multiplicity for compound **1** (400/100 MHz, DMSO-d_6).

Pos.	δ_H [ppm]	Multiplicity (int., J [Hz])	δ_C [ppm]	COSY	HMBC
1 & 2	3.31	s (2H)	49.1	-	All carbons
3 & 5	-	-	171.5	-	-
6 & 9	5.35	s (2H)	81.6	7, 8	All carbons
7 & 8	6.58	s (2H)	136.8	6, 9	6, 7, 8, 9

Chemical shifts for ^{1}H-NMR were in accordance with earlier reported spectra.[114,115] All proton shifts shows as singlets, but were expected to be seen as triplets since they all have two neighboring protons to split the signal. The spectra reported by Yu *et al*.[114] and Gramlich *et al*.[115] shows the same appearance of singlets for all protons.

Designation of chemical shifts for ^{1}H- and ^{13}C-NMR analysis are summarized in Table 3 and Figure 11. All NMR spectra's and IR are given in appendix A.

4.2.2 Direct condensation of compound 1

The next step of the three-step synthesis of compound **3**, is the direct condensation by nucleophilic attack of an amine to one of the carbonyl carbons of compound **1**. The two hydroxyl groups in APO will later function as a diol when reacting this compound with MDI and PTMG to synthesize compound **8**. Proposed mechanism for the nucleophilic attack of an amino group to the protected anhydride (**1**) is given in Scheme 19 The initial runs for this synthesis-step followed the same procedure as reported in section 3.2.1., but were eventually changed to achieve higher yields than reported values.[114,115]

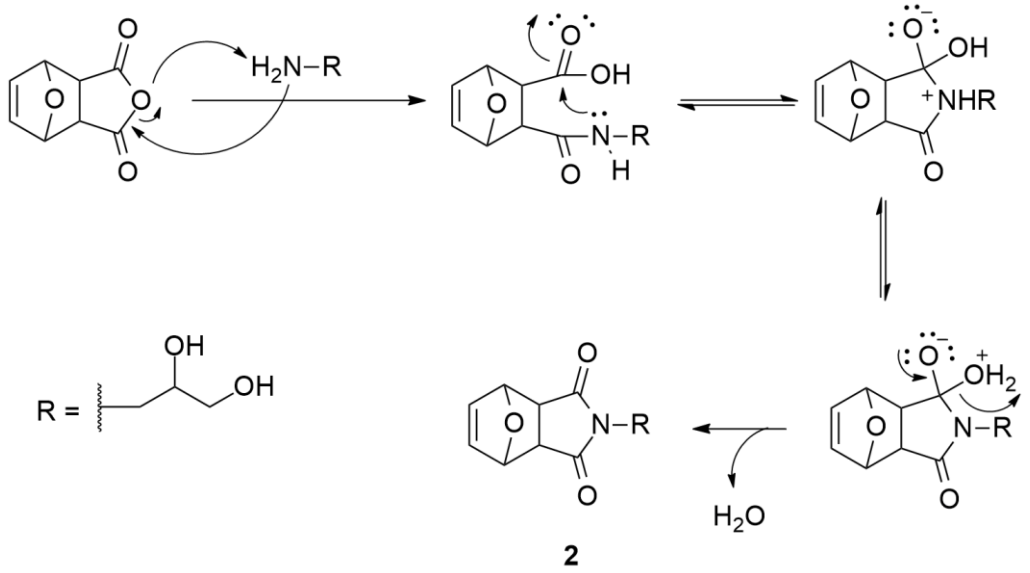

Scheme 19. Mechanism for nucleophilic attack of an amino group to compound **1**.[121,122]

Table 4. Reactant amounts and conditions for direct condensation of APO and **1**.

Run	Compound 1 [g]	APO [equiv.]	Solvent	Rx temp. [°C]	Rx time [h]	Yield [%]
1	0.49	1.07	EtOH	85	5	-
2	1.00	1.03	EtOH	85	12	-
3	0.99	1.03	DMF	150	72	-
4	0.72	1.03	MeOH	65	5	-
5	0.75	1.03	MeOH	65	24	47[a]
6	0.95	1.03	MeOH	65	72	32[b]
7	0.98	1.03	MeOH	65	72	33[b]
8	3.63	1.03	MeOH	65	72	**86**[b]
9	1.75	1.03	MeOH	65	48	44[b]
10	1.48	1.03	MeOH	65	72	42[b]
11	3.18	1.03	MeOH	60	48	51[b]
12	3.23	1.03	MeOH	60	48	56[b]
13	3.14	1.03	MeOH	60	72	53[b]

a) Rx stopped as rx-setup was not tight and solvent evaporated off

b) Hot filtrated and purified by recrystallization with MeOH

The synthetic pathway for compound **2** was followed based on the synthetic parameters suggested by Yu *et al*.[114] and Gramlich *et al*.[115], both with yields around 49%. The first few reactions runs did not yield any product. Different scales, reaction durations, temperatures and solvents were explored. The solution to this problem was found on run 8 where the product was found in the aqueous phase during extraction. This was not expected because the water phase was checked earlier in run 1 and 2 which gave no yields. By backtracking to stored water phases of run 5-7, more yields were obtained by removal of water.

Longer reaction times combined with exchanging the solvent from EtOH to MeOH led to an improvement in earlier reported yields. Run 8, a relatively large batch turned a yield of 4.48 g, 86% of compound **2** after recrystallization and drying.

A total of 13 experiments were completed at a 0.49 – 3.63 g scale, with yields ranging in the 32-56% range, with one outlier result reaching 86% yield. Designation of chemical shifts for ^{1}H- and ^{13}C-NMR analysis are summarized in Table 5 and Figure 12. All NMR spectra's, IR and MS are given in appendix B.

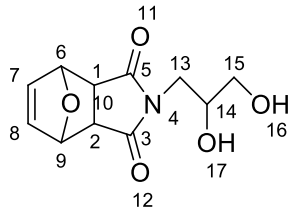

Figure 12. The structure of compound **2** and peak assignment numbering.

NMR

Table 5. Assignment of ^{1}H- and ^{13}C-NMR shifts, coupling constants and multiplicity for compound N (400/100 MHz, DMSO-d_6).

Pos.	δ_H [ppm]	Multiplicity (int., J [Hz])	δ_C [ppm]	COSY	HMBC
1 & 2	2.91-2.95	m (2H)	47.5	-	1, 2, 3, 5, 6, 7, 8, 9
3 & 5	-	-	177.0	-	-
6 & 9	5.13	s (2H)	80.8	7, 8	1, 2, 3, 5, 6, 7, 8, 9
7 & 8	6.55	s (2H)	136.9	6, 9	6, 7, 8, 9
13	3.33-3.35	m (2H)	42.3	14	3, 5, 14, 15
14	3.64-3.71	m (1H)	68.5	13, 15, 17	13, 15
15	3.26-3.28	t (2H, J = 5.4)	64.4	14, 16	13, 14
16	4.56-4.59	t (1H, J = 5.7)	-	15	14,15
17	4.79-4.80	d (1H, J = 5.2)	-	14	13, 14, 15

Chemical shifts for ^{1}H-NMR were in accordance with earlier reported spectra reported for compound **2**.[114,115] The same singlets could be seen at positions 6-9, which were expected to be split by neighboring protons. Besides showing the correct mass for compound **2**, mass spectrometry showed that the furan protection group had fractioned off during MS analysis to show the target compound **3**, cementing the conclusion of the correct mass and structure of this compound.

4.2.3 Retro Diels-Alder de-protection of compound 2

The third and last step of the three-step synthesis of maleimide (**3**), is the de-protection of compound **2** by removing furan through retro Diels-Alder (rDA). To achieve rDA, compound **2** was refluxed at (110°C) for 7 hours in toluene, and the mechanism for this reaction is given in Scheme 20. For de-protection of compound 2, an adaptation of the experimental procedure earlier reported by Yu *et al*.[114] and Gramlich *et al*.[115] was used.

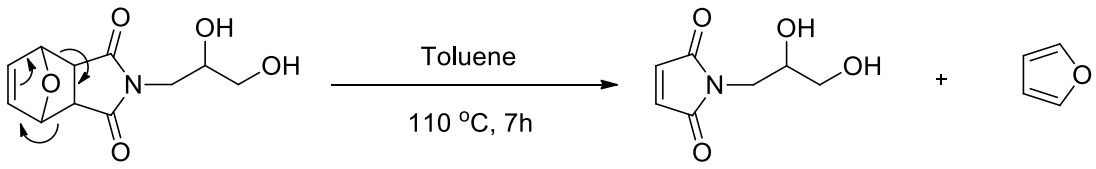

2 **3**

Scheme 20. De-protection of **2** by rDA to yield compound **3**.[35,114]

Table 6. Reactant amounts and conditions for rDA of compound **2**.

Run	Compound 2 [mg]	Rx temp. [°C]	Rx time [h]	Yield [%]
1	470	110	6	32[a]
2	270	110	7	67[b]
3	1000	110	7.5	38[a]
4	543	110	7.5	43[b]
5	1029	110	7.5	37[b]
6	1020	115	5	**89**[b]
7	2300	115	6	11[b]
8	2100	115	6	72[b]

a) Washed with EtOAc

b) Reaction liquid filtered to leave unreacted material

The synthesis of the final maleimide compound proceeded without major issues. In some cases, some of the starting material would not dissolve in the reaction solvent (toluene). Additional pre-heated toluene was added to the reaction to solubilize the remaining material without stopping the reflux. Some of the material remained insoluble, turning to a pink color as the reaction progressed. This was measured to be <1% of the material used, and was separated from the reaction crude, as it would have a minimal impact on the overall yield. For run 1 and 3, the crystallized product was dissolved in EtOAc and filtered, removing the pink residue (insoluble in EtOAc). The EtOAc was evaporated off to

yield maleimide **3**. For the remaining runs (2, 4-8), this separation was simplified by filtrating of the residue right after reaction termination. As the reaction mixture went towards room temperature, crystals instantly started to form, turning the mixture cloudy. Freezing overnight accelerated this process. The final product was subsequently collected through suction filtration and dried overnight under reduced pressure to yield the final maleimide (**3**).

A total of 8 experiments were completed at a 270 mg – 2.30 g scale, with yields ranging from 11 to 89%. Run 6 (giving the highest yield at 89%), was left to react at a slightly higher temperature and 2-hour shorter run time. Earlier reported yields for this, were listed around 80%.[114,115] Designation of chemical shifts for ^{1}H- and ^{13}C-NMR analysis are summarized in Table 7 and Figure 13. All NMR spectra's and IR are given in appendix C.

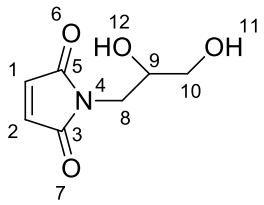

Figure 13. The structure of compound **3** and peak assignment numbering.

NMR

Table 7. Assignment of ^{1}H- and ^{13}C-NMR shifts, coupling constants and multiplicity for compound **3** (400/100 MHz, DMSO-d_6).

Pos.	**δ_H [ppm]**	**Multiplicity (int., J [Hz])**	**δ_C [ppm]**	**COSY**	**HMBC**
1 & 2	7.00	s (2H)	134.5	11	1, 2, 3, 5
3 & 5	-	-	171.2	-	1, 2, 8
8	3.38-3.40	m (2H)	41.2	9	3, 5, 9, 10
9	3.63-3.71	m (1H)	68.4	8, 10, 12	8, 10
10	3.30-3.33	m (2H)	64.1	9, 11	8, 9
11	4.59-4.62	t (1H, J = 6.0)	-	10	9, 10
12	4.82-4.83	d (1H, J = 5.2)	-	9	8, 9, 10

Peak assignment for compound **3** matched with those earlier reported.[114,115] Chemical shifts allocated to position 9 showed three neighboring proton shifts, and the integral showed 1H resulting in its assignment. Further, shifts at position 8 and 10 both had integrals for two protons, and with position 8 only showing 9 in the COSY spectra placed the shifts allocated to position 8 and 10 to their respective places. The shift at 4.59-4.62 ppm showed a triplet placing it in position 11 next to the two protons at position 10. The same reasoning was used for position 12 with a doublet, placing it next to position 9 with one proton. The high shift singlet at 7.00 ppm with two protons placed them next to the carbonyls. COSY and HMBC further cemented the assignment of peaks. One anomaly was detected as the COSY signal for positions 1 and 2 showed the proton at position 11 as a neighbor, although the hydroxyl proton at position 11 showed no signal for 1 and 2.

As suggested by Sheremeteva *et al*.[123], a quick and simple quantitative experiment to test the formation of cyclic imide, is to add KOH, potassium hydroxide to the cyclic imide in an alkaline solution in a 2 to 1 molar ratio. By adding an excess of KOH, the solution quickly turned dark red because of the ring opening of the cyclic imide from the formation of dipotassium salt of the maleimide (see Scheme 21 and Figure 14).

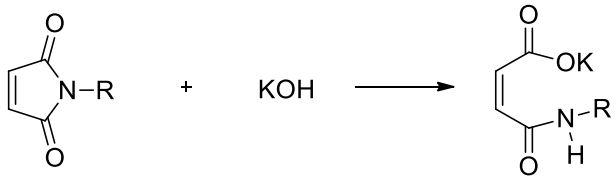

Scheme 21. Ring-opening of cyclic imide.

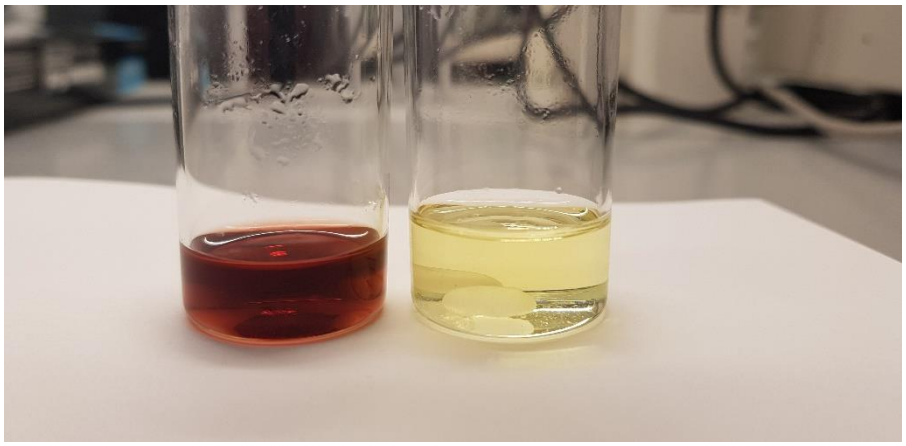

Figure 14. Cyclic Imide and KOH in NaOH (left), KOH in NaOH (right).[123]

4.3 Synthesis of compound **4**

4.3.1 Pyridine catalyzed esterification between acyl chloride and an alcohol

As introduced in section 2.2.1, functional groups can be decorated with malonate groups through a pyridine-catalyzed esterification with ethyl oxopropionates. Furan-3-methanol was used as the component with a hydroxyl-functionality for the esterification. The pyridine catalyzed esterification reaction is given in Scheme 22., and was synthesized in accordance to literature procedures.[124]

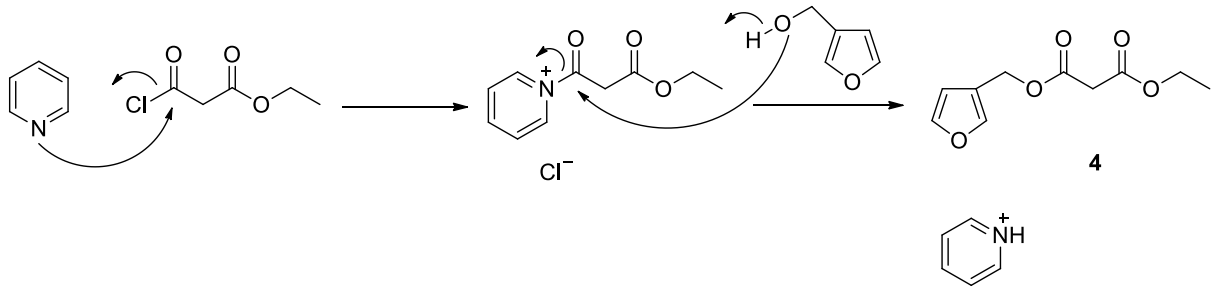

Scheme 22. Pyridine catalysed esterification between Ethyl 3-chloro-3-oxopropionate and Furan-3-methanol to yield compound **4**.[124,125]

All runs were completed with Ethyl 3-chloro-3-oxopropionate and furan-3-methanol in a 1 to 1 ratio with pyridine as catalyst in excess. The first runs for this reaction were tried with reactions times at both 24 hours and 48 hours, with the latter, giving an 84% yield with some impurities. Nevertheless, a run time at 72 hours was concluded to yield a purer product, as well as maintaining high yields. Proton NMR initially showed some impurities, but resolving the product in THF several times resulted in the NMR spectra's given in appendix D. The run purified through washes of THF resulted in a yield at 83%, and further functionalized onto graphene. For TLC analysis, staining with a solution of 5% vanillin in sulfuric acid and MeOH were used. Compound **4** were stored at 4°C as an orange viscous oil. Designation of chemical shifts through ^{1}H- and ^{13}C-NMR analysis are summarized in Table 8 and Figure 15. All NMR spectra's, IR and MS are given in appendix D.

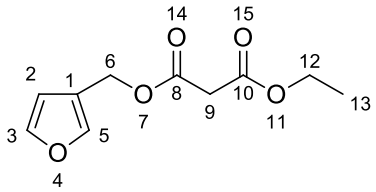

Figure 15. The structure of compound **4** and peak assignment numbering.

NMR

Table 8. Assignment of ^{1}H- and ^{13}C-NMR shifts, coupling constants and multiplicity for compound **4** (400/100 MHz, DMSO-d_6).

Pos.	δ_H [ppm]	Multiplicity (int., J [Hz])	δ_C [ppm]	COSY	HMBC
1	-	-	119.8	-	
2	6.40	d (1H, J = 1.2)	110.4	3	1, 3, 5, 6
3	7.36-7.37	t (1H, J = 2.0)	143.3	2	1, 2, 5
5	7.46	d (1H, J = 0.8)	141.7	-	1, 2, 3
6	5.03	s (2H)	58.5	-	1, 2, 5, 8
8	-	-	166.3	-	
9	3.36	s (2H)	41.4	-	8, 10
10	-	-	166.4	-	
12	4.13-4.18	q (2H, J = 7.2)	61.4	13	10, 13
13	1.20-1.24	t (3H, J = 7.2)	13.9	12	12

Assignment of peaks for compound **4** were quite straightforward for the malonate-structure of the molecule. Both multiplicity, integrals and ^{13}C-NMR helped assigning position 12 and 13, and COSY contributed to that conclusion. The most similar peaks for this elucidation were position 6 and 9, both with similar integrals and multiplicity, as both were CH_2-groups with no neighboring protons. The higher chemical shift (5.03 vs. 3.36 ppm) of position 6 placed it next to the oxygen of the ester, and the 3.36 shift were naturally placed on the carbonyl side of the ester. The shifts allocated to position 3 and 5 were a result of the carbon signals relevant to these proton shifts were slightly higher to the one for the 6.40 shift, placing position 3 and 5 close to the oxygen in the furan. COSY spectra finally placed shifts for position 2 and 3 on the same side, and the shift allocated to position 5 alone on the other side. Lastly, mass spectrometry reported the expected mass for compound **4**.

4.4 Preparation and synthesis of compound **6**

For the preparation of compound **6**, graphite was exfoliated into graphene (**5**), and **5** were subsequently functionalized with the furan-malonate derivative (**4**) via the microwave assisted Bingel reaction. The pathway is shown in the synthesis strategy in Scheme 15 and completed in accordance to literature procedures.[124,126,127] MicroRaman spectroscopy was further used to analyze the quality of exfoliated graphene and malonate hybrid. In the following sections, graphene production, graphene functionalization and microRaman spectra will be discussed.

4.4.1 Solvent assisted exfoliation of graphite powder

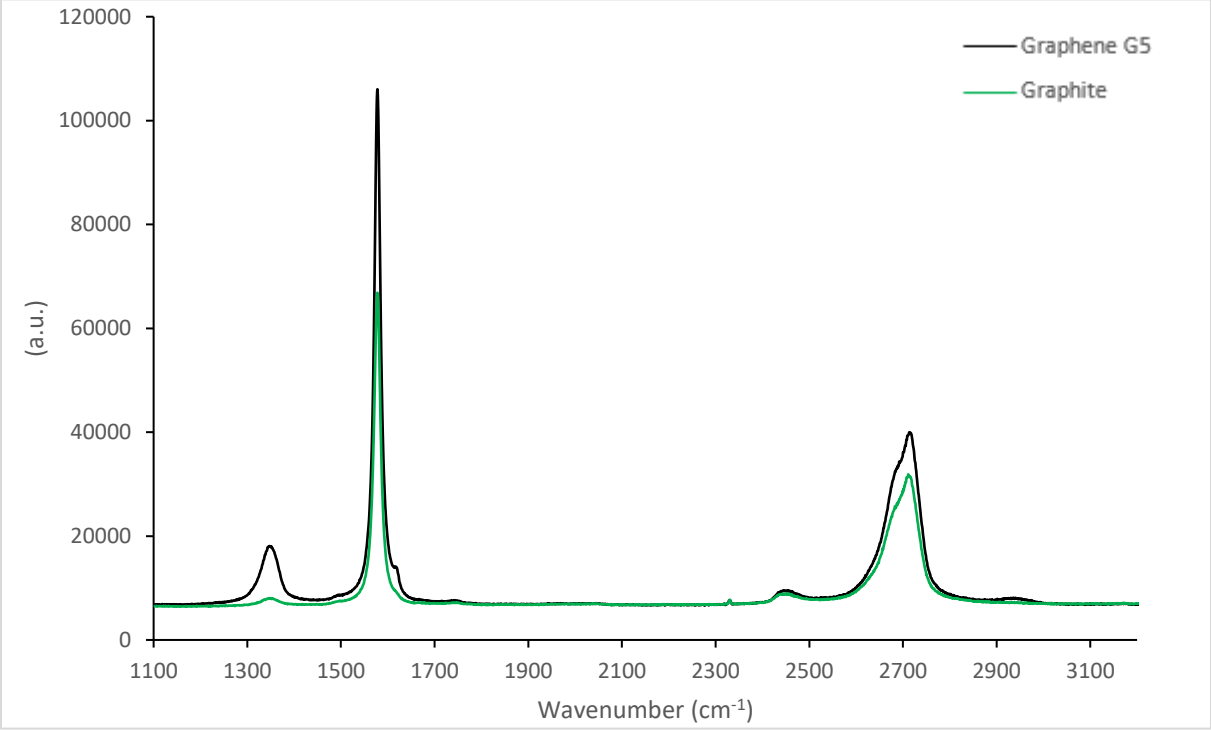

Figure 16. Raman spectra of graphite powder (green) and exfoliated graphene (black)

The standard method as described in the experimental section 6.4, was used to make several batches of exfoliated graphene. At first, centrifugation at 3000 RPM for 2 min was used for removal of bulk graphite after tip sonication, but was later changed to 4000 RPM for 5 min to remove even more non-exfoliated graphite. Graphene runs **G5-G8** seen in appendix I all yielded exfoliated graphene, stable in NMP for long periods. Aggregation and subsequent precipitation occurred after 2-3 weeks. The samples had a D/G ratio ranging from 0.17 to 0.24, and had an opaque black color. The **G5** run yielded the most promising

graphene with a D/G ratio of 0.17, good stability in NMP and a good ability to absorb light. The defect formation indicated by the intensity increase of the D band from graphite to exfoliated graphene, is expected as larger particles are broken down and new edges are introduced from the exfoliation process.

In comparison with the work of Ferrari et al.[107] in Figure 10 in section 2.3, all G' peaks centered around 2670cm^{-1} of exfoliated graphene runs **G1-G8** had a slight shift to the right. This indicates that the graphene yielded is likely few-layered graphene.

4.4.2 [2+1] Cycloaddition of compound **4**

Using an adaptation of earlier reported procedures, the [2+1] cycloaddition of compound **4** onto exfoliated graphene **5** were completed through the MW assisted Bingel reaction.[100,124,127,128] Through altering the amounts of graphene used and output power of the microwave, an optimized procedure was developed for the production of graphene hybrid containing the furan group.

Several Bingel reactions failed to functionalize the graphene with compound **4**. This was a result of not reaching the desired reaction temperatures around 125°C, and was caused by using too much exfoliated graphene and too little power output on the MW. Runs **BG2** and **BG6** were scaled to use 20 mL exfoliated graphene instead of 3 mL previously tested, which resulted in not reaching desired temperatures. For runs **BG1** and **BG8A**, too little power output was used, resulting in failure to functionalize the exfoliated graphene. From testing variations of graphene amounts used and power output, a more stable method was developed and resulted in several promising graphene hybrids, with **BG8B** and **BG5** as the most promising hybrids.

Figure 17 and 18 shows the Raman spectra of graphene hybrids **BG8B** and **BG5** with the exfoliated graphene it originated from respectively. Graphene hybrid **BG8B** has a D/G ratio of 0.50, and the graphene it originated from has a D/G ratio of 0.24. Graphene hybrid **BG5** has a D/G ratio of 0.40, and the graphene it originated from has a D/G ratio of 0.17. Of the 2 graphene hybrids, **BG5** was chosen for further synthesis because it showed better stability in common organic solvents, and better light absorption meaning a higher concentration of graphene hybrid. The exfoliated graphene it originated from also had less defect formation than **G8**.

Another interesting observation from the Raman spectra of **BG8B** and **BG5**, is the change of the G' band shape after the Bingel reaction. The peak which earlier shifted slightly to the right indicating formation of few-layer graphene has shifted to the middle showing band shapes more correlated towards formation of single-layer graphene as reported by Ferrari *et al*.[107] This could be a result of the newly introduced organic molecules to the graphene lattice, further promoting exfoliation of graphene particles. The Raman spectra was acquired after the Bingel reaction mixture was centrifuged again. From this, one can expect that multi-layered graphene was centrifuged off, resulting in fewer-layer graphene hybrids.

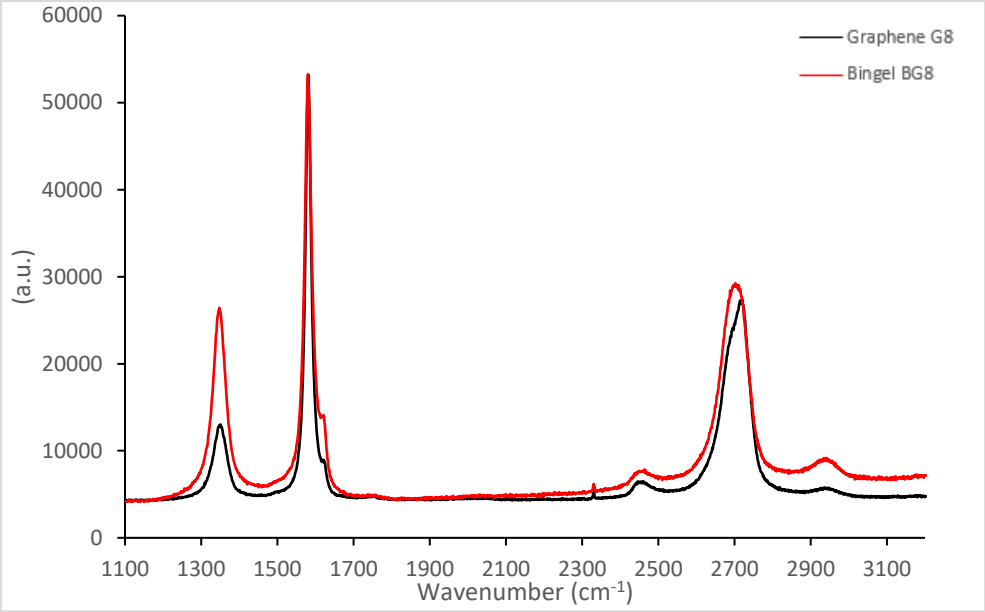

Figure 17. Raman spectra of exfoliated graphene **G8** (black) and Bingel graphene **BG8B** (red).

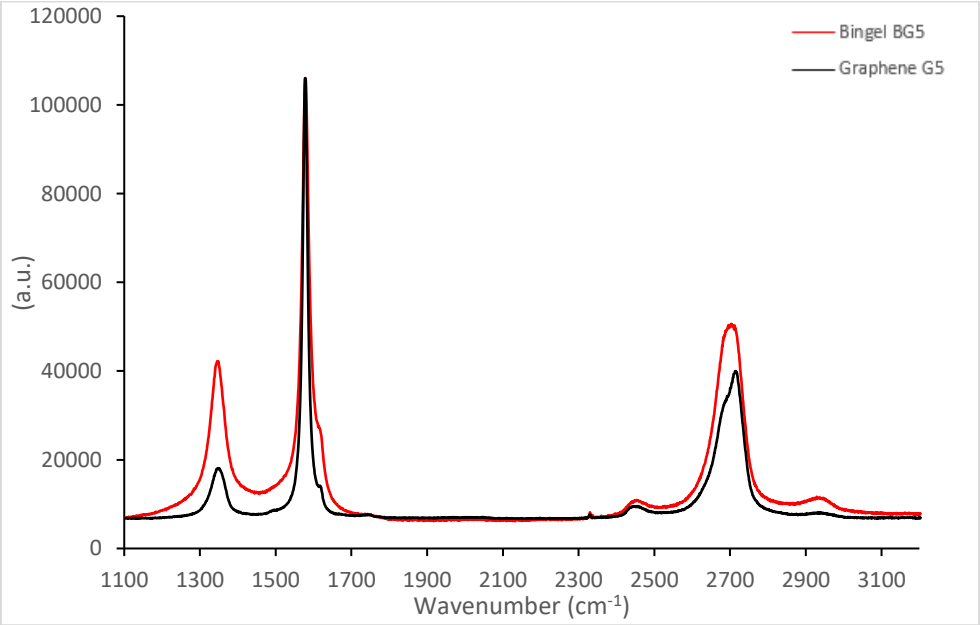

Figure 18. Raman spectra of exfoliated graphene **G5** (black) and Bingel graphene **BG5** (red) further used in film forming for target material **9**.

Figure 19. Exfoliated Graphene in DCM (left), graphene hybrid in DCM (mid), and graphene hybrid in THF (right).

Stability of the exfoliated graphene versus graphene hybrids was also tested using common organic solvents such as DCM and THF. Exfoliated graphene and graphene hybrids were redispersed in DCM as described in experimental section 6.5. DCM is a bad solvent for pristine exfoliated graphene resulting in aggregation and within minutes after dispersion in DCM. In comparison, the graphene hybrids showed great stability in both DCM and THF as seen in Figure 19, further verifying the formation of the hybrid.

4.5 Polyurethane Synthesis

Using an adaptation of the procedure described by Yu *et al*.[114], and Lin *et al*.[16], polyurethane was synthesized both with and without compound **3**. Synthesis of polyurethane without the maleimide compound was mostly to study the progress of polymerization and familiarize ourselves with the reaction without exhausting synthesized maleimide. Procedures for polyurethane synthesis are described in sections 6.7.1 and 6.7.2. Synthesized polyurethanes were analyzed using ^{1}H-NMR, IR and GPC, appendix G and H. The polyol used in this synthesis is difunctional PTMG ($M_n \approx 1000$), the isocyanate used is MDI, and the polyaddition (Scheme 33 in section 6.7.2) was catalyzed by TEA (Et_3N). The mechanism for this TEA catalyzed polyaddition is shown in Scheme 23, following the mechanism suggested by Farka *et al*.[61,63]

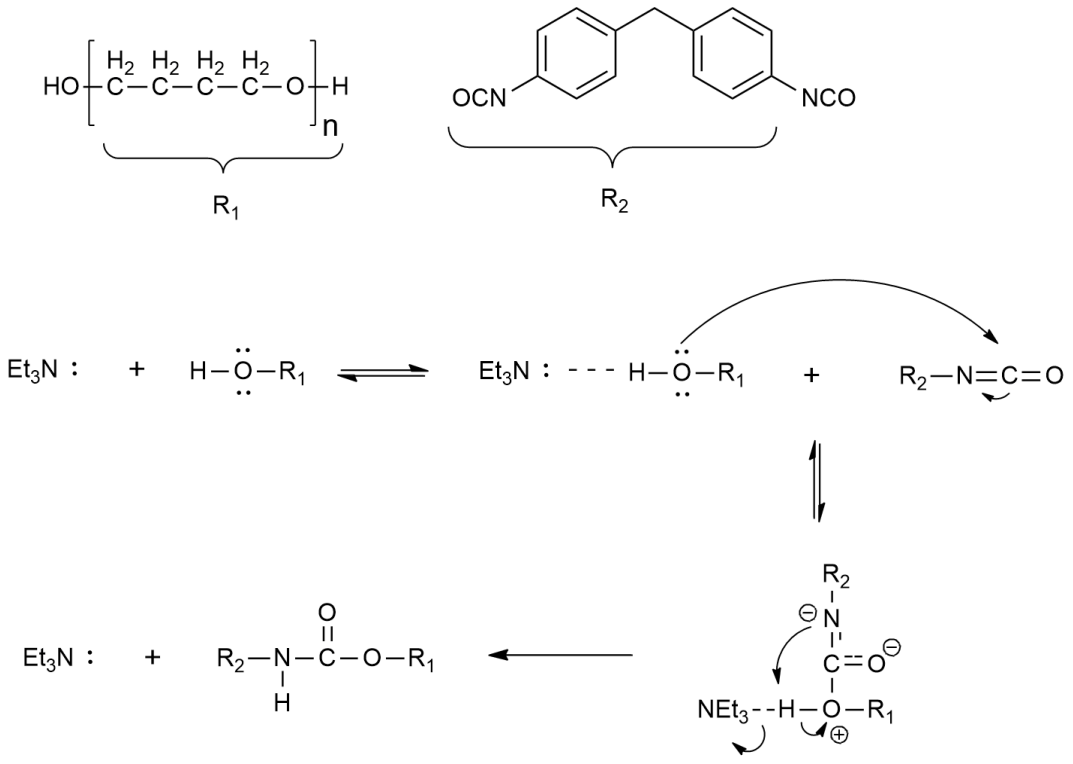

Scheme 23. TEA catalysed Polyurethane synthesis.[61,63,129]

4.5.1 Polyaddition of isocyanate and diol

As mentioned on the previous page, Polyaddition without maleimide were done to study the progress of polymerization and familiarize ourselves with the reaction without exhausting synthesized maleimide. Initial polymerizations were completed with anhydrous DMF at 80 °C. These polymerizations were supposed to react overnight, but were cut short as the polymerization progressed faster than expected. After 30 min reaction time, the whole reaction mixture had turned into a clear gel. Although polymerization was achieved, the polymer would not dissolve in solvents such as $CHCl_3$, DMSO, DMF, THF, rendering it useless for further work. When adding the various solvents, the polymer crude would either swell or shrink. After switching over to toluene as the organic solvent, improved control of the polyaddition was achieved. Furthermore, a solubility table for the polymer was developed to better understand which solvents are useful for precipitation and purification of the polymeric products, and to dissolve the polymers for further use and analysis. From these solubility tests, MeOH was found to be the solvent best suited for precipitation of polyurethane. MDI, PTMG and maleimide (**3**) were all soluble in MeOH, but it would not dissolve the polymer. This led to MeOH being a suitable solvent for purification of polyurethane as all unreacted monomers would stay in solution and polyurethane polymer would precipitate. IR spectra before and after purification shows the effect of precipitation as peaks correlated to unreacted monomers were gone, and in some cases almost gone. From Figure 20, a presence of –NCO groups (2263 cm^{-1}) can be seen showing traces of unreacted isocyanate. The bottom spectrum is acquired after precipitation, and here the isocyanate peak at 2263 cm^{-1} is almost gone. Further, the broad peak at 3289 cm^{-1} shows the formation of the NH group, which is part of the urethane linkage of polyurethane. Peaks centered around 1710 cm^{-1} shows the presence of carbonyls, while strong peaks around 1100 and 1220 cm^{-1} shows the formation of –C-O-C-, which is also a crucial part of the urethane linkage.

GPC data of compound **7** are given in appendix G.

M_w = 104000 g/mol^{-1}, M_n 38000 = g/mol^{-1}, PDI = 2.72.

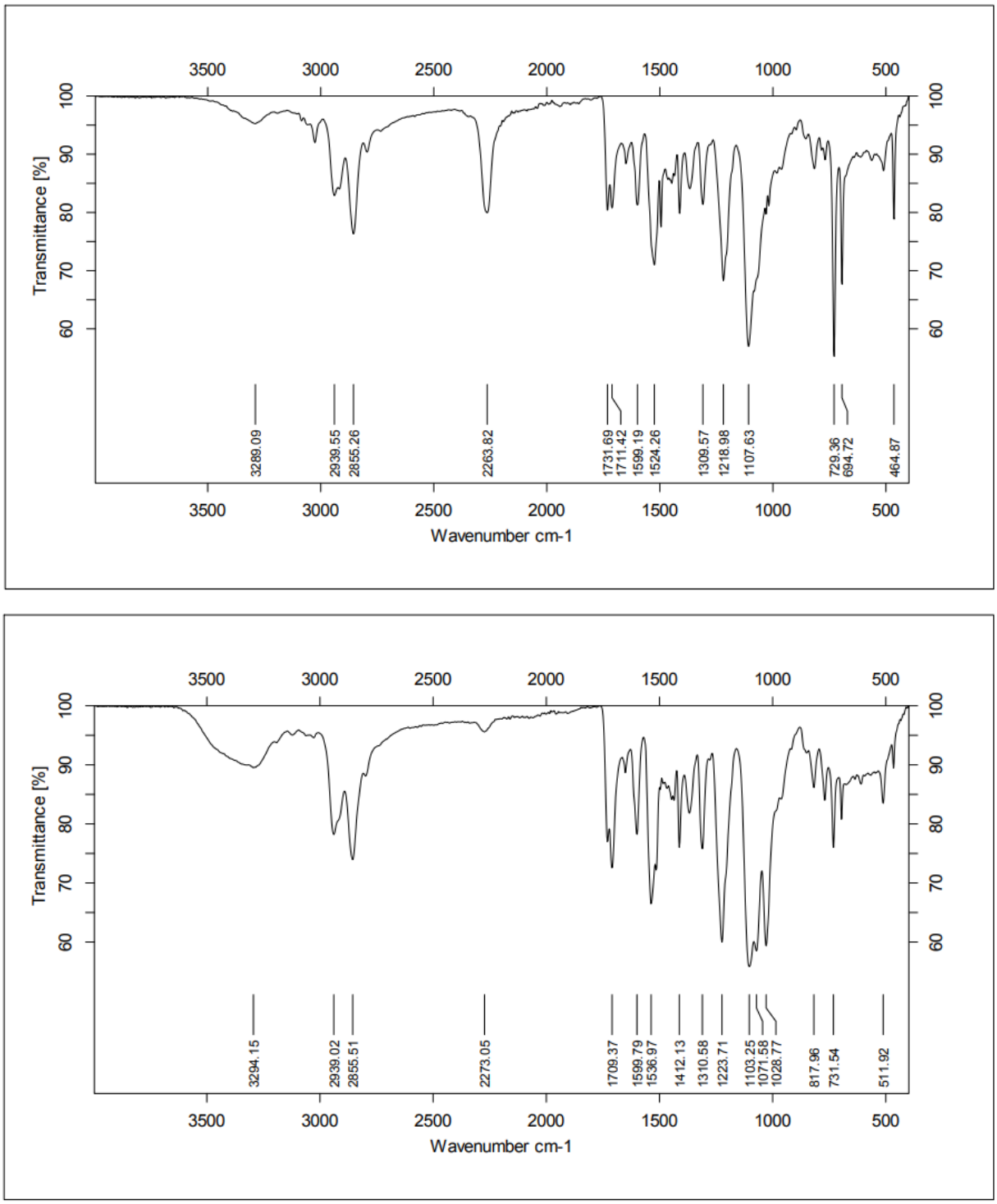

Figure 20. Difference in IR for polyurethane before (top) and after (bottom) precipitation in MeOH. The example shown is a run with maleimide (**3**).

4.5.2 Polyaddition of PTMG and maleimide (**3**) with MDI

The Polyaddition of PTMG and maleimide (**3**) with MDI were initially reacted in toluene as the organic solvent after testing without maleimide. To dissolve maleimide (**3**) in toluene, a temperature way above the reaction temperature of 80 °C was needed. After several runs, there were issues with confirming that maleimide (**3**) had reacted with any isocyanate groups. Both NMR and IR showed no cyclic imide group in the reacted polymer. One theory is that maleimide would precipitate out of solution as the temperature decreased after dissolving it in toluene. In some cases, specs of white powder or crystals would be visible sometime after addition of maleimide (**3**). Because of this, other solvents were explored for the Polyaddition. Earlier used by Yu *et al.*,[114] DMAc proved useful as a reaction solvent as it easily dissolved maleimide. Several runs with the new solvent were completed, and solubility was tested as shown in Table 9. MeOH was able to precipitate the polymer as a dark orange (some cases red) liquid. THF showed adequate polymer solubilizing properties, and was selected for further use. THF solubility was crucial as this is the solvent used for gel permeation chromatography to characterize our polymer products. The parts that were dissolved was analyzed with GPC, and furthermore used for the final mixing with graphene nanohybrid (**6**).

Table 9. Solubility table for all three monomers, polyurethane (**7**) and maleimide polyurethane (**8**).

Solvent	PTMG	MDI	Maleimide (**3**)	PU (**7**)	M-PU (**8**)
$CHCl_3$	++	++	++	++	-
DCM	++	S	+	+	
DMF	++	++	++	++	++
DMSO	-	++	++	++	++
EtOAc	++	-	++	-	-
Et_2O	++	S		P	
EtOH	++	+	++	P	
MeOH	++	+	+++	P	P
THF	++	+++	++	+++	++
Toluene	++	+	+		-

+) Soluble with heat, ++) Soluble, +++) Very Soluble, P) Precipitation, S) Suspension -) Not soluble

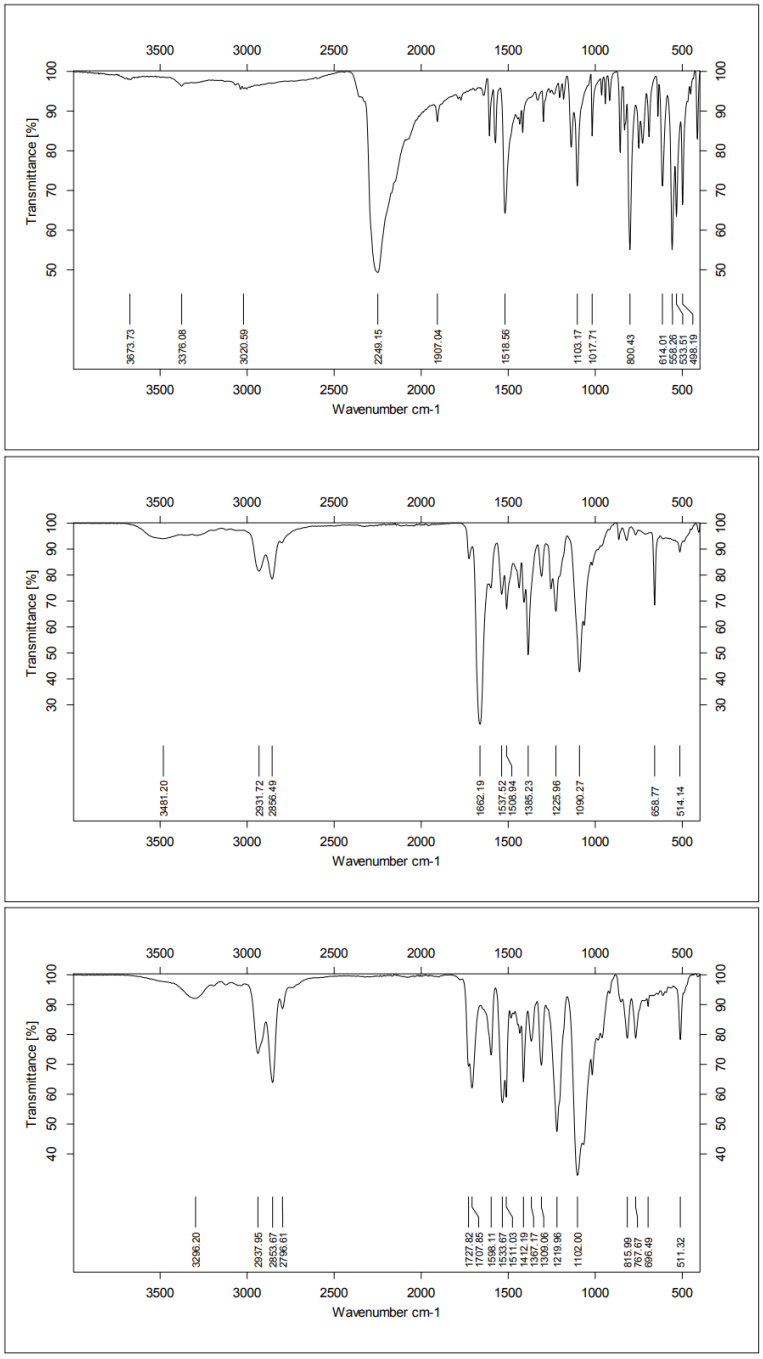

Figure 21. IR spectra of MDI (top), polyurethane (**7**)(mid), and maleimide-polyurethane (**8**)(mid).

From the comparison of IR spectra in Figure 21 and Table 10 there is a visible difference between polyurethane (**7**) and maleimide polyurethane (**8**). This is mostly owed to the change of reaction solvent, molar ratios and the presence of cyclic imide introduced by the maleimide monomer. Symmetric C-N-C stretching vibration at 1367 cm^{-1} is a sign of

successful maleimide functionalization as reported by Engel *et al*.[118] and Hsiao *et al*.[130] Furthermore, the peak at 696 cm^{-1} is due to imide ring deformation. Peaks centered around 1710 cm^{-1} are visible due to symmetric C=O stretching from cyclic imide, but also due to the carbonyls in the formed urethane linkages.

NMR analysis of maleimide polyurethane (**8**) shows chemical shifts for the imide protons (7.21 ppm, s) and a chemical shift (4.01-4.07 ppm, m) for alkyl protons situated on the "bridge" between the two hydroxyls of maleimide (**3**).[114] Two shifts situated along the alkyl chain of the maleimide is missing, but could be overlapping with shifts from the PTMG, as its shifts are much more prominent than maleimide.

Table 10. FTIR characteristics for MDI, polyurethane (**7**) and maleimide polyurethane (**8**)

Functional groups	MDI	PU (**7**)	M-PU (**8**)
N-H	-	3481	3296
C=O	~1600	1662	1707
C=C	1518	1537	1511
C-N	1600	~1600	1598
N=C=O	2249	-	-
C-O-C	-	1225/1095	1102
Imide C-N	-	-	1367
Imide ring	-	-	696

GPC data of compound **8** are given in appendix H.

GPC-data: M_w = 27300 g/mol^{-1}, M_n = 7030 g/mol^{-1}, PDI = 3.88

4.6 Preparation and casting of nanohybrid polymer film

The amount of functionalized grapehene (**6**) used for the final graphene-polyurethane hybrid are approximated amounts as precise amounts of graphene requires intricate instrumentation since these are well-below µg scale quantities. TGA experiments are needed in order to estimate actual quatnitites of graphene hybrid used. TGA is not available in our facilites, and due to time constraints, only RAMAN was used for the spectroscopic verification. Dispersibility in common organic solvents provided facile experimental verification for the formation of the hybrid.

Assisted by a bath sonication for 5 seconds, the graphene was redispersed in THF to make an uniform dispersion. From this, one can conclude that different volumes of graphene dispersed in THF will have the same concentration if split before aggregation of graphene occurs. From this, four different concentrations of graphene dispersion were made with volumes given in Table 11. As the equivalents of redispersed graphene varied from 1 to 3, there was possible to make a study to compare the impact of the different amounts used. Figure 22 shows how the different amounts of graphene acted right after adding it to the polymer solution. All samples were once again bath sonicated to evenly distribute the graphene hybrid, making all the vials have a variation of grey color similar to **9D** in the bottom picture of Figure 22.

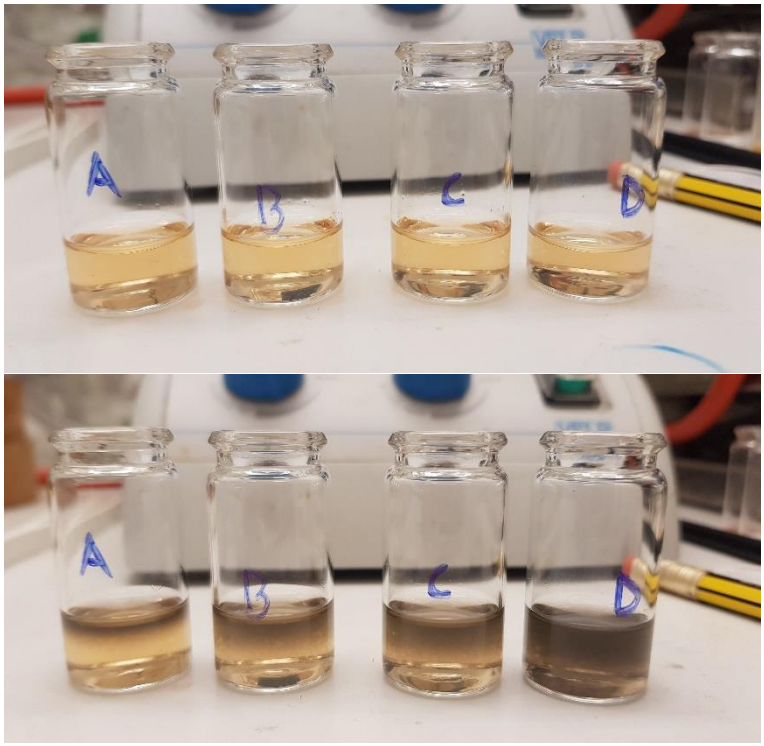

Figure 22. Solution of pristine maleimide polyurethane (**8**) in THF (top), graphene hybrid (**6**) in THF added to the polymer (bottom).

Table 11. Parameters for nanohybrid polymer **9A-9D**. Compound **8** solved in THF and compound **6** redispersed in THF.

Nanohybrid Polymer	Maleimide polyurethane (**8**)	Graphene hybrid (**6**)
9A	2 mL	0.2 mL
9B	2 mL	0.3 mL
9C	2 mL	0.4 mL
9D	2 mL	0.6 mL

Two sets of each solution of compound **6** and compound **8** were further dropcasted onto Si wafers situated on a hot plate at 60 °C. Film forming happened almost instantaneously as drops were applied to the wafers. An extra film were casted without graphene to study the differences in film forming for linear polyurethane vs. graphene crosslinked polyurethane via furan maleimide linkage. The films casted with graphene hybrid (**6**) had noticeable faster film forming, plus initiating film forming on the test vial edges. Each of the films were cut evenly with a surgical knife after films had hardened. One of the sets was subsequently heated at 160 °C overnight to initiate the rDA, initiating the cycloreversion of maleimide and furan. The temperature was then lowered to around 60 °C for 2 hours to allow for the furan and maleimide to once again react through DA to self-heal the cut films. The rDA cycloreversion of furan and maleimide does not take place below temperatures of 125 °C.[29] From this, two comparable set of films casted onto wafers, one with cuts, and one set further heat treated to allow for new bonds to form in damaged areas. Heating of polyurethane also facilitate the self-healing process as the mobility of the polymer chains increases.[14]

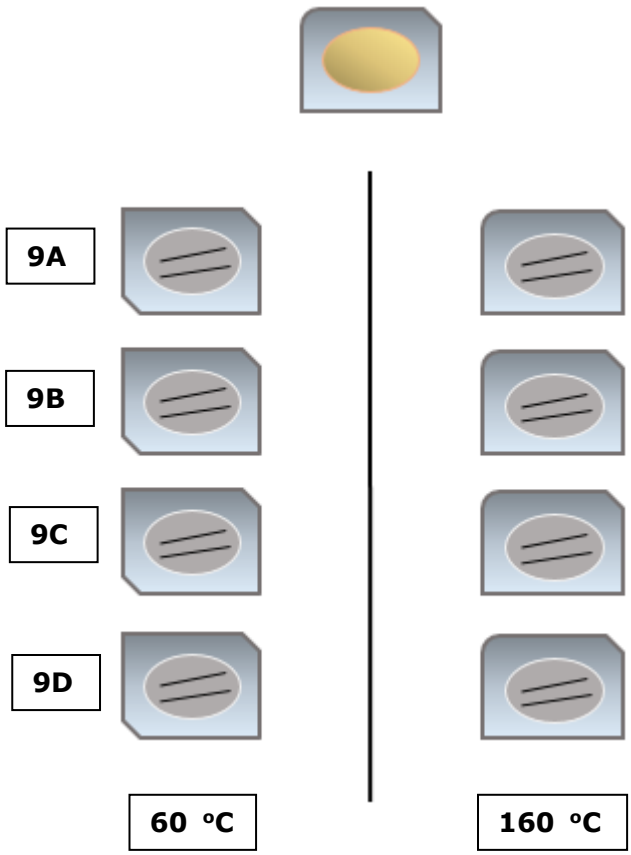

Figure 23. Target material **9A-9D** drop casted onto cleaned Si wafers. The single Si Wafer on top was maleimide polyurethane (**8**) drop casted without graphene hybrid (**6**).

Figure 23 above is simply used as an overview of the film casting. The gradient plates are the Si wafers, the grey circles are graphene crosslinked polyurethane, the yellow circle is the blank sample without graphene, and the black lines indicates inflicted cuts onto the polymeric films.

From SEM imaging, a difference was evident between the cut films and those who were heat-treated. Furthermore, a trend in the amount of graphene used had a visible impact one the self-healing process, cementing the conclusion that self-healing had happened. From the pictures in Figures 24-31, an increase in self-healing is visible as more graphene is used in the polyurethane-graphene composite. Pictures from each sample 9A-D are presented over the next four pages in the order from A to D with an increase in self-healing. First, pictures of the cut film without heat treatment for cycloreversion is showed, followed by those who were heated to initiate the rDA cycloreversion. For each Si wafer, an overview picture in the magnification range x100-x200 is shown. As self-healing increased, a focal point were hard to achieve using the SEM, as edges functioned as a way to find focus when acquiring pictures in the magnification range x1768-x2500.

SEM imaging of compound 9A

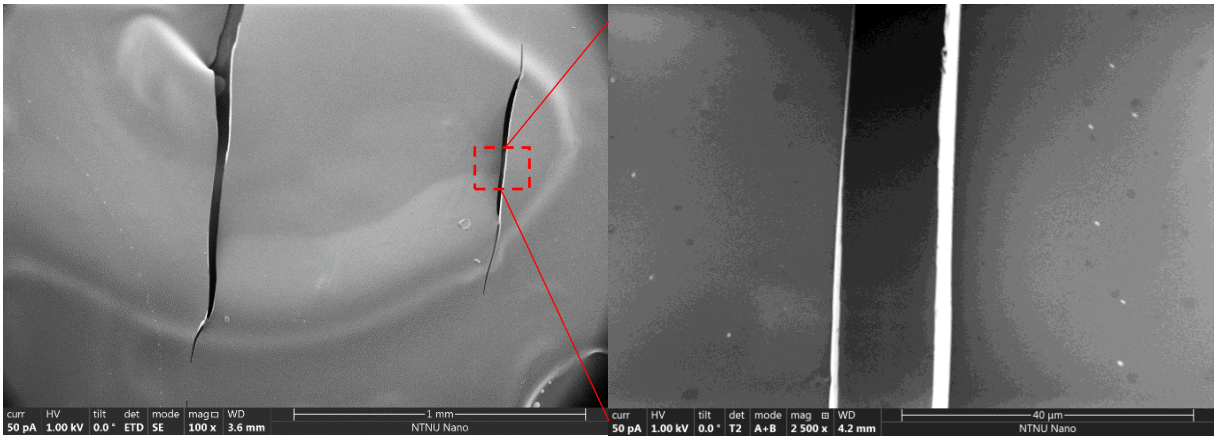

Figure 24. Sample **9A** not heat-treated.

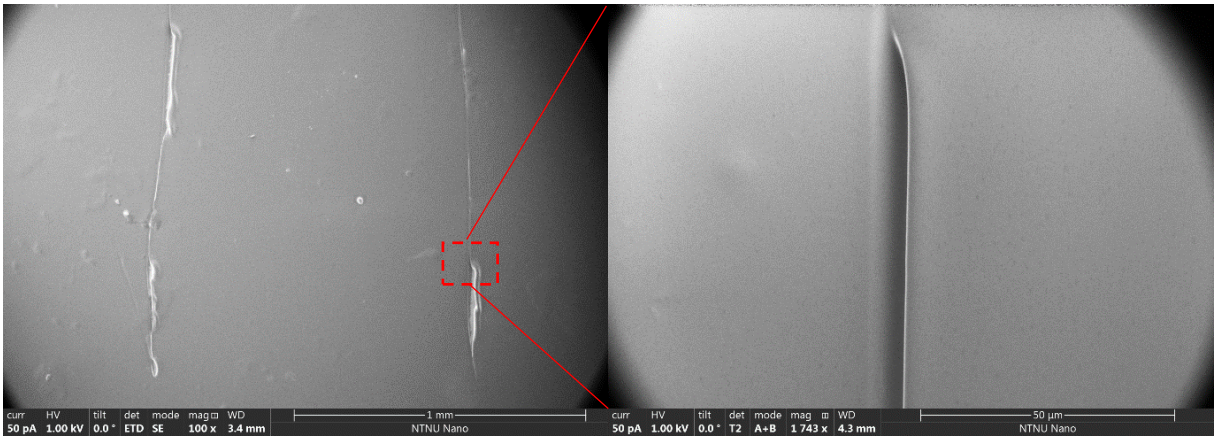

Figure 25. Sample **9A** Heat-treated to facilitate self-healing.

Sample **9A** with 2.0 mL graphene hybrid showed good signs of self-healing as the topography of the film was scanned. Some places had not achieved self-healing, often near the edges of the applied cuts as seen in Figure 25 (right). The width of the cuts were measured to vary from 15 to 50 µm, and it is expected that some places are too wide to self-heal. The heat applied for rDA also helps with the mobility of the polymer chains, so the furan and maleimide pendants can reach each other to form new covalent bonds.

SEM imaging of compound 9B

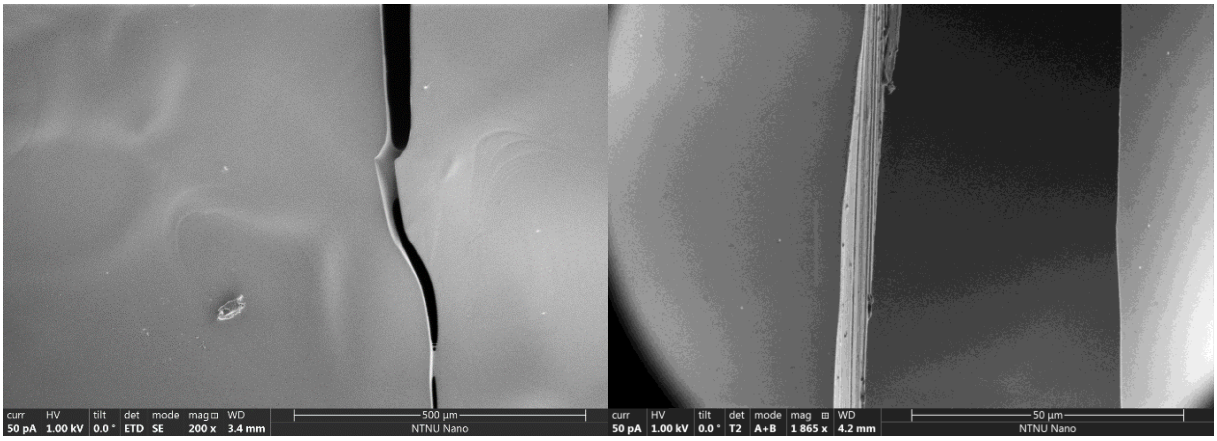

Figure 26. Sample **9B** not heat-treated.

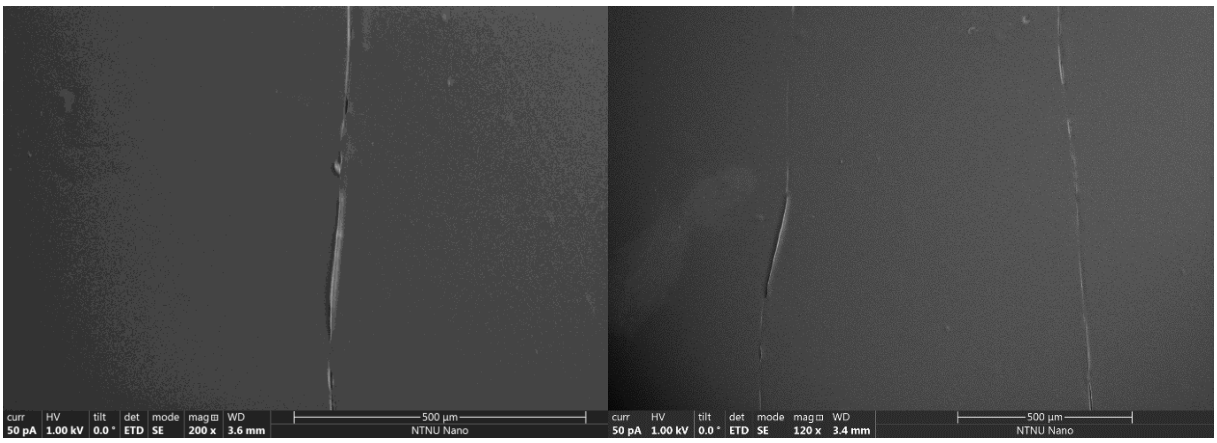

Figure 27. Sample **9B** Heat-treated to facilitate self-healing.

Sample **9B** with 3.0 mL graphene hybrid also showed signs of self-healing of the film heated at 160 °C overnight. The right picture in Figure 27 shows one cut that has self-healed on the right side, while the cut to the left still shows some damage to the film. The left picture (Figure 27) also shows some cuts that most likely have been too wide, but still has achieved some self-healing nonetheless.

SEM imaging of compound 9C

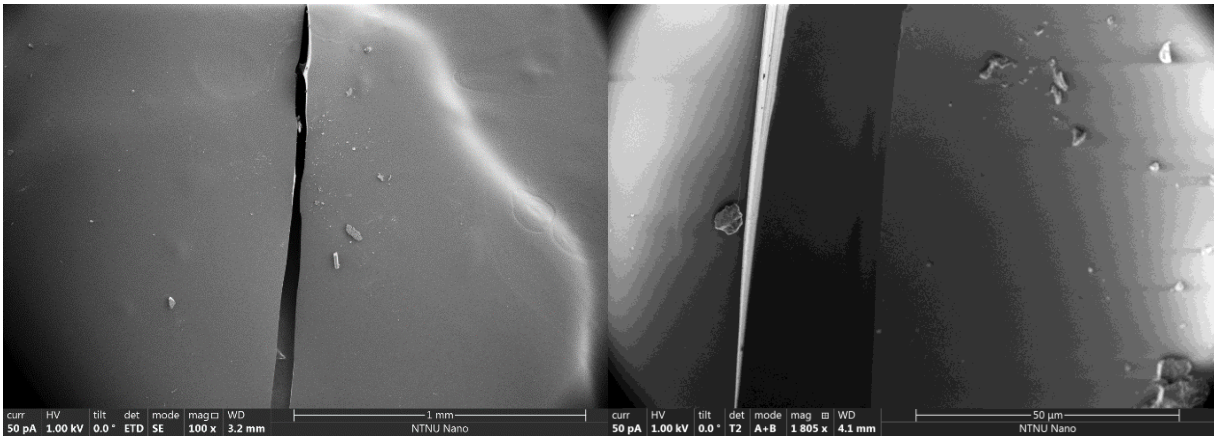

Figure 28. Sample **9C** not heat-treated.

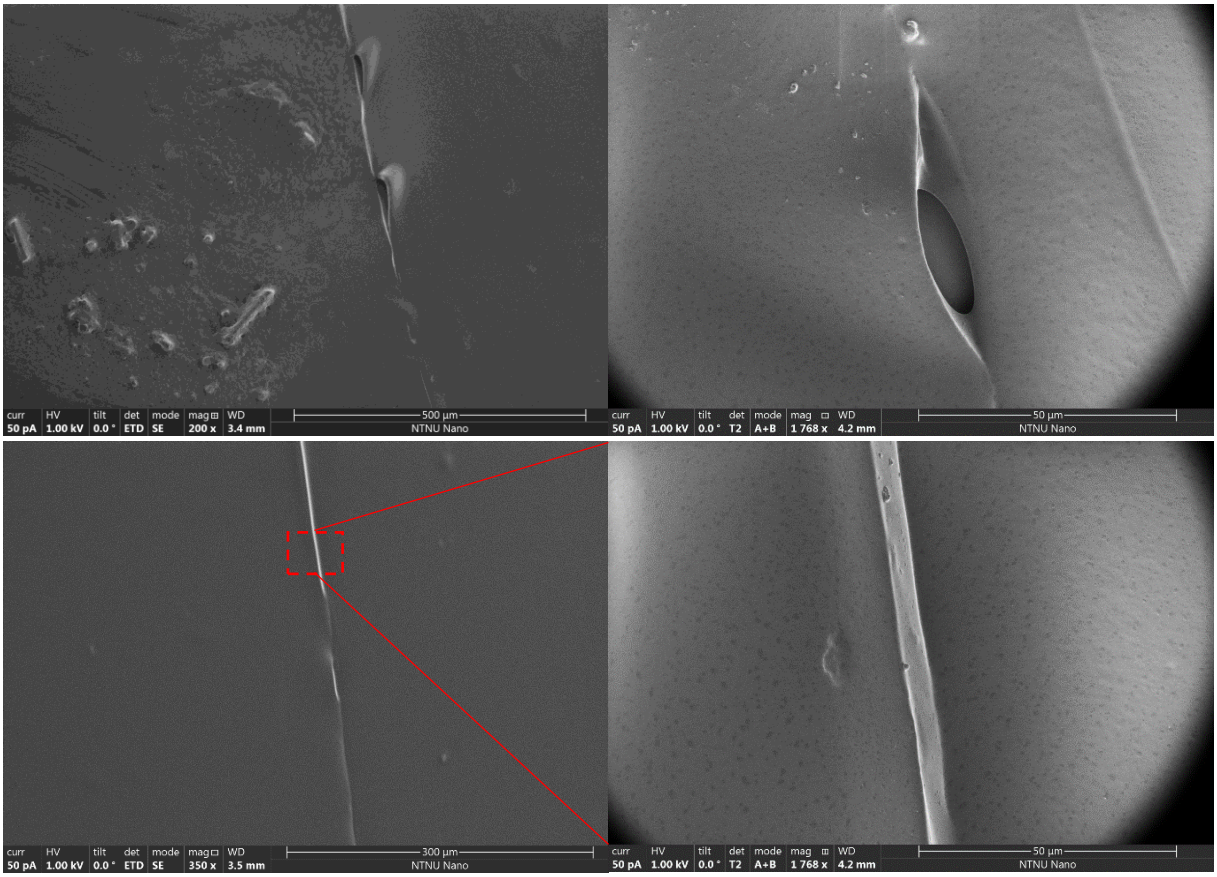

Figure 29. Sample **9C** Heat-treated to facilitate self-healing.

Sample **9C** with 4.0 mL graphene hybrid showed that increasingly more self-healing of the polymer film, and the cuts ranged from 10 to 50 µm. Some places showed traces of earlier cuts, while some small "pockets" were not healed, most likely due to the width of the cut being too wide. From the upper right picture in Figure 29, the T2 mode of SEM allowed for observation of the topography of the non-healed part showing the depth of the polymer film.

SEM imaging of compound 9D

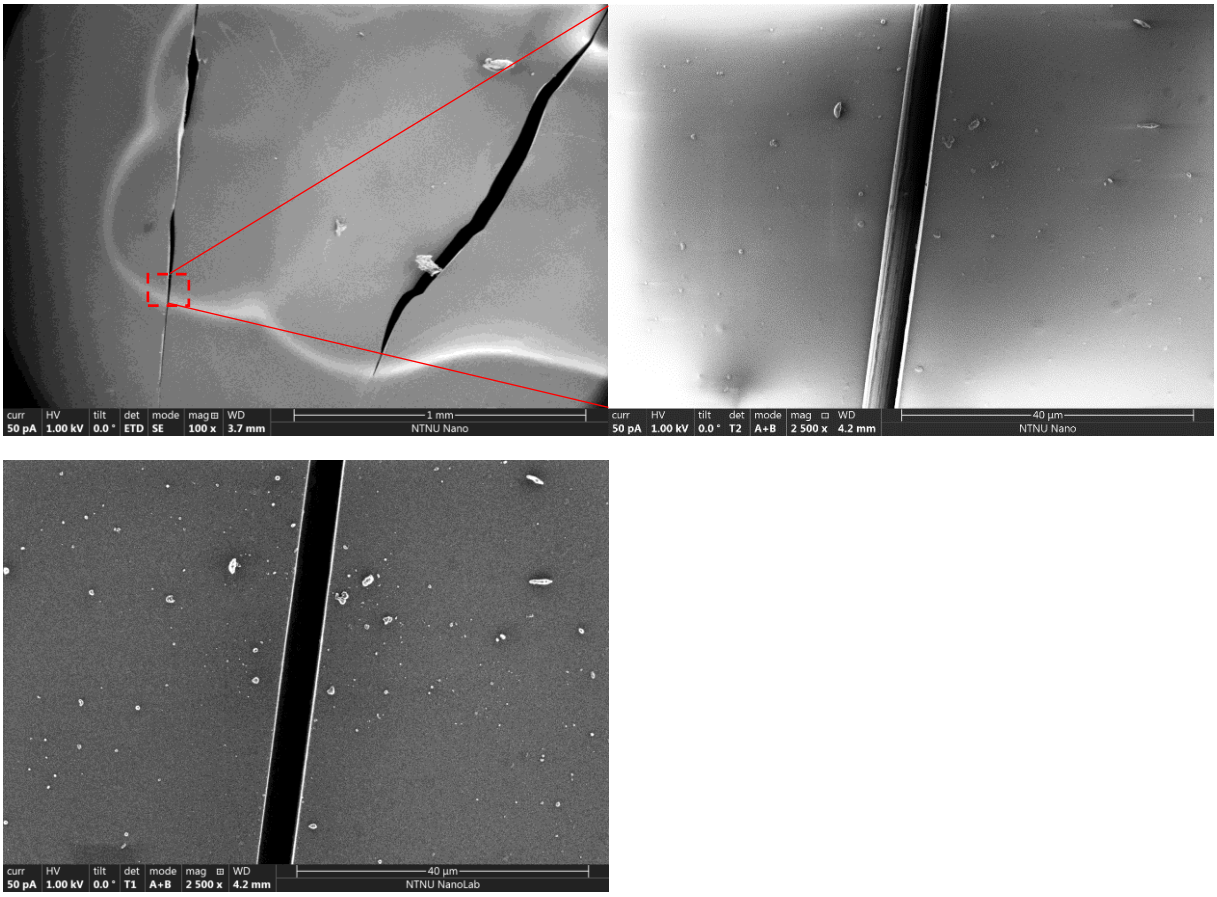

Figure 30. Sample **9D** not heat-treated.

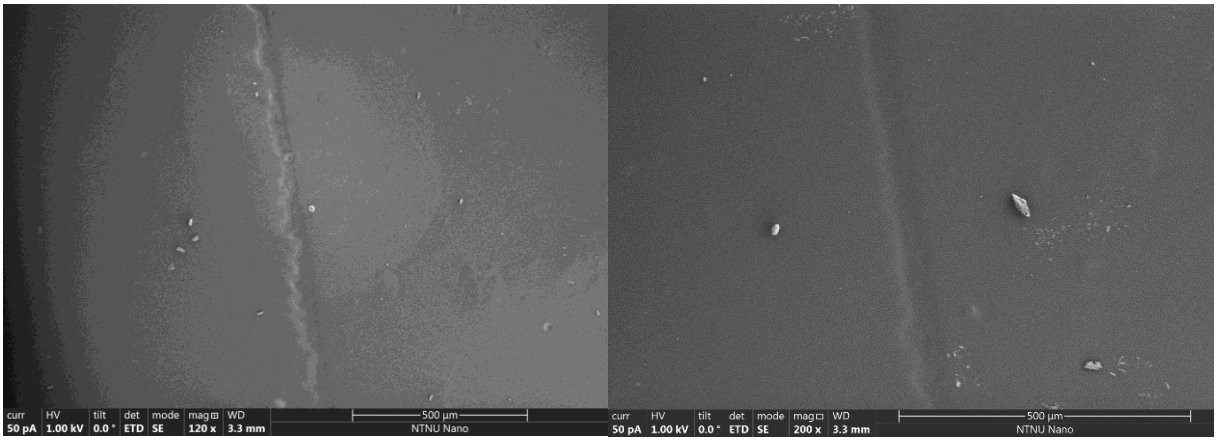

Figure 31. Sample **9D** Heat-treated to facilitate self-healing.

Sample **9D** with 6.0 mL graphene hybrid showed that full self-healing was achieved, and only traces of the original cuts were visible. The trend of increased healing following the increase of added graphene hybrid also contribute to the conclusion that self-healing was realized. Because of the self-healing, there was not possible to find any closer focal points in Figure 31 for close up imaging with magnification up to x2500.

5 Conclusion and further work

A multistep synthesis for a graphene-crosslinked polyurethane with self-healing capabilities were planned and developed as shown in Scheme 15 in section 4.1. The key mechanism for this thesis is the thermoreversible Diels-Alder reaction between a diene (furan) and a dienophile (maleimide) as shown in Scheme 24.

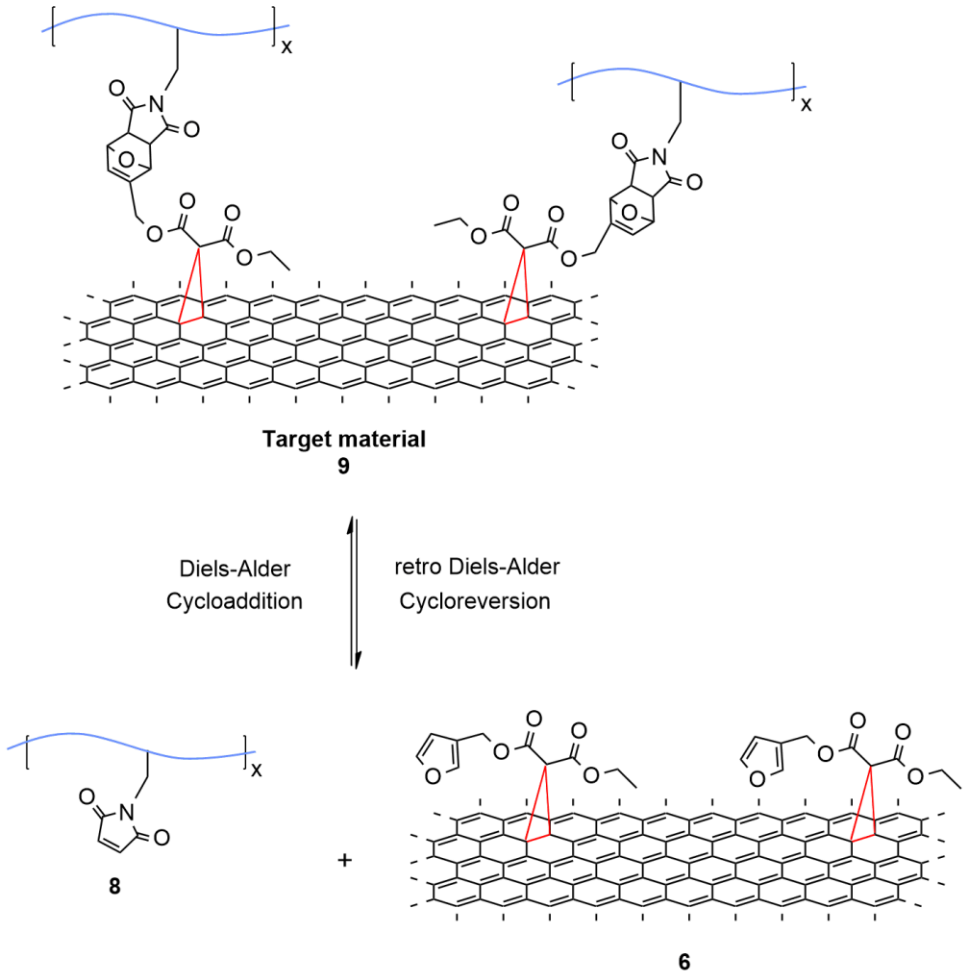

Scheme 24. Diels-Alder/retro Diels-Alder of graphene hybrid **6** and maleimide polyurethane **8** to yield target material **9**.

The overall synthesis were carried out in 2 main parts. The first part consisted of pyridine catalysed esterification between Ethyl 3-chloro-3-oxopropionate and Furan-3-methanol to yield compound **4**, which was further functionalized onto exfoliated graphene via the MW assisted Bingel reaction. The other part consisted of a 3-step synthesis to yield a maleimide equipped with two hydroxyl groups for further Polyaddition into a polyurethane with MDI and PTMG resulting in maleimide polyurethane **8**. Finally, the graphene hybrid **6** and the maleimide polyurethane **8** were mixed together for film forming of the novel target material

9A-D. Cuts were applied to each of the films, and they were heated to reach the temperatures for retro Diels-Alder, making it possible to form new bonds and self-heal the damaged polymer films. Self-healing of the target material was confirmed through SEM imaging, with an increase in self-healing ability correlated to the amount of graphene hybrid utilized.

Pyridine catalysed esterification between Ethyl 3-chloro-3-oxopropionate and Furan-3-methanol afforded compound **4** with the purest run yielding 83 %. Several parameters were tested for exfoliation of graphene, and further functionalization via Bingel reaction to successfully yield a novel nanohybrid **6**. This nanohybrid was confirmed through microRaman characterization, and dispersibility in common organic solvents were tested as experimental verification.

Diels Alder reaction of maleic anhydride and furan afforded compound **1** in yields ranging from 15-58%. The biggest margin of error was unreacted maleic anhydride precipitating during the reaction process. Further, compound **2** was prepared through direct condensation of **1** with APO resulting in yields ranging from 32-86%. The maleimide monomer **3** was prepared by rDA of **2**, resulting in yields ranging from 11-89%. Overall yield for the 3-step synthesis of maleimide **3** was 44.4%. Maleimide **3** was further functionalized into a TEA catalyzed Polyaddition with MDI and PTMG (M_n = 1000) to yield maleimide polyurethane **8**.

Further work of this thesis should include optimization work for some of the synthetic pathways. By achieving better control of the synthesis of compound **1**, the overall yield for synthesis of maleimide **3** could be improved. Both the second and third step of this synthesis were improved through this master thesis, making the overall yield an acceptable result compared to earlier reported results.[114,115]

Although the study of polyurethane polymerization consisted of 20-25 reactions, more catalysts and different reaction setups could be explored to better understand the implementation of the maleimide monomer. Exploring other types of polyols and isocyanates would also be a focus to study the change in properties of polyurethane.

Further work would also include TGA analysis of graphene hybrids to better estimate the quantities of graphene hybrid acquired. This to better control the amounts of graphene hybrid when preparing the target material. Additional characterization of the polymer films to include conductivity (or the incorporation of the maleimide functional group to other semiconducting polymers) should also be explored as this would open up new application pathways for the material.

6 Experimental

6.1 General

All reagents used in this thesis were purchased from Merck and were used without further purification, unless otherwise stated. NorFab, NTNU NanoLab, provided Si wafers used for final graphene-polyurethane film forming experiments. Dry solvents were collected from an MBraun SPS-800 solvent purifier. TLC was performed with Merck silica gel 60 F254 plates with 254 and 312 nm UV detection or staining with 5% vanillin in sulfuric acid and MeOH.

All graphene liquid exfoliation experiments were performed using a SONOPULS HD2070 tip sonicator. Microwave assisted Bingel reaction was performed using Biotage Initiator microwave synthesizer. Exfoliated graphene and Bingel graphene were centrifuged using a Heraeus labofuge 200 (4000 rpm, t = 5 mins).

NMR spectra were acquired using a Bruker DPX 400 MHz Avance III HD NMR spectrometer, and generated spectra were further developed using Topspin 3.6.2 software.

GPC was performed on an Agilent 1260 Infinity II instrument with THF as eluent at 1.0 mL/min flow rate with 15 minutes run length. Recorded wavelengths were 650 nm. Agilent GPC/SEC software was used for data analysis. An Agilent PLgel MIXED-C (300 x 7.5mm) column with 5.0 µm pore size was used for all analyses. Standards for column calibration was prepared using Agilent EasiCalA/EasiCalB, polystyrene standards.

Accurate mass determination in positive and negative mode was performed on a "Synapt G2-S" Q-TOF instrument from Waters. Samples were ionized by the use of ASAP probe (APCI) or ESI probe. No chromatographic separation was used previous to the mass analysis. Calculated exact mass and spectra processing was done by Waters Software Masslynx V4.1 SCN871. Acquisition of IR spectra's were recorded using the attenuated total reflection technique (ATR) on an FTIR Thermo Nicolet Nexus FTIR Spectrometer with a Smart Endurance reflection cell. Peaks are reported in cm^{-1}.

Graphite used in this thesis Sigma Aldrich: 99% carbon basis, - 325 mesh particle size (>99%), graphite grade 230U, Lot # MKBX6591V

Raman Renishaw InVia Reflex Spectrometer System was used for Raman spectra collection with a 532 nm laser excitation at 5% power output. Spectrum processing was performed using the WiRE software.

6.2 Synthesis of maleimide pendant

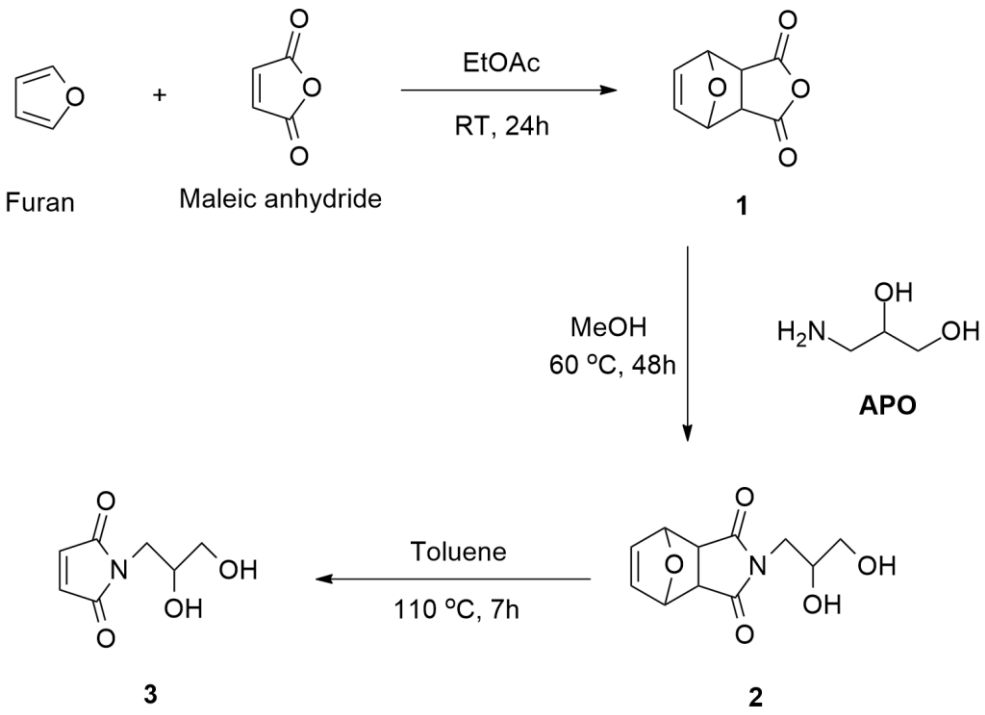

Scheme 25. **3** is synthesized from maleic anhydride and 3-amino-1,2-propanediol through a three-step synthesis.[114]

The synthesis of the maleimide pendant was carried out in three steps as shown in Scheme 25. The first step is a Diels-Alder cycloaddition of furan to protect the carbon-carbon double bond on the cyclic anhydride. Next, the conversion of cyclic anhydride to a cyclic imide is preformed through direct condensation by nucleophilic attack from a primary amine. Lastly, the protective group is removed by retro Diels-Alder, yielding our maleimide monomer and furan as a bi product. This is completed by refluxing **2** in toluene. The procedure of each step is explained in the following sections.

6.2.1 Synthesis of 3a,4,7,7a-tetrahydro-4,7-epoxyisobenzofuran-1,3-dione, compound **1**[114]

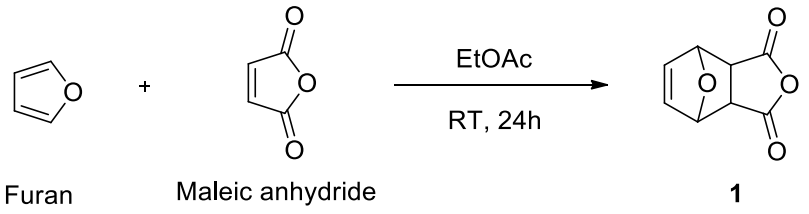

Scheme 26. **1** is synthesized from furan and maleic anhydride

To an oven dried round bottom flask filled with N_2, furan (6.334 g, 93 mmol) was added to a solution of maleic anhydride (9.125 g, 93.0 mmol) in EtOAc (80 mL). The mixture was stirred at room temperature for 24 hours. After stirring, the reaction mixture was placed at room temperature overnight to allow for the formation of colorless crystals. The crystals were removed via suction filtration and dried under reduced pressure overnight, resulting in a total of 8.96 g (54 mmol, 58.06 %) of white crystals. The product was used in the next synthesis step without further purification. Spectroscopic data of **1**: ^{1}H-NMR (400 MHz, DMSO-d_6) δ (ppm): 6.58 (s, 2H), 5.35 (s, 2H), 3.31 (s, 2H). ^{13}C-NMR (100 MHz, DMSO-d_6): 49.1, 81.6, 136.8, 171.5. IR (neat, cm^{-1}) v: 1857 (m), 1779 (s), 1210 (s), 1083 (s), 1018 (s), 920 (s), 877 (s), 848 (s).

^{1}H-NMR were in accordance with previously reported literature.[114] ^{1}H-NMR, ^{13}C-NMR and IR data are given in appendix A.

6.2.2 Synthesis of 2-(2,3-dihydroxypropyl)-3a,4,7,7a-tetrahydro-1H-4,7-epoxyisoindole-1,3(2H)-dione, compound **2**[114]

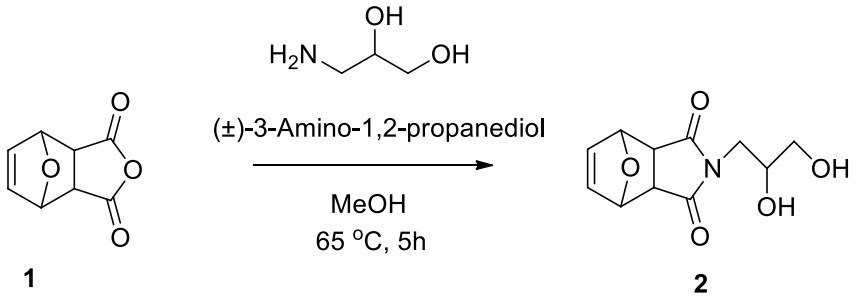

Scheme 27. **2** Synthesized through direct condensation between compound **1** and APO

Using an adaption of a procedure described by Yu *et al.*,[114] compound **1** (3.63g, 21.8 mmol) and APO (2.03 g, 22.2 mmol) and MeOH (140 mL) were added to an oven dried and evacuated round bottom flask with a magnetic stirrer. APO were used in a 1.03 molar excess to furan-A. The reaction mixture was refluxed at 60°C for 48 hours under N_2 purging. Subsequently, the colorless reaction mixture was concentrated to approximately half its original volume. DCM (100mL) and distilled water (100mL) were added to the crude, resulting in an emulsion leading to a phase separation. The organic phase was extracted with distilled water (3x70 mL) and the water phase was washed with DCM (3x70 mL). The combined water phases were concentrated under reduced pressure to form white crystals further treated through hot filtration using MeOH (60mL). Next, the filtrate was cooled in freezer overnight to yield white crystals followed by drying under reduced pressure for 20 hours, resulting in a total of 4.48 g (18.74 mmol, 85.96 %) of compound **2**. Spectroscopic data of **2**: ^{1}H-NMR (400 MHz, DMSO-d_6) δ (ppm): 2.91-2.95 (m, 2H), 3.26-3.28 (t, J = 5.4, 2H), 3.33-3.35 (m, 2H), 3.64-3.71 (m, 1H), 4.56-4.59 (t, J = 5.7, 1H), 4.79-4.80 (d, J = 5.2, 1H), 5.13 (s, 2H), 6.55 (s, 2H). ^{13}C-NMR (100 MHz, DMSO-d_6): 42.3, 47.5, 64.4, 68.5, 136.9, 177.0. IR (neat, cm^{-1}) v: 3390 (br. m), 2998 (w), 2932 (w), 1772 (w), 1681 (br. s), 1401 (s), 1337 (s), 1186 (m), 1117 (m), 1018 (m), 1000 (m), 851 (s), 602 (s). HRMS (TOF MS ES+): *m/z* calcd. For $C_{11}H_{13}NO_5Na$: $[M+Na]^+$: 262.0691, found: 262.0695.

^{1}H-NMR were in accordance with previously reported literature.[114] ^{1}H-NMR, ^{13}C-NMR, IR and HRMS data of compound **2** are given in appendix B.

6.2.3 Synthesis of 1-(2,3-dihydroxypropyl)-1H-pyrrole-2,5-dione, compound **3**[114]

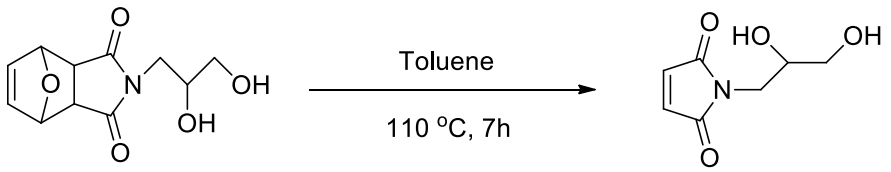

2 **3**

Scheme 28. **3** is synthesized from compound **2** through retro Diels-Alder

Compound **2** (1.02 g, 4.26 mmol) and toluene (80 mL) were added to an oven dried and evacuated round bottom flask with a magnetic stirrer. The solution was purged with N_2 as the solution was refluxed at 110°C for 7 hours. By lowering the temperature to room temperature, the reaction was terminated. After reaction stop, pink residue was visible at the bottom of the reactor vessel, and were removed by filtration. As the reaction mixture cooled down towards room temperature, white crystals started to form, further accelerated by cooling of the mixture overnight at -18°C. The crystals were removed by suction filtration and dried under reduced pressure overnight, resulting in a total of 0.65 g (3.79 mmol, 88.8 %) of compound **3**. Spectroscopic data of **3**: ^{1}H-NMR (400 MHz, DMSO-d_6) δ (ppm): 3.30-3.33 (m, 2H), 3.38-3.40 (m, 2H), 3.63-3.71 (m, 1H), 4.59-4.62 (t, J = 6.0, 1H), 4.82-4.83 (d, J = 5.2, 1H), 7.00 (s, 2H). ^{13}C-NMR (100 MHz, DMSO-d_6): 41.2, 64.1, 68.4, 134.5, 171.2. IR (neat, cm^{-1}) v: 3495 (br. w), 3404 (br. m), 3101 (w), 1692 (br. s), 1444 (m), 1412 (m), 1331 (m), 1097 (m), 1046 (s), 889 (m), 831 (s), 694 (s). HRMS (TOF MS ES+): *m/z* calcd. For $C_7H_9NO_4Na$: $[M+Na]^+$: 194.0429, found: 194.0431.

^{1}H-NMR and ^{13}C-NMR were in accordance with previously reported literature.[114] ^{1}H-NMR, ^{13}C-NMR, IR and HRMS data of compound **3** are given in appendix C.

6.3 Synthesis of malonate derivative

6.3.1 Synthesis of ethyl (furan-3-ylmethyl) malonate, compound **4**

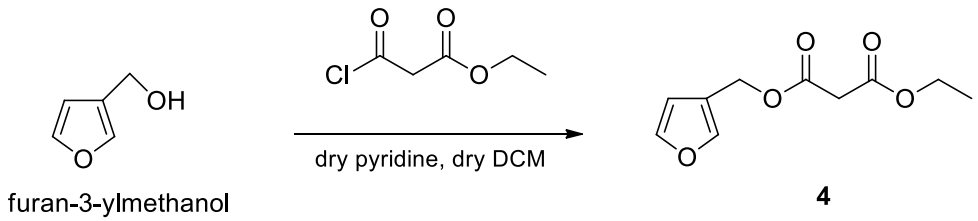

Scheme 29. Synthesis of compound **4** from furan-3-ylmethanol and Ethyl 3-chloro-3-oxopropionate

Anhydrous CH_2Cl_2 (50 mL) was added to an oven dried and evacuated round flask together with a magnetic stirrer. Further, the reaction vessel was cooled down to 0°C before furan-3-ylmethyl (1.25 g, 12.8 mmol) was added by syringe, followed by dry pyridine in excess (g, mmol). Subsequently, Ethyl 3-chloro-3-oxopropionate (1.92 g, 12.8 mmol) were added dropwise to the reaction vessel. The ice bath was kept to keep the reaction at 0°C, before the reaction was stirred in inert atmosphere for 72 hours at room temperature. Termination of the reaction was completed by adding brine (50 mL).

The quenched reaction mixture was then extracted by 3 x 70 mL distilled water and 70 mL CH_2Cl_2. The combined organic layers were dried with $MgSO_4$ and the solvent was evaporated under reduced pressure to yield a crude of orange oil. Lastly the orange oil were dried under reduced pressure for 20 hours, resulting in a total of 2.24 g (10.6 mmol, 83%) of compound **4**. Spectroscopic data of compound **4**: ^{1}H-NMR (400 MHz, $CDCl_3$) δ (ppm): 1.20-1.24 (t, J = 7.2, 3H), 3.36 (s, 2H), 4.13-4.18 (q, J = 7.2, 2H), 5.03 (s, 2H), 6.40 (d, J = 1.2, 1H), 7.36-7.37 (t, J = 2.0, 1H), 7.46 (d, J = 0.8, 1H). ^{13}C-NMR (100 MHz, $CDCl_3$): 13.9, 41.4, 58.5, 61.4, 110.4, 119.8, 141.7, 143.3, 166.3, 166.4. IR (neat, cm^{-1}) v: 2984 (br. w), 1728 (s), 1504 (w), 1370 (w), 1145 (br. s), 1020 (s), 874 (m), 797 (m). HRMS (TOF MS ES+): *m/z* calcd. For $C_{10}H_{12}O_5Na$: $[M+Na]^+$: 235.0582, found: 235.0585.

^{1}H-NMR, ^{13}C-NMR, IR and HRMS data of compound **4** are given in appendix D.

6.4 Exfoliation of graphene

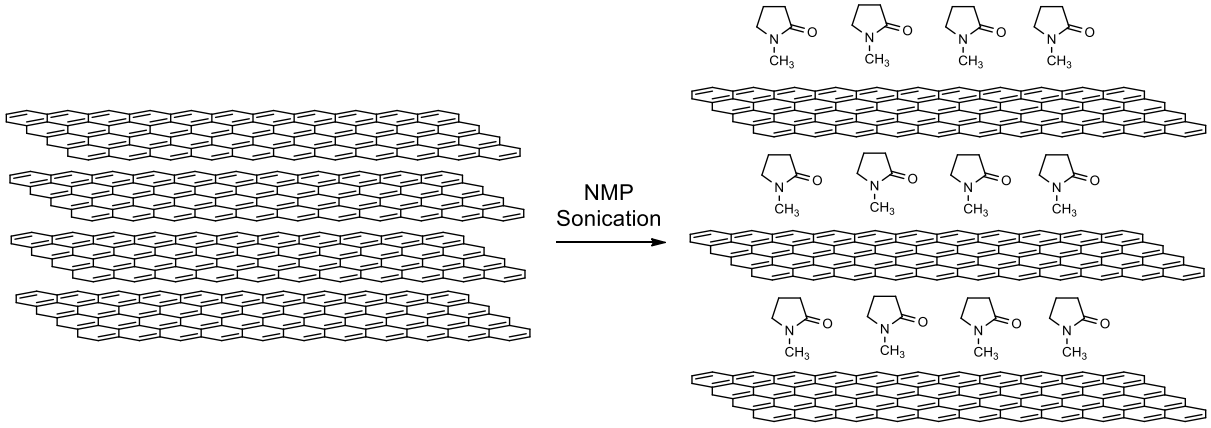

Scheme 30. NMP assisted exfoliation of graphite into graphene sheets, compound **5**.[80]

Graphite powder (100 mg) and NMP (20 mL) were added to a 40 mL cylindrical sample bottle in a 5 mg/mL ratio. The sample bottle was affixed to a tip sonicator and put in a 300 mL ice bath as shown in Figure 8 in section 2.2.1. The sonication was processed at 90 % output power for 30 minutes using a VS70T probe, yielding a black dispersion. Further, centrifuged for 5 minutes at 4000 rpm (1252 RCF). The upper 90 % of the supernatant was collected, yielding a black opaque dispersion of exfoliated graphene sheets.

Standards of the exfoliated graphene were prepared by filtrating small amounts of exfoliated graphene through an Omnipore hydrophilic membrane filter (JHWP04700), pore size 0.45 µm, affixed to a vacuum filtration setup with a porous glass filter. 3 mL of graphene in NMP were diluted with DMF (3 mL) and filtered off, resulting in a black solid product. Further, the graphene was washed with DMF (30 mL), MeOH (100 mL) and DCM (50 mL). The Omnipore filter with its contents were carefully transferred to a beaker with DCM (3 mL), and bath sonicated for 10 seconds to disperse the graphene into the DCM. Finally, the dispersion was centrifuged for 5 minutes at 4000 rpm (1252 RCF). A black opaque supernatant was collected from the centrifuged vial, resulting in a standard of compound **5** dispersed in DCM. MicroRaman of compound **5** is shown in appendix E.

6.5 Microwave-assisted Bingel reaction of exfoliated graphene

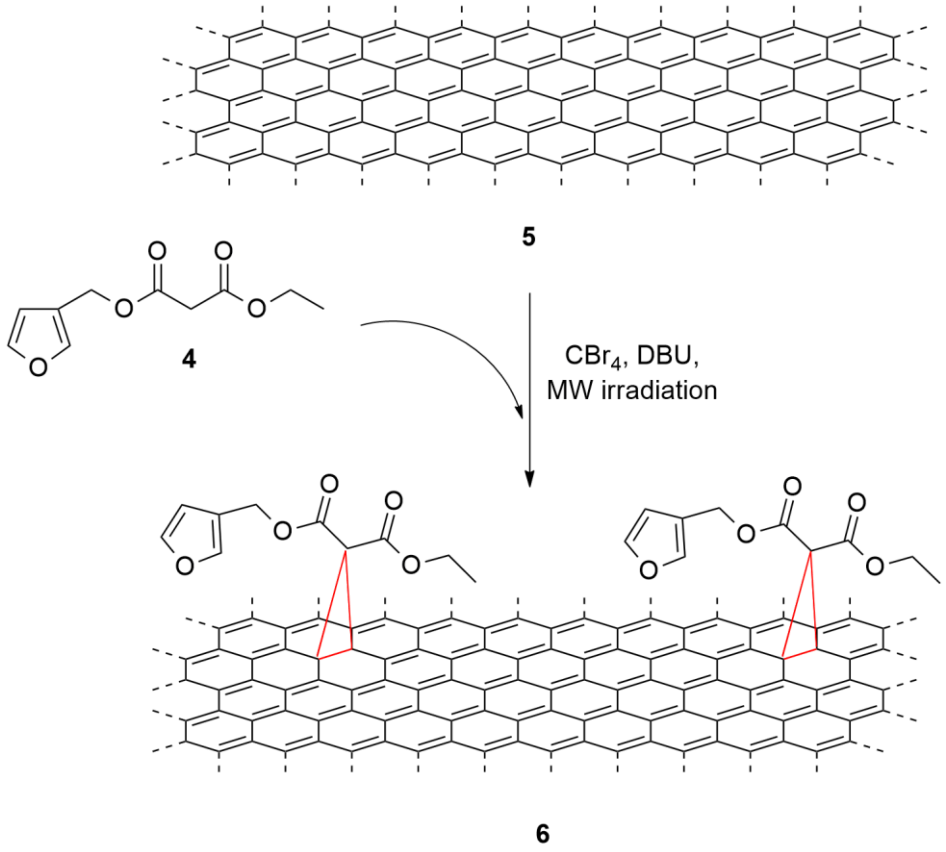

Scheme 31. Compound **6** synthesized through MW assisted Bingel reaction of **4** and **5**.[127]

CBr_4, functionalized malonate (**4**), exfoliated graphene (**5**) and DBU were added to a sealable vial (size type 2.0-5.0 mL) with a magnetic stirrer while under N_2 purging. The vial was sealed and the reactants were processed in a Biotage initiator microwave reactor. Both reactant quantities and reactor settings is listed in appendix I. After the MW assisted Bingel reaction, the vial was cooled to room temperature and excess pressure inside the vial released before removing the sealing cap. An Omnipore hydrophilic membrane filter (JHWP04700), pore size 0.45 µm, were affixed to a vacuum filtration setup with a porous glass filter. The reacted vial contents were diluted with DMF (3 mL) and filtered off, resulting in a black solid product. Further, the product was washed with DMF (30 mL), MeOH (100 mL) and DCM (50 mL). The Omnipore filter with its contents were carefully transferred to a beaker with DCM (3 mL), and bath sonicated for 10 seconds to disperse the product into the DCM. Finally, the dispersion was centrifuged for 5 minutes at 4000 rpm (1252 RCF). A black opaque supernatant was collected from the centrifuged vial, resulting in compound **6**. MicroRaman is shown in appendix F.

6.6 MicroRaman characterization

Raman spectrometry was used to analyze the quality of exfoliated graphene (**5**) and functionalized graphene (**6**) as prepared in **section 6.4** and **6.5** respectively. Samples of graphene **5** and graphene hybrid **6** dispersed in DCM were prepared for microRaman by applying them dropwise to small square sample glass plates, which was heated at 50^{o}C on a hot plate to quickly evacuate the DCM. Further, the samples were oven dried for 1 hour at 110 ^{o}C before microRaman analysis.

Using a Raman spectroscope with a VIS excitation at 532 nm and a power output of 5%, the samples were analyzed in the 1100-3200 cm^{-1} region, which is most important for graphene. Initially, probing with shorter scans at 10 s were completed to obtain an average representation of the sample quality, reflected in the D/G ratio of the Raman spectra. Final Raman spectra were obtained by doing a longer scan at 180s to achieve higher precision and resolution.

Raman spectra of compound **5** and **6,** as well as non-exfoliated graphite is shown in appendix E and F and are further compared in sections 4.4.1 and 4.4.2.

6.7 Polyurethane synthesis

6.7.1 Preliminary tests of Polyurethane synthesis

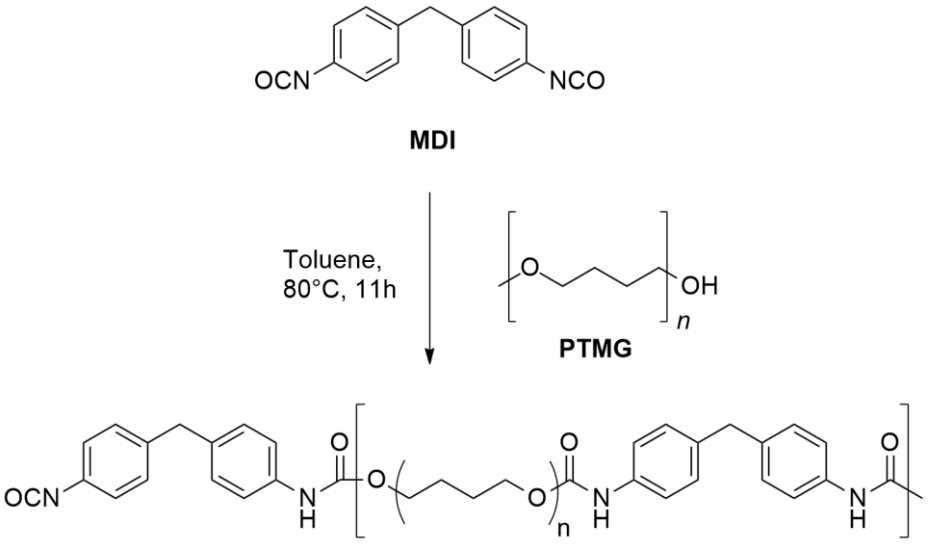

Scheme 32. Synthesis of compound **7** from condensation between MDI and PTMG.[16]

MDI (239 mg, 0.95 mmol) and toluene (4 mL) were added to a 50 mL round bottom flask fitted with a condenser and a magnetic stir bar. Next, a mixture of PTMG (921 mg, 0.92 mmol) and toluene (mL) was added dropwise to the solution in the round-bottom flask. The mixture was allowed to react at 80°C for 11 h under N_2-flow. Cooling the reaction to room temperature terminated the polymerization to yield a colourless crude of polyurethane. Further, the polyurethane crude was precipitated in cold MeOH (mL) under vigorous stirring. Lastly, the white precipitate was dried under reduced pressure for 20 hours, resulting in 1.02 g of compound **7**. GPC-data: M_w = 104000 g/mol^{-1}, M_n 38000 = g/mol^{-1}, PDI = 2.72.

GPC and IR data of compound **7** are given in appendix G.

6.7.2 Synthesis of maleimide functionalized polyurethane **8**

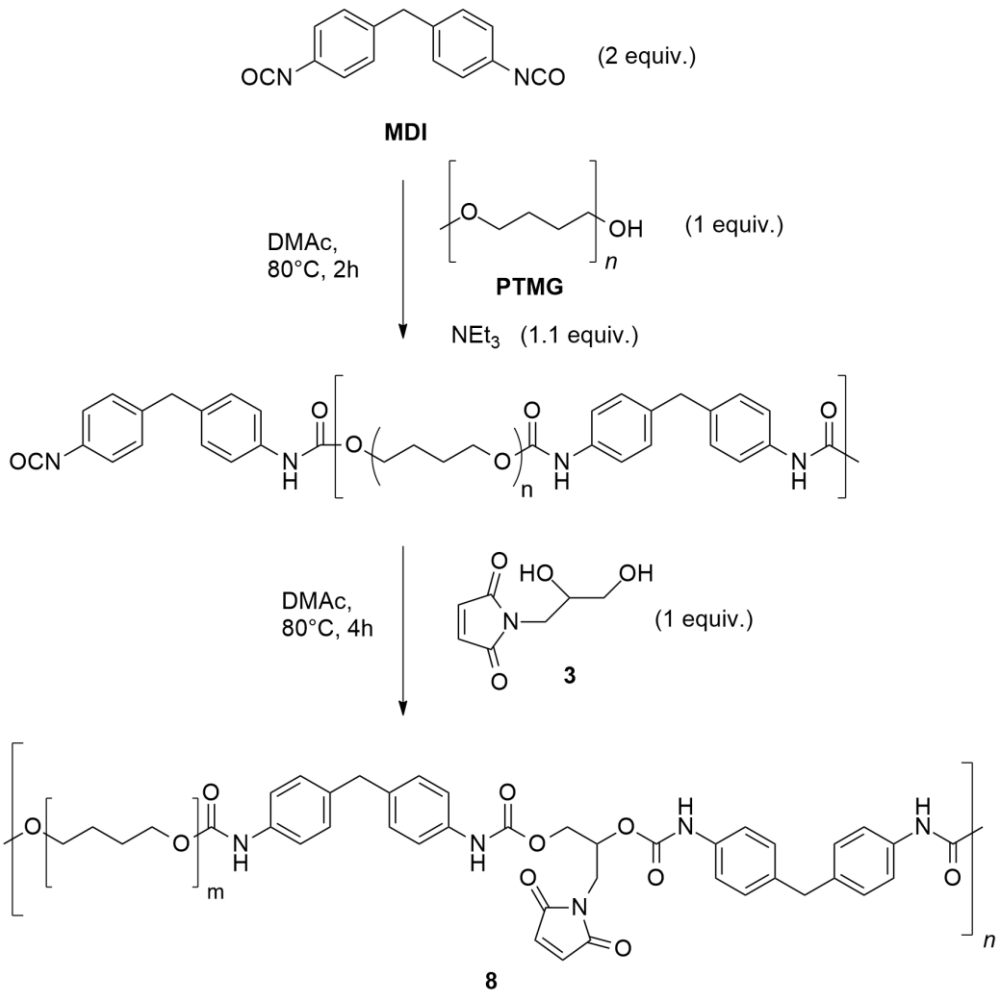

Scheme 33. Synthesis of Maleimide pendant polyurethane, compound **8**.[114]

MDI (351 mg, 1.4 mmol) and DMAc (2 mL) were added to a 50 mL round bottom flask fitted with a condenser and a magnetic stir bar. Next, a mixture of PTMG (701 mg, 0.7 mmol), NEt_3 (0.1 mL, 0.72 mmol) and DMAc (6 mL) was added dropwise to the solution in the round-bottom flask. The mixture of MDI, PTMG and NEt_3 was allowed to react at 80°C for 2 hours under N_2-flow. After 2 hours, a solution of compound **3** (120 mg, 0.7 mmol) and DMAc (2 mL) were added dropwise to the pre-polymerized isocyanate end-capped polyurethane. The reaction was further progressed for 4 h at 80°C with magnetic stirring under N_2-flow. Cooling to room temperature terminated the polymerization to yield a dark red viscous crude of maleimide-functionalized polyurethane. Further, the polymer crude was precipitated in cold MeOH (200 mL) under vigorous stirring. The precipitation solvent was filtered off, and the dark red solids collected were dried under reduced pressure for 20 hours, resulting in 1.21 g of compound **8**.

GPC-data: M_w = 27300 g/mol^{-1}, M_n = 7030 g/mol^{-1}, PDI = 3.88. ^{1}H-NMR (400 MHz, THF-d_8) δ (ppm): 7.70 (s, 1H, -CO-**NH**-C), 7.37-7.35 (m, 4H, -NH-C-(**CH**)$_2$-), 7.21 (s, 1H, -CO-**CH**=**CH**-CO-) 7.04-7.02 (m, 4H, (**CH**)$_2$CCH$_2$), 4.01-4.07 (m, 2.5H, -O-CH-**CH$_2$**-O-/other), 3.81 (s, 2H, **CH2** in MDI), 3.36 (broad peak, 29.5H, -O-**CH$_2$**-CH$_2$-CH$_2$-**CH$_2$**-O-), 3.36 (broad peak, 29H, -O-CH$_2$-**CH$_2$**-**CH$_2$**-CH$_2$-O-).

^{1}H-NMR and IR data of compound **8** are given in appendix H.

6.8 Graphene-crosslinked Polyurethane, compound **9A-D**

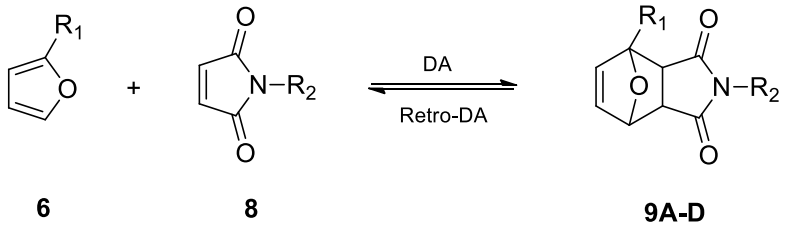

6 **8** **9A-D**

R_1: Graphene hybrid

R_2: Polyurethane backbone

Scheme 34. Diels-Alder/ retro Diels-Alder between compound **6** and **8**.

To form the graphene/polyurethane films **9A-D**, several solutions of compound **6** and **8** in THF were prepared with different concentrations of the graphene component. Further, four different solutions were cast on cleaned silicon wafers. Si wafers (approx. 0.5x1.0 cm) were cleaned by placing them in an airtight beaker with isopropanol (50 mL) followed by bath sonication for 2x 30 minutes. After the first bath sonication, the dirty isopropanol was exchanged for clean isopropanol (50 mL). Lastly, the wafers were oven dried at 110°C overnight.

Compound **8** were prepared by solving 496 mg of dried polymer in THF (16 mL). A dispersion of compound **6** were made by bath sonication an amount of **6** for 10 sec in THF (2 mL) to make a uniform dispersion. By combining solutions of **6** and **8** in THF, four different concentrations of the graphene/polyurethane hybrid were made specified in Table 11 in section 4.6. Each vial was subsequently bath sonicated for 10 secs to properly disperse the graphene hybrid in the polyurethane solution. Further, each solution was drop-casted (10 drops) onto the Si wafers prepared earlier. Each Si wafer were heated to 60°C for 2 h, resulting in four different graphene-crosslinked polyurethane films, **9A-D**.

Using a Swann-Morton sterile Surgical Blade (BS 2982), small cuts were applied to each film of compound **9**. Each damaged film was heated at 160°C to facilitate retro Diels-Alder overnight, followed by 2 h at 60°C the next day. Each film was analysed using SEM APREO after damage were applied to the film and after heating to initiate Diels-Alder as described in section 6.9 on the following page.

6.9 Scanning Electron Microscope analysis

Graphene-crosslinked polyurethanes, **9A-D** were analyzed using a FEI APREO, Field Emission scanning electron microscope (SEM) by using electrons for imaging of material surfaces. This allowed high magnification to closer analyze the topography of compound **9**. Four different samples were prepared as described in section 5.8 by drop casting of polymer onto Si Wafers. Each wafer was affixed onto a sample holder using soft EM-Tec conductive copper SEM tape foil to establish a grounding path. The polymer surface was analyzed using a beam current at 50 pA, acceleration voltage of 1.00 kV and a working distance (WD) of 3.6-4.3mm between the lens and the samples. Overview pictures at the range 500 µm and 1 mm were acquired using the EDT detector inside the main chamber at a magnification of x200 and x100 respectively. Close up image acquisition of the surface were acquired using the T1 and T2 detectors inside the lens to analyze the topography in the 10-50 µm range with magnification up to x2500. Imaging of each sample is showed in Figures 24-31 in section 4.6.

References

1 Staudinger, H. Über Polymerisation. *Berichte der deutschen chemischen Gesellschaft (A and B Series)* **53**, 1073-1085 (1920).

2 Mülhaupt, R. Hermann Staudinger and the origin of macromolecular chemistry. *Angewandte Chemie International Edition* **43**, 1054-1063 (2004).

3 Wu, D. Y., Meure, S. & Solomon, D. Self-healing polymeric materials: A review of recent developments. *Progress in polymer science* **33**, 479-522 (2008).

4 Yoon, D., Sundararajan, P. & Flory, P. Conformational characteristics of polystyrene. *Macromolecules* **8**, 776-783 (1975).

5 Young, R. J. & Lovell, P. A. *Introduction to polymers*. (CRC press, 2011).

6 Strobl, G. R. & Strobl, G. R. *The physics of polymers*. Vol. 2 (Springer, 1997).

7 Olivera, S., Muralidhara, H. B., Venkatesh, K., Gopalakrishna, K. & Vivek, C. S. Plating on acrylonitrile–butadiene–styrene (ABS) plastic: a review. *Journal of materials science* **51**, 3657-3674 (2016).

8 Akindoyo, J. O. *et al.* Polyurethane types, synthesis and applications–a review. *Rsc Advances* **6**, 114453-114482 (2016).

9 Carothers, W. H. Polymerization. *Chemical Reviews* **8**, 353-426 (1931).

10 Stille, J. K. (ACS Publications, 1981).

11 Rogers, M. E. & Long, T. E. *Synthetic methods in step-growth polymers*. (John Wiley & Sons, 2003).

12 Ortega, R. A., Carter, E. S. & Ortega, A. E. Nylon 6, 6 nonwoven fabric separates oil contaminates from oil-in-water emulsions. *Plos one* **11**, e0158493 (2016).

13 Van Der Zwaag, S. Self-healing materials: an alternative approach to 20 centuries of material science. *Delft: Springer* (2007).

14 Du, Y., Li, D., Liu, L. & Gai, G. Recent achievements of self-healing graphene/polymer composites. *Polymers* **10**, 114 (2018).

15 Wu, S. *et al.* Ultrafast self-healing nanocomposites via infrared laser and their application in flexible electronics. *ACS applied materials & interfaces* **9**, 3040-3049 (2017).

16 Lin, C. *et al.* A self-healable nanocomposite based on dual-crosslinked Graphene Oxide/Polyurethane. *Polymer* **127**, 241-250 (2017).

17 Sarkar, S., Bekyarova, E., Niyogi, S. & Haddon, R. C. Diels– Alder chemistry of graphite and graphene: graphene as diene and dienophile. *Journal of the American Chemical Society* **133**, 3324-3327 (2011).

18 Hu, H., Zhao, Z., Wan, W., Gogotsi, Y. & Qiu, J. Ultralight and highly compressible graphene aerogels. *Advanced materials* **25**, 2219-2223 (2013).

19 Zhu, Y. *et al.* Microwave assisted exfoliation and reduction of graphite oxide for ultracapacitors. *Carbon* **48**, 2118-2122 (2010).

20 Thakur, V. K. & Kessler, M. R. Self-healing polymer nanocomposite materials: A review. *Polymer* **69**, 369-383 (2015).

21 Yuan, Y., Yin, T., Rong, M. & Zhang, M. Self healing in polymers and polymer composites. Concepts, realization and outlook: A review. *Express Polymer Letters* **2**, 238-250 (2008).

22 Zhu, D. Y., Rong, M. Z. & Zhang, M. Q. Self-healing polymeric materials based on microencapsulated healing agents: From design to preparation. *Progress in Polymer Science* **49**, 175-220 (2015).

23 Garcia, S. & Fischer, H. in *Smart Polymers and their Applications* 271-298 (Elsevier, 2014).

24 Brown, E. N., Kessler, M. R., Sottos, N. R. & White, S. R. In situ poly (urea-formaldehyde) microencapsulation of dicyclopentadiene. *Journal of microencapsulation* **20**, 719-730 (2003).

25 Garcia, S. J. Effect of polymer architecture on the intrinsic self-healing character of polymers. *European Polymer Journal* **53**, 118-125 (2014).

26 de Espinosa, L. M., Fiore, G. L., Weder, C., Foster, E. J. & Simon, Y. C. Healable supramolecular polymer solids. *Progress in Polymer Science* **49**, 60-78 (2015).

27 White, S. R. *et al.* Autonomic healing of polymer composites. *Nature* **409**, 794-797 (2001).

28 Li, J., Zhang, G., Sun, R. & Wong, C.-P. A covalently cross-linked reduced functionalized graphene oxide/polyurethane composite based on Diels–Alder chemistry and its potential application in healable flexible electronics. *Journal of Materials Chemistry C* **5**, 220-228 (2017).

29 Sanyal, A. Diels–Alder Cycloaddition-Cycloreversion: A Powerful Combo in Materials Design. *Macromolecular Chemistry and Physics* **211**, 1417-1425 (2010).

30 Gandini, A. The furan/maleimide Diels–Alder reaction: A versatile click–unclick tool in macromolecular synthesis. *Progress in Polymer Science* **38**, 1-29 (2013).

31 Willocq, B. *et al.* One-component Diels–Alder based polyurethanes: a unique way to self-heal. *RSC advances* **7**, 48047-48053 (2017).

32 An, S. Y., Arunbabu, D., Noh, S. M., Song, Y. K. & Oh, J. K. Recent strategies to develop self-healable crosslinked polymeric networks. *Chemical Communications* **51**, 13058-13070 (2015).

33 Nicolaou, K. C., Snyder, S. A., Montagnon, T. & Vassilikogiannakis, G. The Diels–Alder reaction in total synthesis. *Angewandte Chemie International Edition* **41**, 1668-1698 (2002).

34 Vollmer, J. & Servis, K. Woodward-Hoffmann rules: Electrocyclic reactions. *Journal of Chemical Education* **45**, 214 (1968).

35 Woodward, R. B. & Hoffmann, R. *The conservation of orbital symmetry*. (Elsevier, 2013).

36 Qiu, Y. Substituent effects in the Diels–Alder reactions of butadienes, cyclopentadienes, furans and pyroles with maleic anhydride. *Journal of Physical Organic Chemistry* **28**, 370-376 (2015).

37 Houk, K. N., Loncharich, R. J., Blake, J. F. & Jorgensen, W. L. Substituent effects and transition structures for Diels-Alder reactions of butadiene and cyclopentadiene with cyanoalkenes. *Journal of the American Chemical Society* **111**, 9172-9176 (1989).

38 Nevejans, S., Ballard, N., Miranda, J. I., Reck, B. & Asua, J. M. The underlying mechanisms for self-healing of poly (disulfide) s. *Physical Chemistry Chemical Physics* **18**, 27577-27583 (2016).

39 Canadell, J., Goossens, H. & Klumperman, B. Self-healing materials based on disulfide links. *Macromolecules* **44**, 2536-2541 (2011).

40 Bracchi, M. E. & Fulton, D. A. Orthogonal breaking and forming of dynamic covalent imine and disulfide bonds in aqueous solution. *Chemical Communications* **51**, 11052-11055 (2015).

41 Godoy-Alcántar, C., Yatsimirsky, A. K. & Lehn, J. M. Structure-stability correlations for imine formation in aqueous solution. *Journal of physical organic chemistry* **18**, 979-985 (2005).

42 Yang, L. *et al.* Improving tumor chemotherapy effect using an injectable self-healing hydrogel as drug carrier. *Polymer Chemistry* **8**, 5071-5076 (2017).

43 Li, Y. *et al.* Self-healing hydrogel with a double dynamic network comprising imine and borate ester linkages. *Chemistry of Materials* **31**, 5576-5583 (2019).

44 Deng, C. C., Brooks, W. L., Abboud, K. A. & Sumerlin, B. S. Boronic acid-based hydrogels undergo self-healing at neutral and acidic pH. *ACS Macro Letters* **4**, 220-224 (2015).

45 Marco-Dufort, B. & Tibbitt, M. Design of moldable hydrogels for biomedical applications using dynamic covalent boronic esters. *Materials Today Chemistry* **12**, 16-33 (2019).

46 Gyarmati, B., Szilágyi, B. Á. & Szilágyi, A. Reversible interactions in self-healing and shape memory hydrogels. *European Polymer Journal* **93**, 642-669 (2017).

47 Adams, J. *et al.* Potent and selective inhibitors of the proteasome: dipeptidyl boronic acids. *Bioorganic & medicinal chemistry letters* **8**, 333-338 (1998).

48 Hentschel, J., Kushner, A. M., Ziller, J. & Guan, Z. Self-healing supramolecular block copolymers. *Angewandte Chemie* **124**, 10713-10717 (2012).

49 Hager, M. D. Self-healing materials. *Handbook of Solid State Chemistry*, 201-225 (2017).

50 Yan, X., Wang, F., Zheng, B. & Huang, F. Stimuli-responsive supramolecular polymeric materials. *Chemical Society Reviews* **41**, 6042-6065 (2012).

51 van Gemert, G. M., Peeters, J. W., Söntjens, S. H., Janssen, H. M. & Bosman, A. W. Self-healing supramolecular polymers in action. *Macromolecular Chemistry and Physics* **213**, 234-242 (2012).

52 Mollet, B. B. *et al.* A modular approach to easily processable supramolecular bilayered scaffolds with tailorable properties. *Journal of Materials Chemistry B* **2**, 2483-2493 (2014).

53 Herbst, F., Seiffert, S. & Binder, W. H. Dynamic supramolecular poly (isobutylene) s for self-healing materials. *Polymer Chemistry* **3**, 3084-3092 (2012).

54 Vaiyapuri, R., Greenland, B. W., Colquhoun, H. M., Elliott, J. M. & Hayes, W. Molecular recognition between functionalized gold nanoparticles and healable, supramolecular polymer blends–a route to property enhancement. *Polymer Chemistry* **4**, 4902-4909 (2013).

55 Greenland, B. W., Burattini, S., Hayes, W. & Colquhoun, H. M. Design, synthesis and computational modelling of aromatic tweezer-molecules as models for chain-folding polymer blends. *Tetrahedron* **64**, 8346-8354 (2008).

56 Das, A. & Mahanwar, P. A brief discussion on advances in polyurethane applications. *Advanced Industrial and Engineering Polymer Research* (2020).

57 Sharmin, E. & Zafar, F. Polyurethane: an introduction. *Polyurethane*, 3-16 (2012).

58 Król, P. & Król, B. Structures, properties and applications of the polyurethane ionomers. *Journal of Materials Science* **55**, 73-87 (2020).

59 Bayer, O. Das di-isocyanat-polyadditionsverfahren (polyurethane). *Angewandte Chemie* **59**, 257-272 (1947).

60 Feng, L. *et al.* Self-healing behavior of polyurethanes based on dual actions of thermo-reversible Diels-Alder reaction and thermal movement of molecular chains. *Polymer* **124**, 48-59 (2017).

61 Dworakowska, S., Bogdał, D., Zaccheria, F. & Ravasio, N. The role of catalysis in the synthesis of polyurethane foams based on renewable raw materials. *Catalysis today* **223**, 148-156 (2014).

62 Baker, J. W. & Gaunt, J. THE MECHANISM OF THE REACTION OF ARYL ISOCYANATES WITH ALCOHOLS AND AMINES. 2. THE BASE-CATALYSED REACTION OF PHENYL ISOCYANATE WITH ALCOHOLS. *Journal of the chemical society*, 9-18 (1949).

63 Farkas, A., Mills, G., Erner, W. & Maerker, J. Triethylenediamine—a new bicyclic intermediate and catalyst for making polyurethane foam. *Industrial & Engineering Chemistry* **51**, 1299-1300 (1959).

64 Brocas, A.-L., Mantzaridis, C., Tunc, D. & Carlotti, S. Polyether synthesis: From activated or metal-free anionic ring-opening polymerization of epoxides to functionalization. *Progress in polymer science* **38**, 845-873 (2013).

65 Bailosky, L. C. *et al.* Synthesis of polyether polyols with epoxidized soy bean oil. *Progress in Organic Coatings* **76**, 1712-1719 (2013).

66 Pavier, C. & Gandini, A. Oxypropylation of sugar beet pulp. 1. Optimisation of the reaction. *Industrial Crops and Products* **12**, 1-8 (2000).

67 Furtwengler, P. & Avérous, L. Renewable polyols for advanced polyurethane foams from diverse biomass resources. *Polymer Chemistry* **9**, 4258-4287 (2018).

68 Carothers, W. H. Studies on polymerization and ring formation. I. An introduction to the general theory of condensation polymers. *Journal of the American Chemical Society* **51**, 2548-2559 (1929).

69 Ionescu, M. *Chemistry and technology of polyols for polyurethanes*. (iSmithers Rapra Publishing, 2005).

70 Fitzer, E., Kochling, K.-H., Boehm, H. & Marsh, H. Recommended terminology for the description of carbon as a solid (IUPAC Recommendations 1995). *Pure and Applied Chemistry* **67**, 473-506 (1995).

71 Novoselov, K. S. *et al.* Electric field effect in atomically thin carbon films. *science* **306**, 666-669 (2004).

72 Boehm, H. P., Setton, R. & Stumpp, E. Nomenclature and terminology of graphite intercalation compounds (IUPAC Recommendations 1994). *Pure and Applied Chemistry* **66**, 1893-1901 (1994).

73 Bonaccorso, F., Sun, Z., Hasan, T. & Ferrari, A. Graphene photonics and optoelectronics. *Nature photonics* **4**, 611 (2010).

74 Tsoukleri, G. *et al.* Subjecting a graphene monolayer to tension and compression. *small* **5**, 2397-2402 (2009).

75 Shao, Y. *et al.* Graphene based electrochemical sensors and biosensors: a review. *Electroanalysis: An International Journal Devoted to Fundamental and Practical Aspects of Electroanalysis* **22**, 1027-1036 (2010).

76 Coroş, M., Pogăcean, F., Măgeruşan, L., Socaci, C. & Pruneanu, S. A brief overview on synthesis and applications of graphene and graphene-based nanomaterials. *Frontiers of Materials Science* **13**, 23-32 (2019).

77 Hummers Jr, W. S. & Offeman, R. E. Preparation of graphitic oxide. *Journal of the american chemical society* **80**, 1339-1339 (1958).

78 Huh, S. *et al.* UV/ozone-oxidized large-scale graphene platform with large chemical enhancement in surface-enhanced Raman scattering. *ACS nano* **5**, 9799-9806 (2011).

79 Jing, Q. *et al.* Chemical functionalization of graphene oxide for improving mechanical and thermal properties of polyurethane composites. *Materials & Design* **85**, 808-814 (2015).

80 Khan, U., O'Neill, A., Lotya, M., De, S. & Coleman, J. N. High-concentration solvent exfoliation of graphene. *small* **6**, 864-871 (2010).

81 Butt, H.-J., Graf, K. & Kappl, M. *Physics and chemistry of interfaces*. (John Wiley & Sons, 2013).

82 Novoselov, K. S. *et al.* A roadmap for graphene. *nature* **490**, 192-200 (2012).

83 Sun, Z. *et al.* Growth of graphene from solid carbon sources. *Nature* **468**, 549-552 (2010).

84 Li, Z. *et al.* Low-temperature growth of graphene by chemical vapor deposition using solid and liquid carbon sources. *ACS nano* **5**, 3385-3390 (2011).

85 Gan, X. *et al.* A simple method to synthesize graphene at 633 K by dechlorination of hexachlorobenzene on Cu foils. *Carbon* **50**, 306-310 (2012).

86 Sharma, S. *et al.* Synthesis of graphene crystals from solid waste plastic by chemical vapor deposition. *Carbon* **72**, 66-73 (2014).

87 Ruan, G., Sun, Z., Peng, Z. & Tour, J. M. Growth of graphene from food, insects, and waste. *ACS nano* **5**, 7601-7607 (2011).

88 Sutter, P. W., Flege, J.-I. & Sutter, E. A. Epitaxial graphene on ruthenium. *Nature materials* **7**, 406-411 (2008).

89 Ueta, H. *et al.* Highly oriented monolayer graphite formation on Pt (1 1 1) by a supersonic methane beam. *Surface science* **560**, 183-190 (2004).

90 De Arco, L. G., Zhang, Y., Kumar, A. & Zhou, C. Synthesis, transfer, and devices of single-and few-layer graphene by chemical vapor deposition. *IEEE Transactions on Nanotechnology* **8**, 135-138 (2009).

91 Chen, Z. *et al.* Bulk growth of mono-to few-layer graphene on nickel particles by chemical vapor deposition from methane. *Carbon* **48**, 3543-3550 (2010).

92 Chan, S.-H. *et al.* Low-temperature synthesis of graphene on Cu using plasma-assisted thermal chemical vapor deposition. *Nanoscale research letters* **8**, 1-5 (2013).

93 Jeon, C. *et al.* Opening and reversible control of a wide energy gap in uniform monolayer graphene. *Scientific reports* **3**, 1-6 (2013).

94 KiangáChua, C. Introducing dichlorocarbene in graphene. *Chemical Communications* **48**, 5376-5378 (2012).

95 Yan, L. *et al.* Chemistry and physics of a single atomic layer: strategies and challenges for functionalization of graphene and graphene-based materials. *Chemical Society Reviews* **41**, 97-114 (2012).

96 Huang, P., Zhu, H., Jing, L., Zhao, Y. & Gao, X. Graphene covalently binding aryl groups: conductivity increases rather than decreases. *ACS nano* **5**, 7945-7949 (2011).

97 Biglova, Y. N. & Mustafin, A. G. Nucleophilic cyclopropanation of [60] fullerene by the addition–elimination mechanism. *RSC advances* **9**, 22428-22498 (2019).

98 Diederich, F., Isaacs, L. & Philp, D. Syntheses, structures, and properties of methanofullerenes. *Chemical Society Reviews* **23**, 243-255 (1994).

99 Choi, J., Kim, K.-j., Kim, B., Lee, H. & Kim, S. Covalent functionalization of epitaxial graphene by azidotrimethylsilane. *The Journal of Physical Chemistry C* **113**, 9433-9435 (2009).

100 Bingel, C. Cyclopropanierung von fullerenen. *Chemische Berichte* **126**, 1957-1959 (1993).

101 Stankovich, S. *et al.* Synthesis of graphene-based nanosheets via chemical reduction of exfoliated graphite oxide. *carbon* **45**, 1558-1565 (2007).

102 Georgakilas, V. *et al.* Organic functionalization of carbon nanotubes. *Journal of the American Chemical Society* **124**, 760-761 (2002).

103 Quintana, M. *et al.* Functionalization of graphene via 1, 3-dipolar cycloaddition. *ACS nano* **4**, 3527-3533 (2010).

104 Roscher, S., Hoffmann, R. & Ambacher, O. Determination of the graphene–graphite ratio of graphene powder by Raman 2D band symmetry analysis. *Analytical methods* **11**, 1224-1228 (2019).

105 Graves, P. & Gardiner, D. Practical raman spectroscopy. *Springer* (1989).

106 Dresselhaus, M., Jorio, A., Souza Filho, A. & Saito, R. Defect characterization in graphene and carbon nanotubes using Raman spectroscopy. *Philosophical Transactions of the Royal Society A: Mathematical, Physical and Engineering Sciences* **368**, 5355-5377 (2010).

107 Ferrari, A. C. *et al.* Raman spectrum of graphene and graphene layers. *Physical review letters* **97**, 187401 (2006).

108 Novoselov, K. S. *et al.* Two-dimensional gas of massless Dirac fermions in graphene. *nature* **438**, 197-200 (2005).

109 Zhang, Y., Tan, Y.-W., Stormer, H. L. & Kim, P. Experimental observation of the quantum Hall effect and Berry's phase in graphene. *nature* **438**, 201-204 (2005).

110 Malard, L., Pimenta, M. A., Dresselhaus, G. & Dresselhaus, M. Raman spectroscopy in graphene. *Physics reports* **473**, 51-87 (2009).

111 Du, P. *et al.* Synthesis of linear polyurethane bearing pendant furan and cross-linked healable polyurethane containing Diels–Alder bonds. *New Journal of Chemistry* **38**, 770-776 (2014).

112 Patel, Y. S. & Patel, H. S. Thermoplastic-thermosetting merged polyimides via furan-maleimide Diels–Alder polymerization. *Arabian Journal of Chemistry* **10**, S1373-S1380 (2017).

113 Truong, T. T., Nguyen, H. T., Phan, M. N. & Nguyen, L. T. T. Study of Diels–Alder reactions between furan and maleimide model compounds and the preparation of a healable thermo-reversible polyurethane. *Journal of Polymer Science Part A: Polymer Chemistry* **56**, 1806-1814 (2018).

114 Yu, S., Zhang, R., Wu, Q., Chen, T. & Sun, P. Bio-Inspired high-performance and recyclable cross-linked polymers. *Advanced Materials* **25**, 4912-4917 (2013).

115 Gramlich, W. M., Robertson, M. L. & Hillmyer, M. A. Reactive compatibilization of poly (l-lactide) and conjugated soybean oil. *Macromolecules* **43**, 2313-2321 (2010).

116 Chen, S. *et al.* A Single Molecular Diels–Alder Crosslinker for Achieving Recyclable Cross-Linked Polymers. *Macromolecular rapid communications* **36**, 1687-1692 (2015).

117 Mather, B. D., Viswanathan, K., Miller, K. M. & Long, T. E. Michael addition reactions in macromolecular design for emerging technologies. *Progress in Polymer Science* **31**, 487-531 (2006).

118 Engel, T. & Kickelbick, G. Thermoreversible reactions on inorganic nanoparticle surfaces: Diels–alder reactions on sterically crowded surfaces. *Chemistry of Materials* **25**, 149-157 (2013).

119 Sammis, G. M., Danjo, H. & Jacobsen, E. N. Cooperative dual catalysis: Application to the highly enantioselective conjugate cyanation of unsaturated imides. *Journal of the American Chemical Society* **126**, 9928-9929 (2004).

120 Nair, D. P. *et al.* The thiol-Michael addition click reaction: a powerful and widely used tool in materials chemistry. *Chemistry of Materials* **26**, 724-744 (2014).

121 Jafari, E. Synthesis and evaluation of antimicrobial activity of cyclic imides derived from phthalic and succinic anhydrides. *Research in pharmaceutical sciences* **12**, 526 (2017).

122 Dhivare, R. S. & Rajput, S. S. Synthesis and antimicrobial activity of five membered cyclic imide derivatives of mono, di and tri substituted aromatic amines and napthyl amine. *World J Pharm Sci* **4**, 1650-1658 (2015).

123 Sheremeteva, T. & Gusinskaya, V. Formation and stability of amide and imide links. *Bulletin of the Academy of Sciences of the USSR, Division of chemical science* **15**, 657-661 (1966).

124 González, S., Martín, N. & Guldi, D. M. Synthesis and Properties of Bingel-type Methanofullerene– π-Extended-TTF Diads and Triads. *The Journal of organic chemistry* **68**, 779-791 (2003).

125 Fersht, A. R. & Jencks, W. P. Acetylpyridinium ion intermediate in pyridine-catalyzed hydrolysis and acyl transfer reactions of acetic anhydride. Observation, kinetics, structure-reactivity correlations, and effects of concentrated salt solutions. *Journal of the American Chemical Society* **92**, 5432-5442 (1970).

126 Economopoulos, S. P., Rotas, G., Miyata, Y., Shinohara, H. & Tagmatarchis, N. Exfoliation and chemical modification using microwave irradiation affording highly functionalized graphene. *ACS nano* **4**, 7499-7507 (2010).

127 Economopoulos, S. P., Pagona, G., Yudasaka, M., Iijima, S. & Tagmatarchis, N. Solvent-free microwave-assisted Bingel reaction in carbon nanohorns. *Journal of Materials Chemistry* **19**, 7326-7331 (2009).

128 Coleman, K. S., Bailey, S. R., Fogden, S. & Green, M. L. Functionalization of single-walled carbon nanotubes via the Bingel reaction. *Journal of the American Chemical Society* **125**, 8722-8723 (2003).

129 Van Maris, R., Tamano, Y., Yoshimura, H. & Gay, K. M. Polyurethane catalysis by tertiary amines. *Journal of cellular plastics* **41**, 305-322 (2005).

130 Hsiao, S.-H., Guo, W., Kung, Y.-C. & Lee, Y.-J. Redox-active and electrochromic aromatic poly (amide-imide) s with 2, 4-dimethoxytriphenylamine chromophores. *Journal of Polymer Research* **18**, 1353-1364 (2011).

Appendices

The appendices are organized so that the synthesis of the pendant groups are listed first, followed by Raman spectra and polyurethane synthesis. This way, the appendices are listed by ascending compound number listed in the "Numbered Compounds" section. Spectra for compound **1-4** are listed and presented in the following order: ^{1}H-NMR, ^{13}C-NMR, COSY, HSQC, HMBC, IR, HRMS. For exfoliated graphene (**5**) and Bingel graphene (**6**), tables for reaction process are presented in appendix I, and microRaman spectra can be viewed in appendices E and F. Spectra for maleimide-polyurethane (**8**) are listed as follow: ^{1}H-NMR, IR and GPC. SEM imaging of the target material is presented in discussion section **4.6**.

A Spectroscopic data - Compound 1

^{1}H-NMR spectrum of compound 1

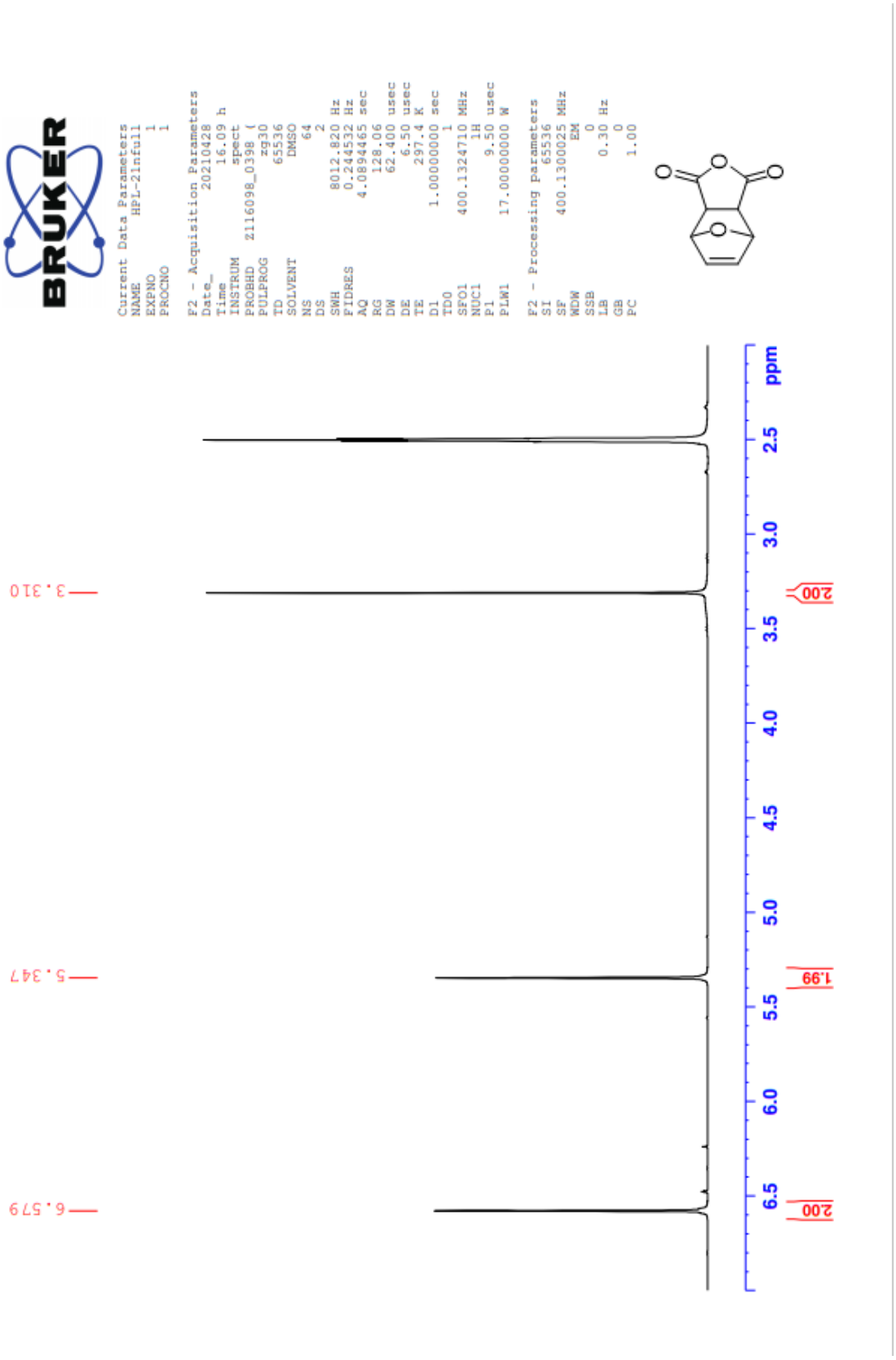

^{13}C-NMR spectrum of compound 1

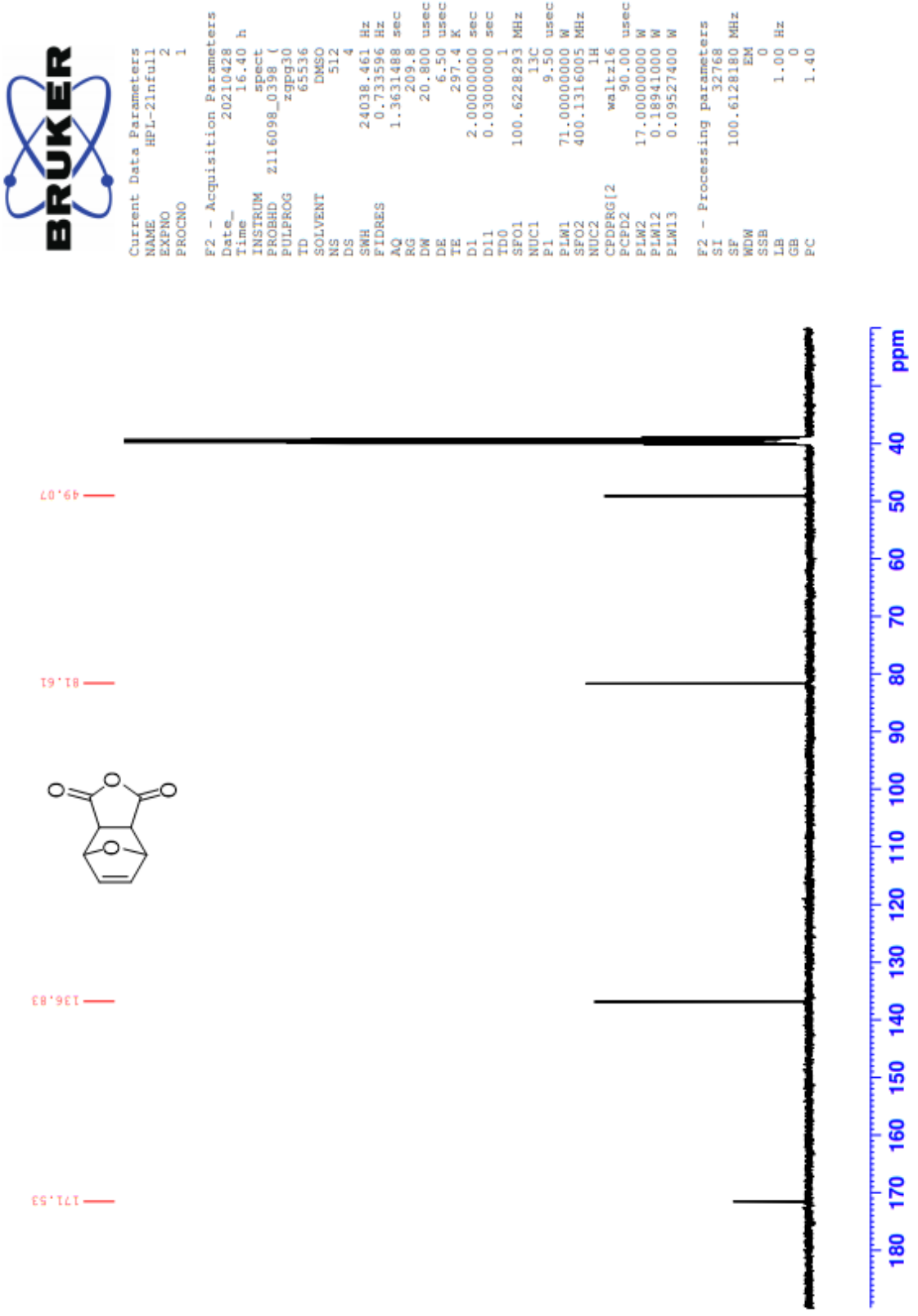

COSY spectrum of compound 1

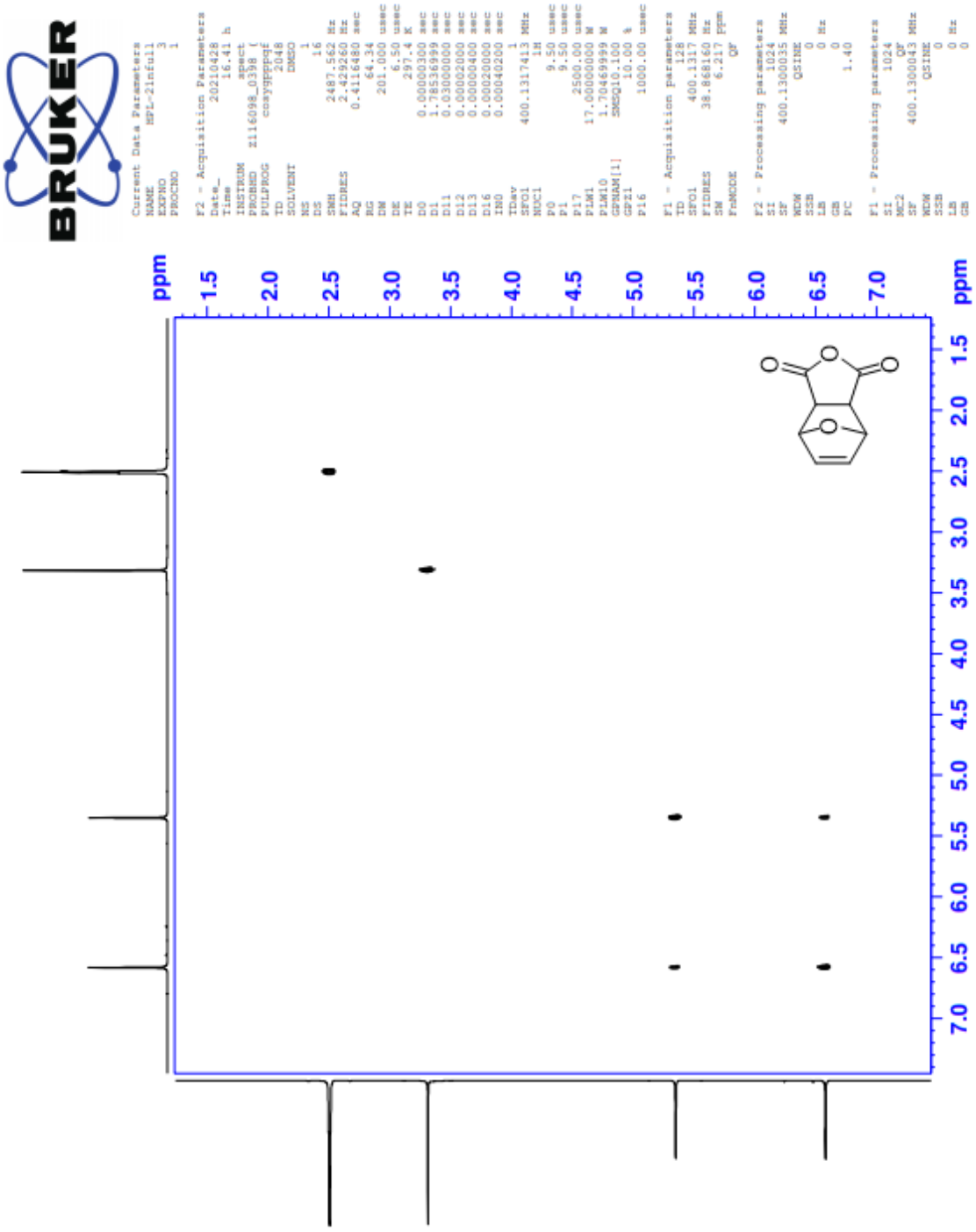

HSQC spectrum of compound 1

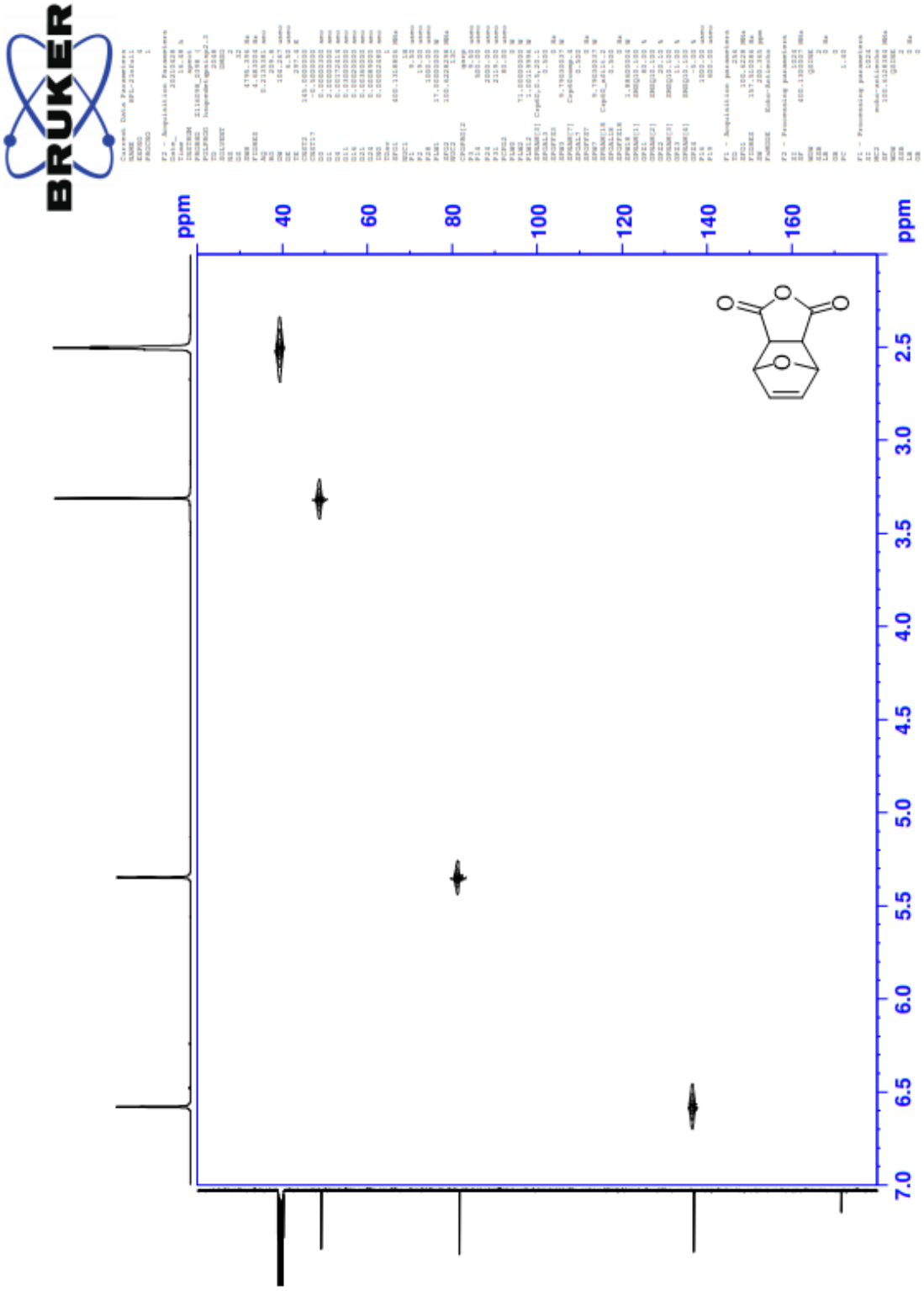

HMBC spectrum of compound 1

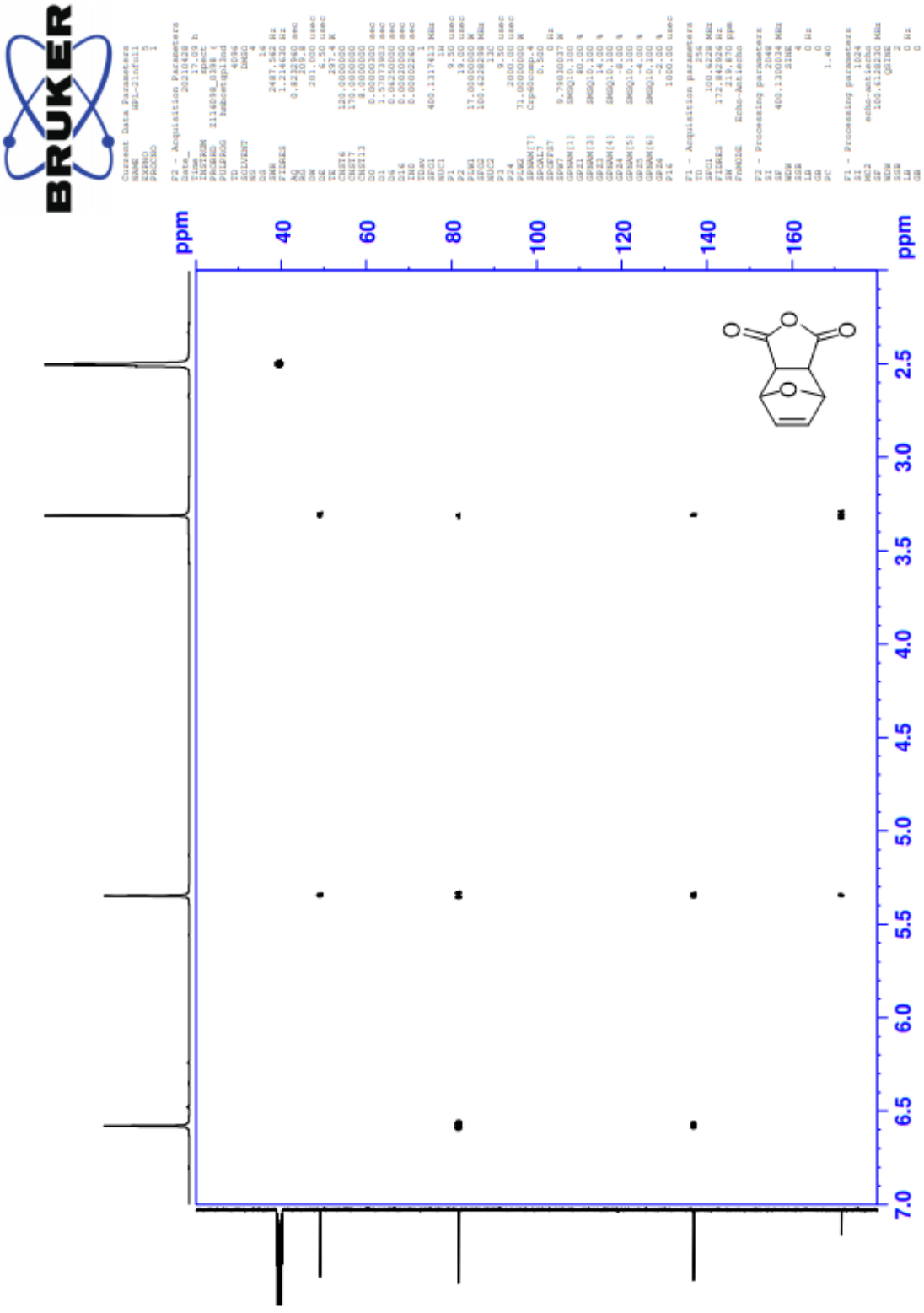

B Spectroscopic data - Compound 2

^{1}H-NMR spectrum of compound 2

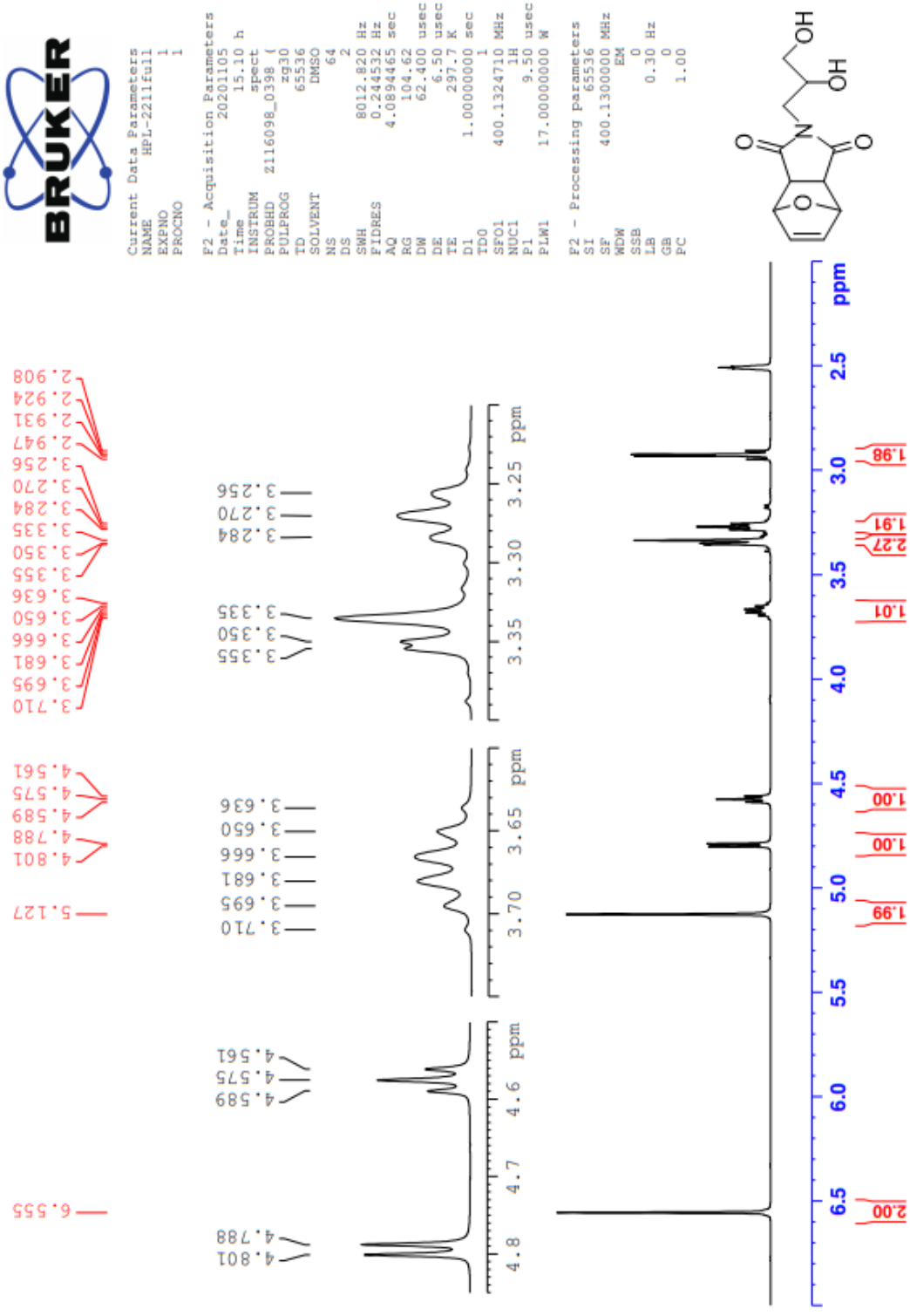

^{13}C-NMR spectrum of compound 2

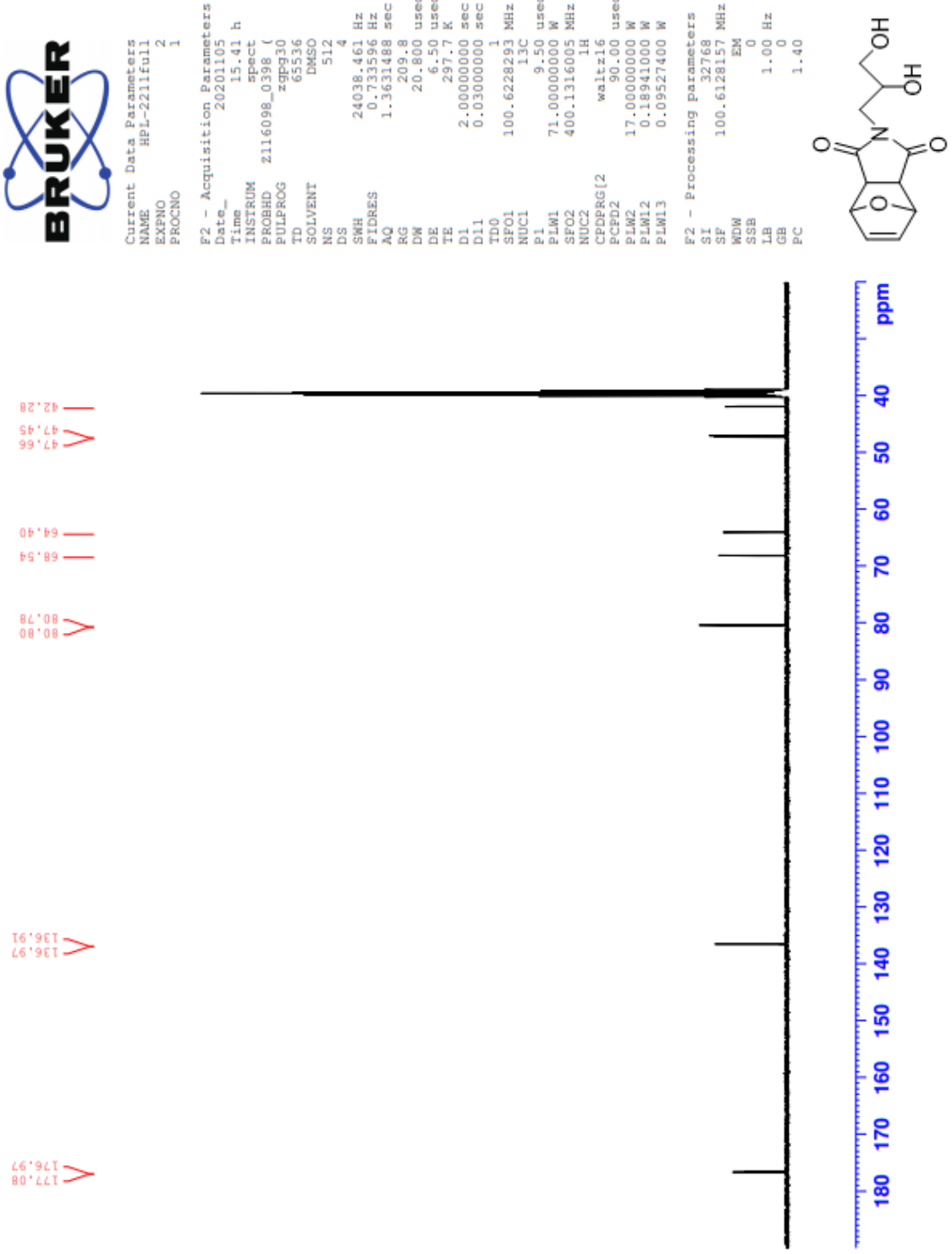

COSY spectrum of compound 2

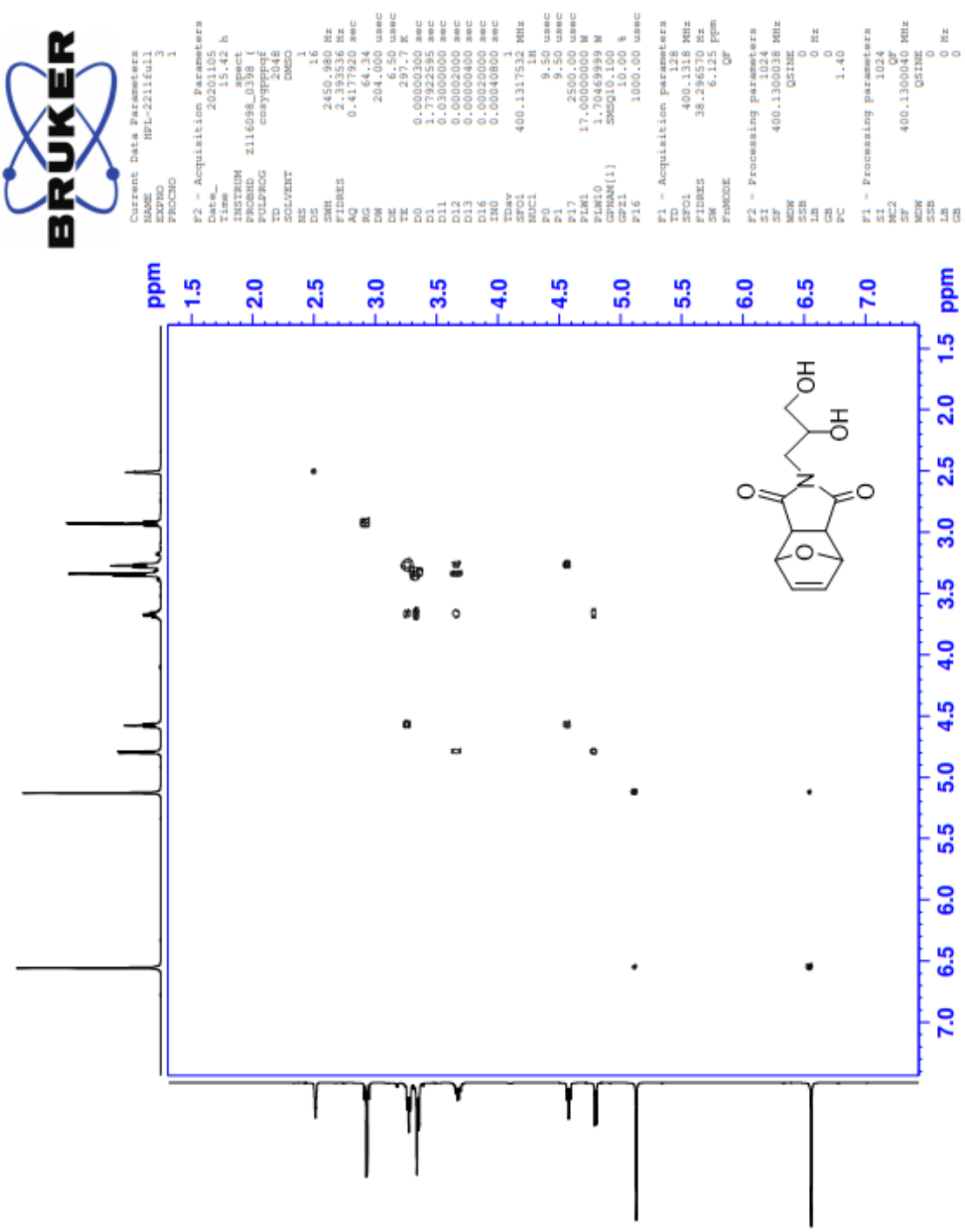

HSQC spectrum of compound 2

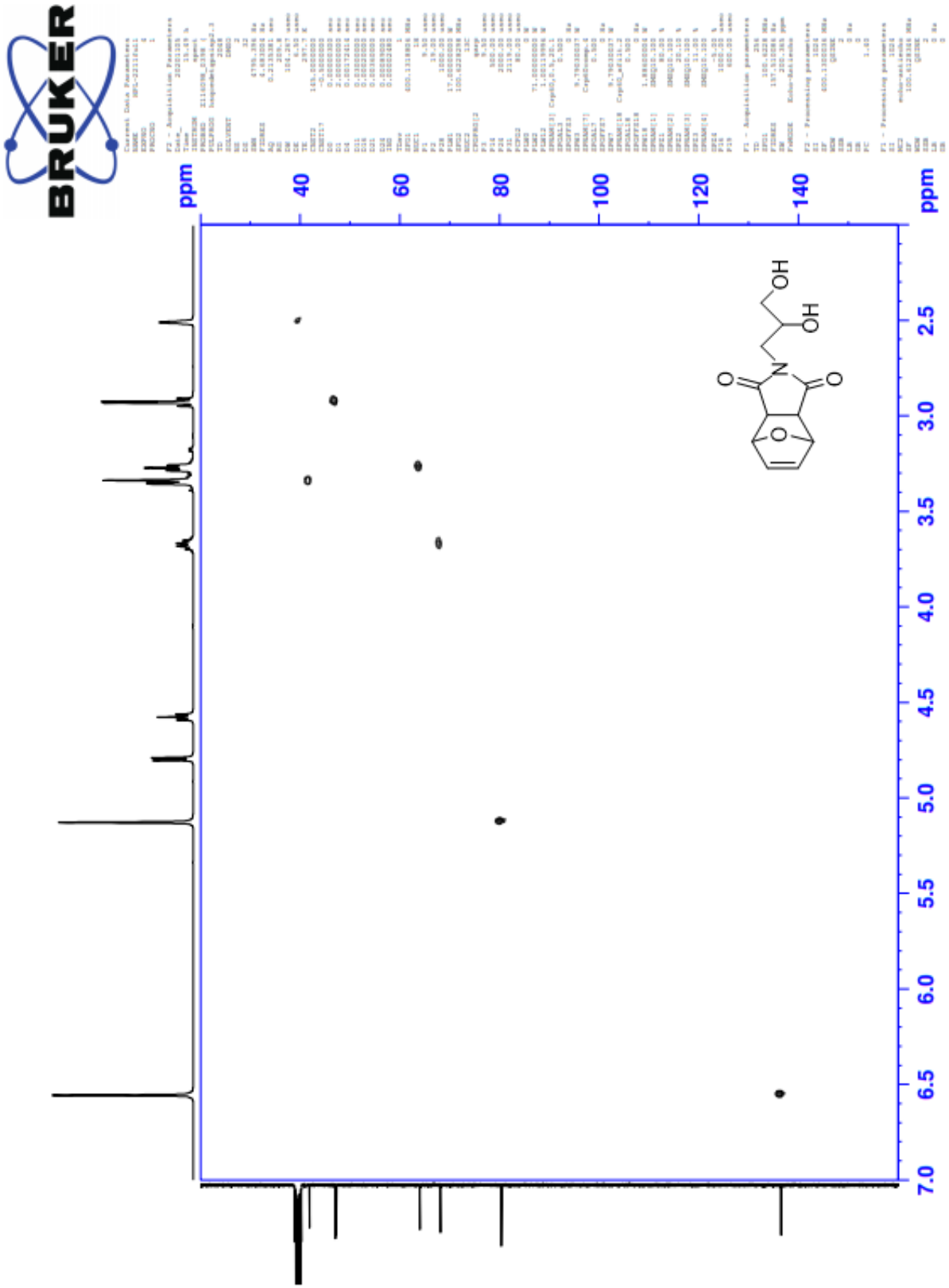

HMBC spectrum of compound 2

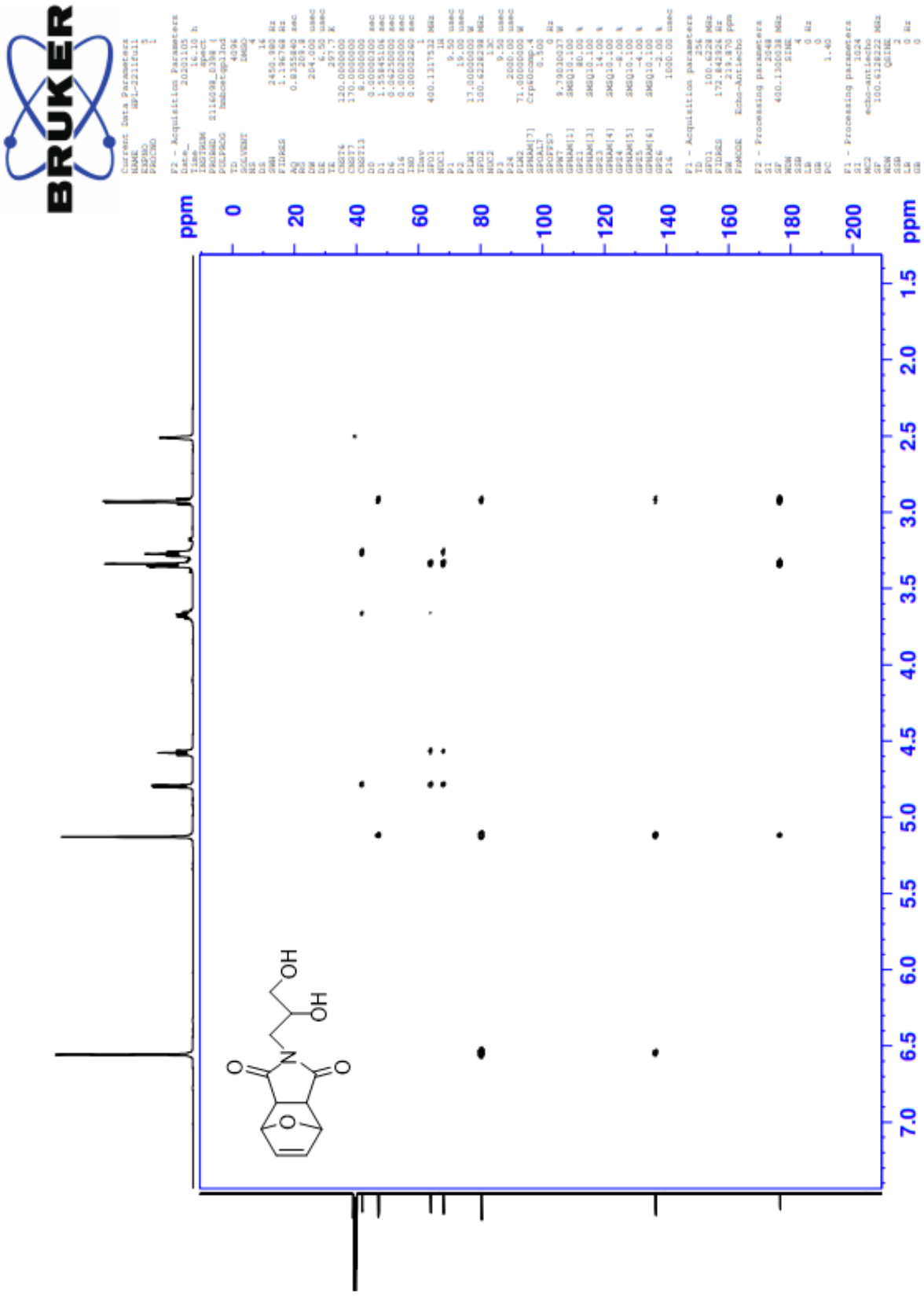

IR spectrum of compound 2

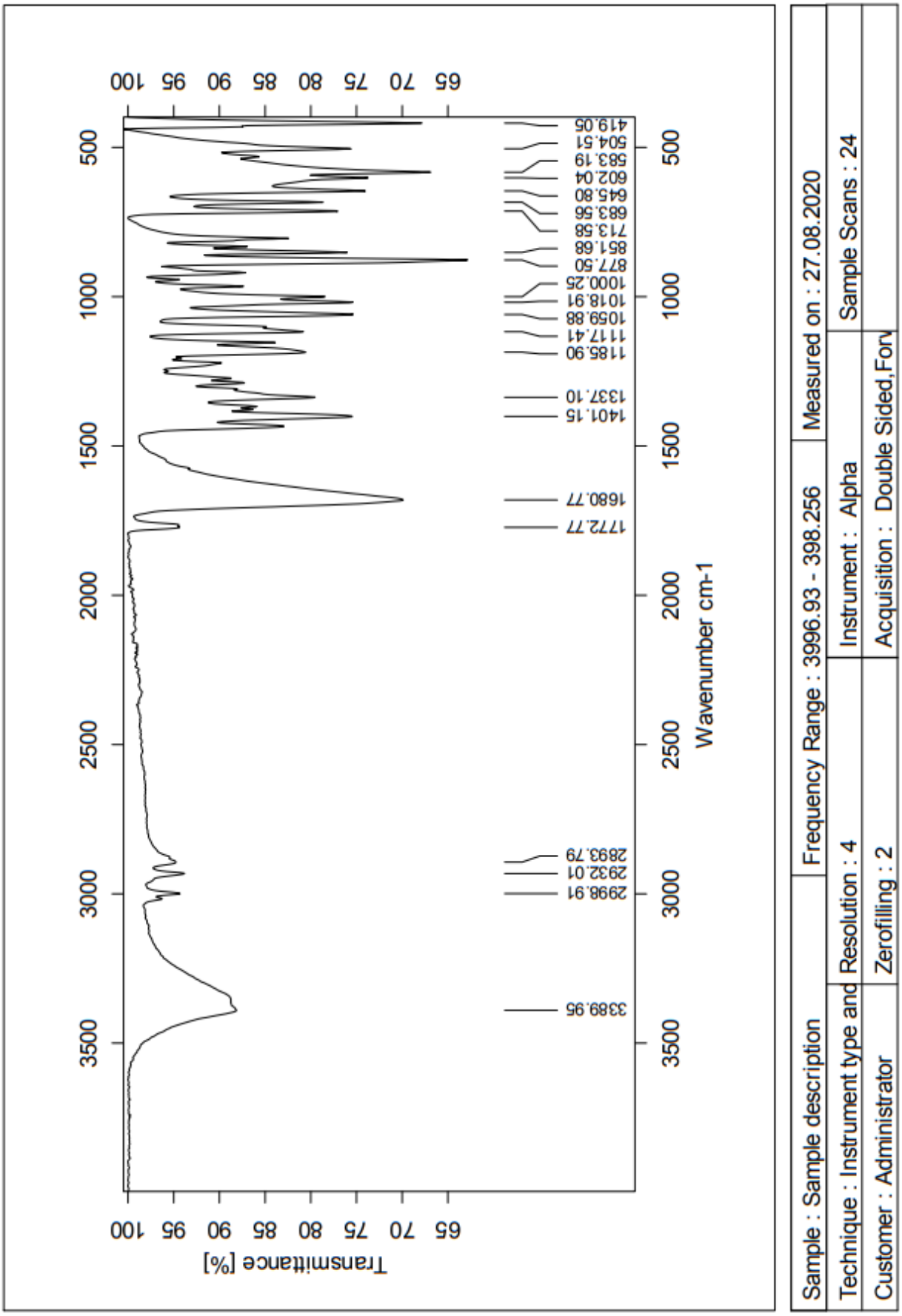

HRMS spectrum of compound 2

Elemental Composition Report **Page 1**

Single Mass Analysis
Tolerance = 2.0 PPM / DBE: min = -10.0, max = 50.0
Element prediction: Off
Number of isotope peaks used for i-FIT = 6

Monoisotopic Mass, Even Electron Ions
753 formula(e) evaluated with 1 results within limits (all results (up to 1000) for each mass)
Elements Used:
C: 0-100 H: 0-100 N: 0-10 O: 0-8 Na: 0-1
2021-251 89 (0.848) AM2 (Ar,35000.0,0.00,0.00); Cm (89:99)
1: TOF MS ES+

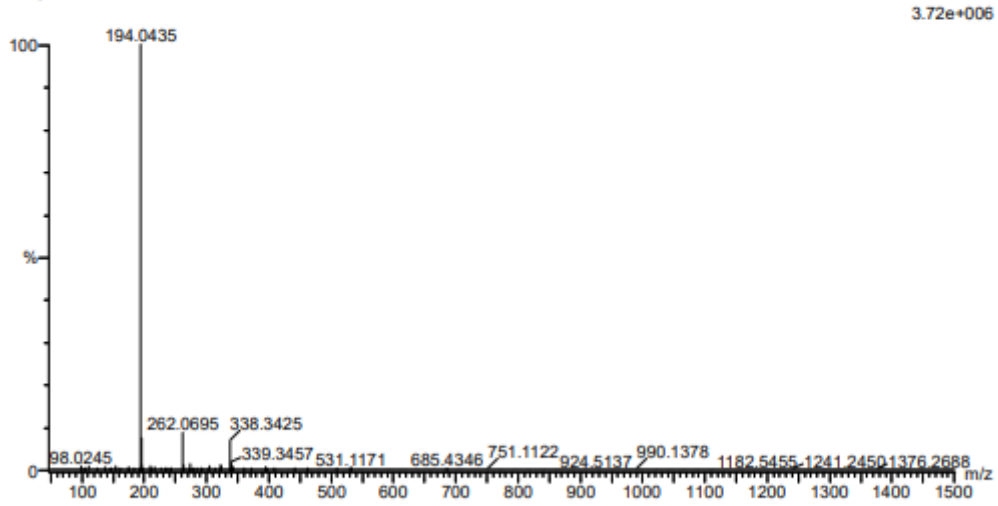

Minimum:				-10.0				
Maximum:		5.0	2.0	50.0				
Mass	Calc. Mass	mDa	PPM	DBE	i-FIT	Norm	Conf(%)	Formula
262.0695	262.0691	0.4	1.5	5.5	2835.9	n/a	n/a	C11 H13 N O5 Na

C Spectroscopic data - Compound 3

^{1}H-NMR spectrum of compound 3

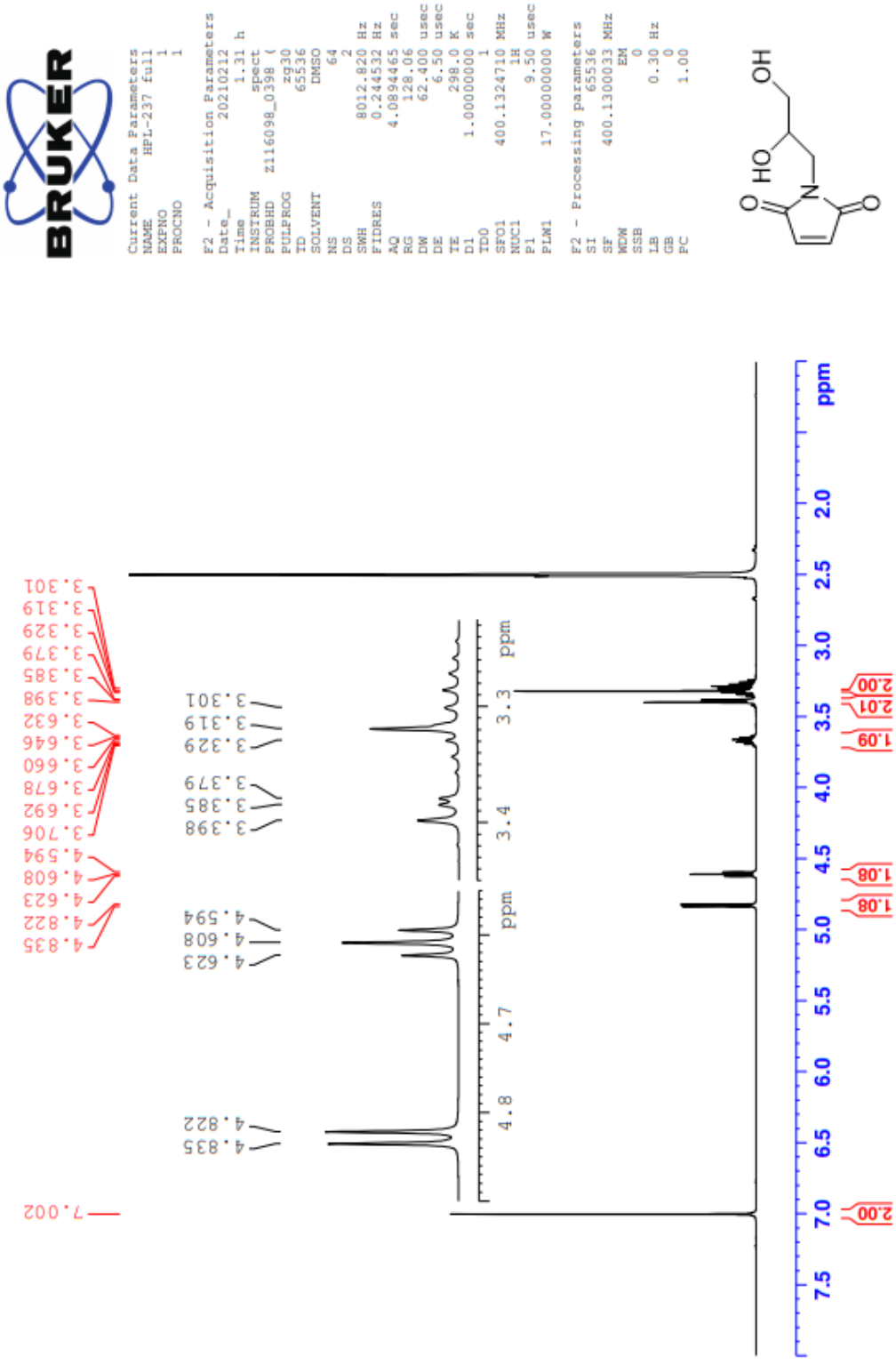

^{13}C-NMR spectrum of compound 3

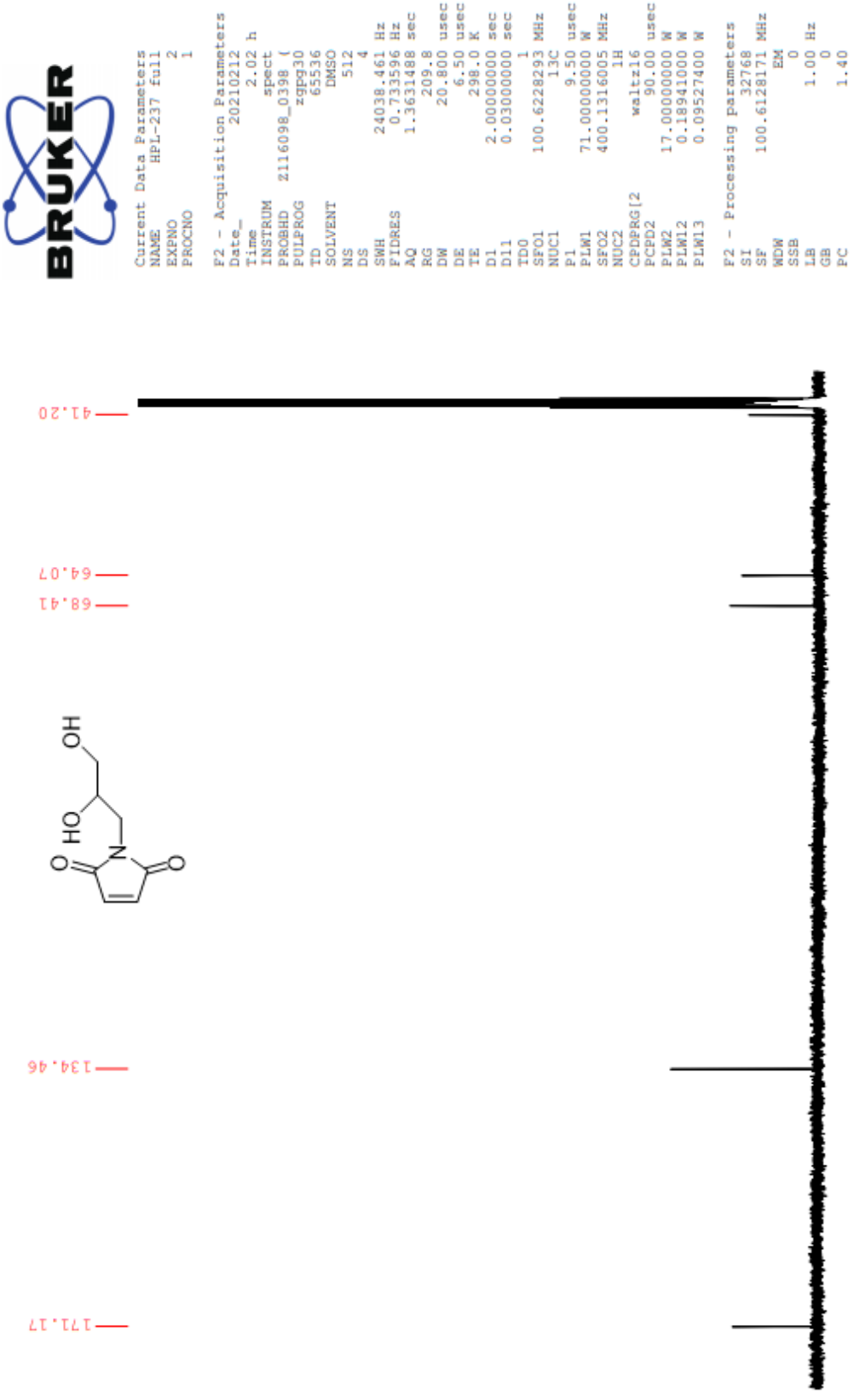

COSY spectrum of compound 3

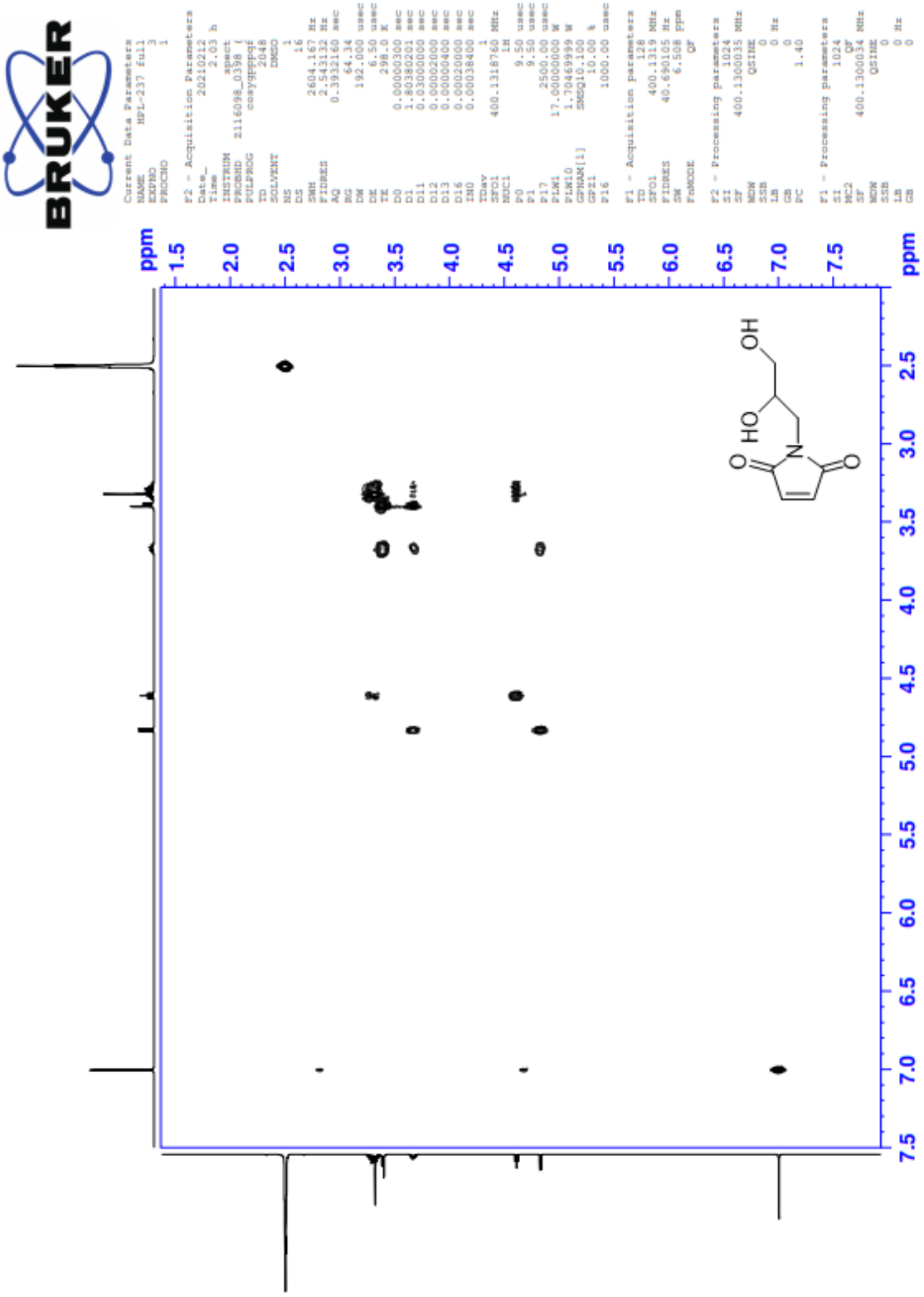

HSQC spectrum of compound 3

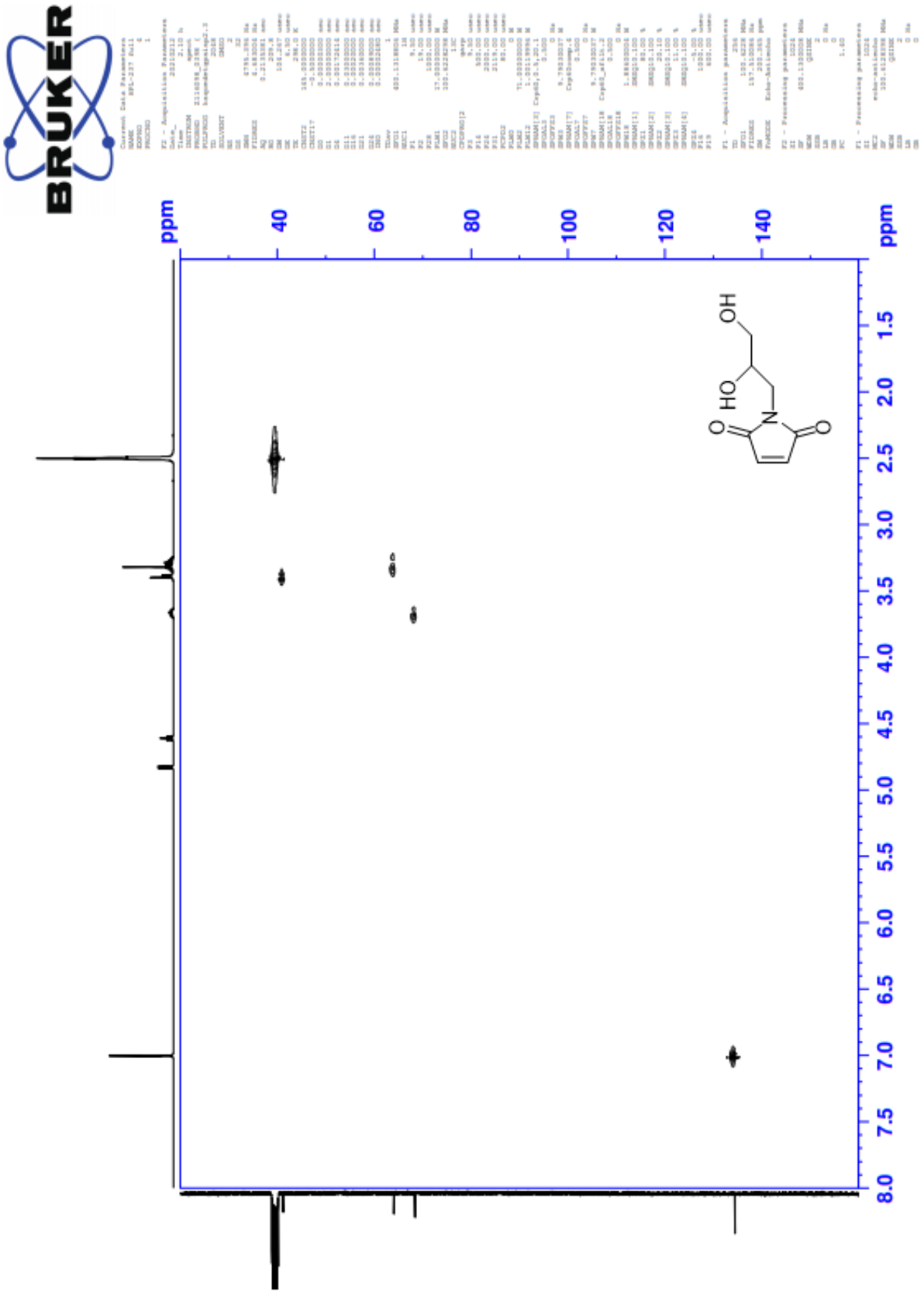

HMBC spectrum of compound 3

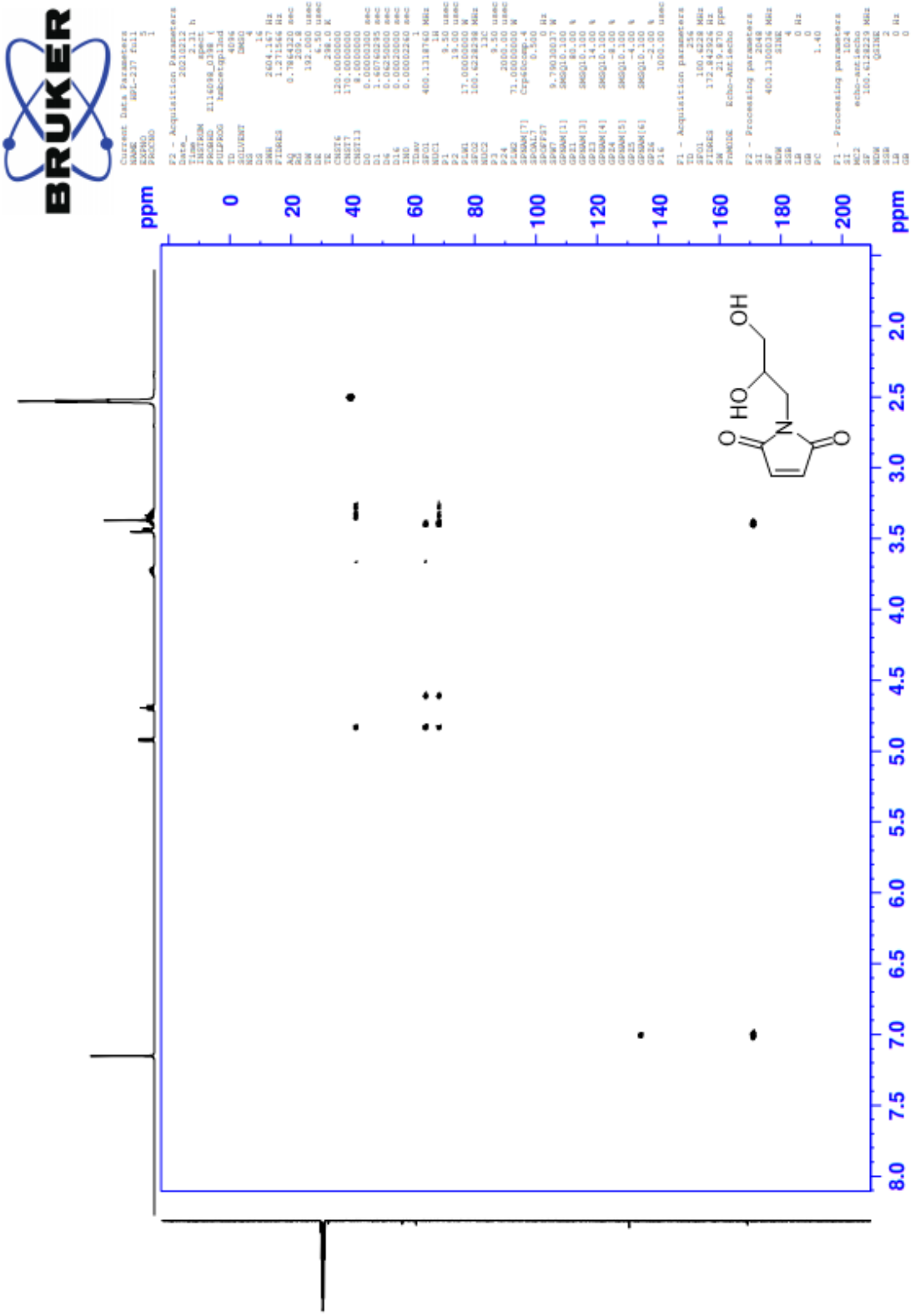

IR spectrum of compound 3

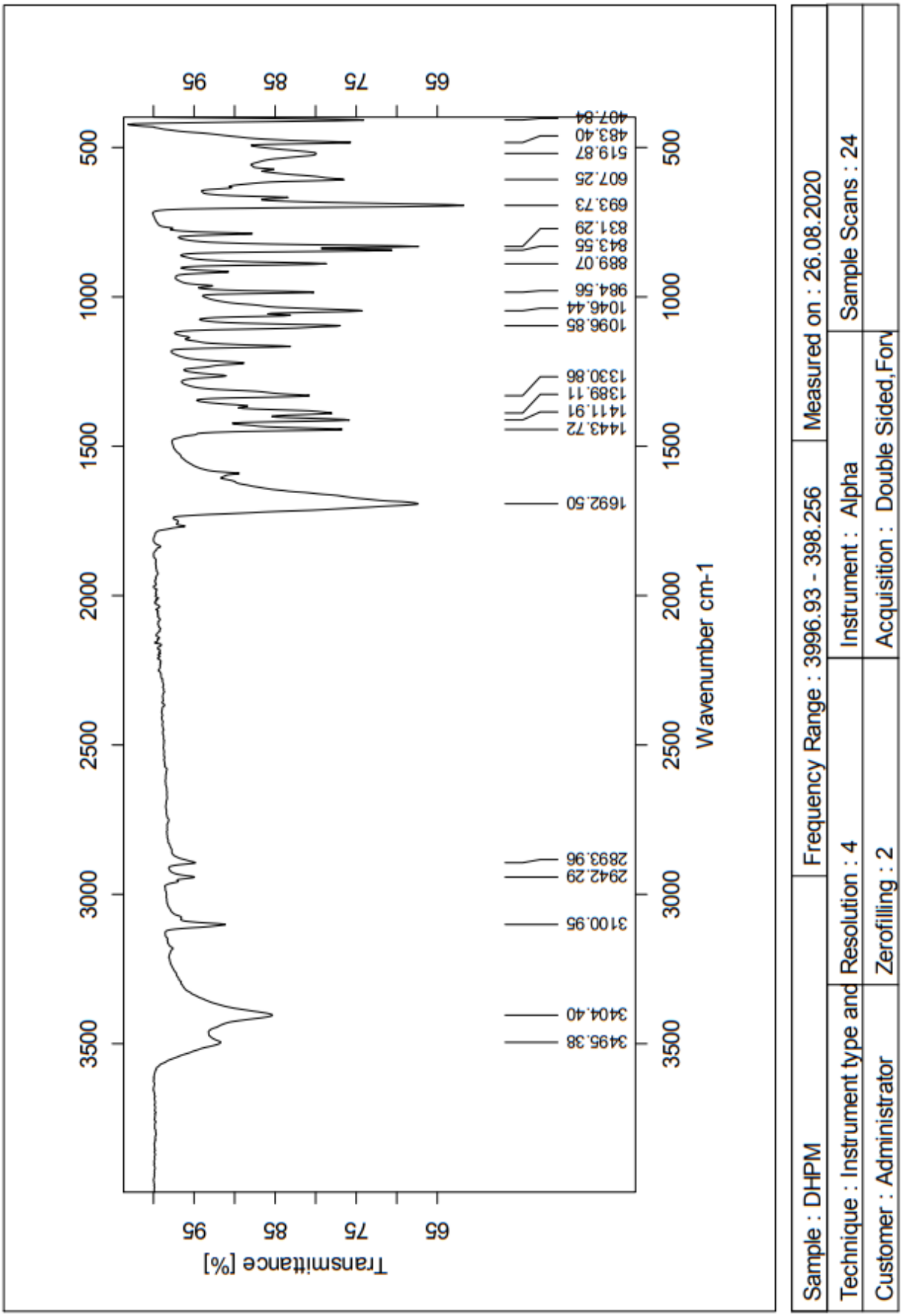

HRMS spectrum of compound 3

Elemental Composition Report **Page 1**

Single Mass Analysis
Tolerance = 2.0 PPM / DBE: min = -10.0, max = 50.0
Element prediction: Off
Number of isotope peaks used for i-FIT = 6

Monoisotopic Mass, Even Electron Ions
485 formula(e) evaluated with 1 results within limits (all results (up to 1000) for each mass)
Elements Used:
C: 0-100 H: 0-100 N: 0-10 O: 0-8 Na: 0-1
2021-250 65 (0.622) AM2 (Ar,35000.0,0.00,0.00); Cm (59:65)
1: TOF MS ES+

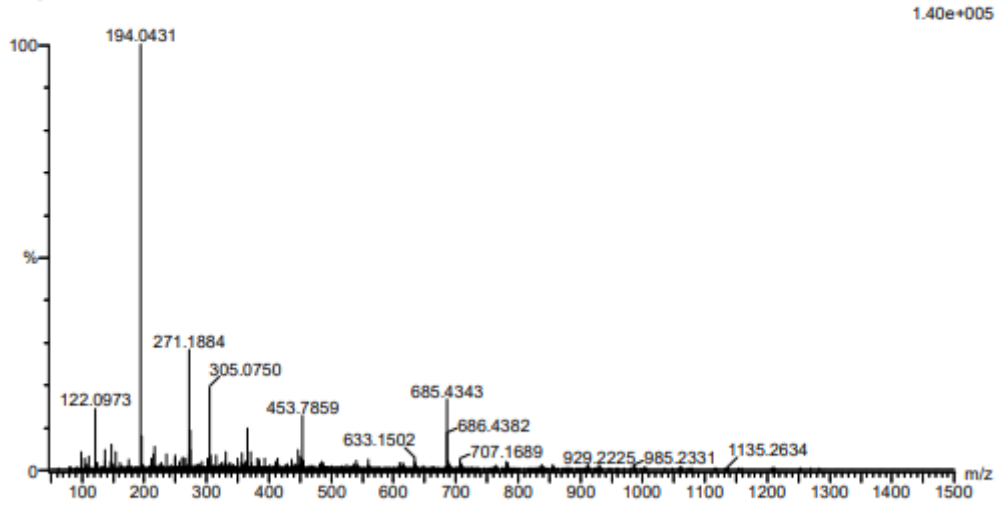

Minimum:				-10.0				
Maximum:		5.0	2.0	50.0				
Mass	Calc. Mass	mDa	PPM	DBE	i-FIT	Norm	Conf(%)	Formula
194.0431	194.0429	0.2	1.0	3.5	2312.1	n/a	n/a	C7 H9 N O4 Na

D Spectroscopic data - Compound 4

^{1}H-NMR spectrum of compound 4

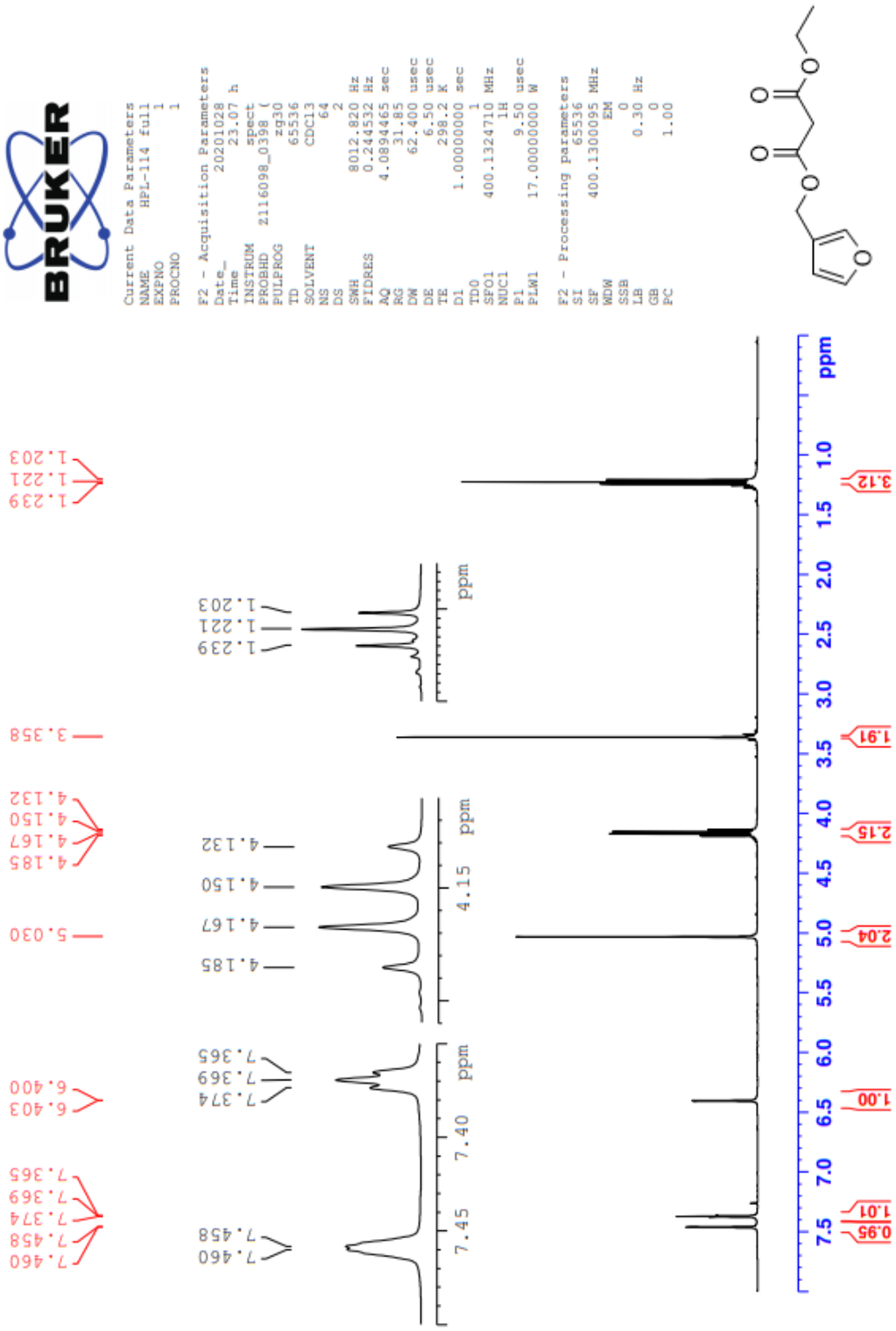

^{13}C-NMR spectrum of compound 4

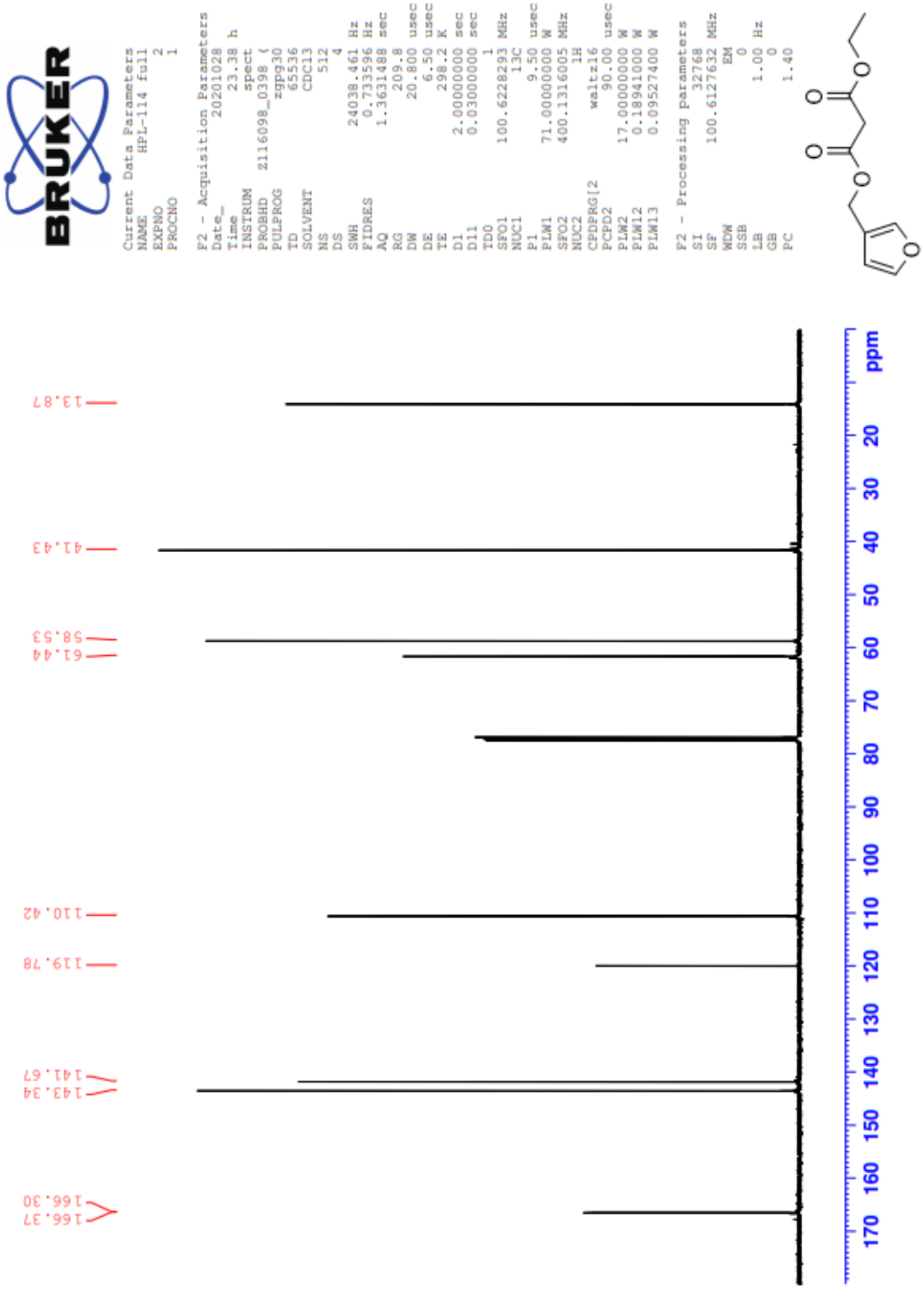

COSY spectrum of compound 4

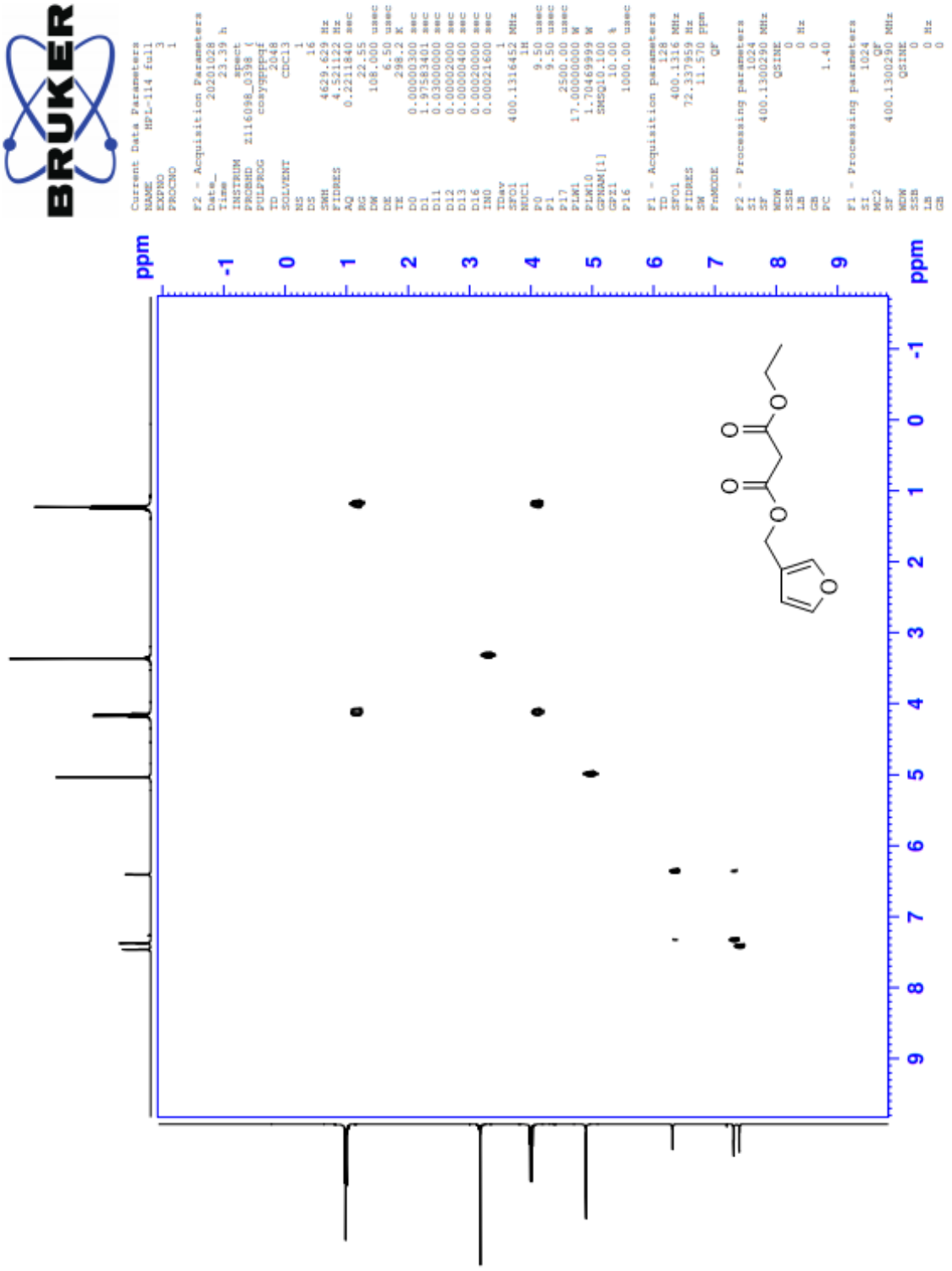

HSQC spectrum of compound 4

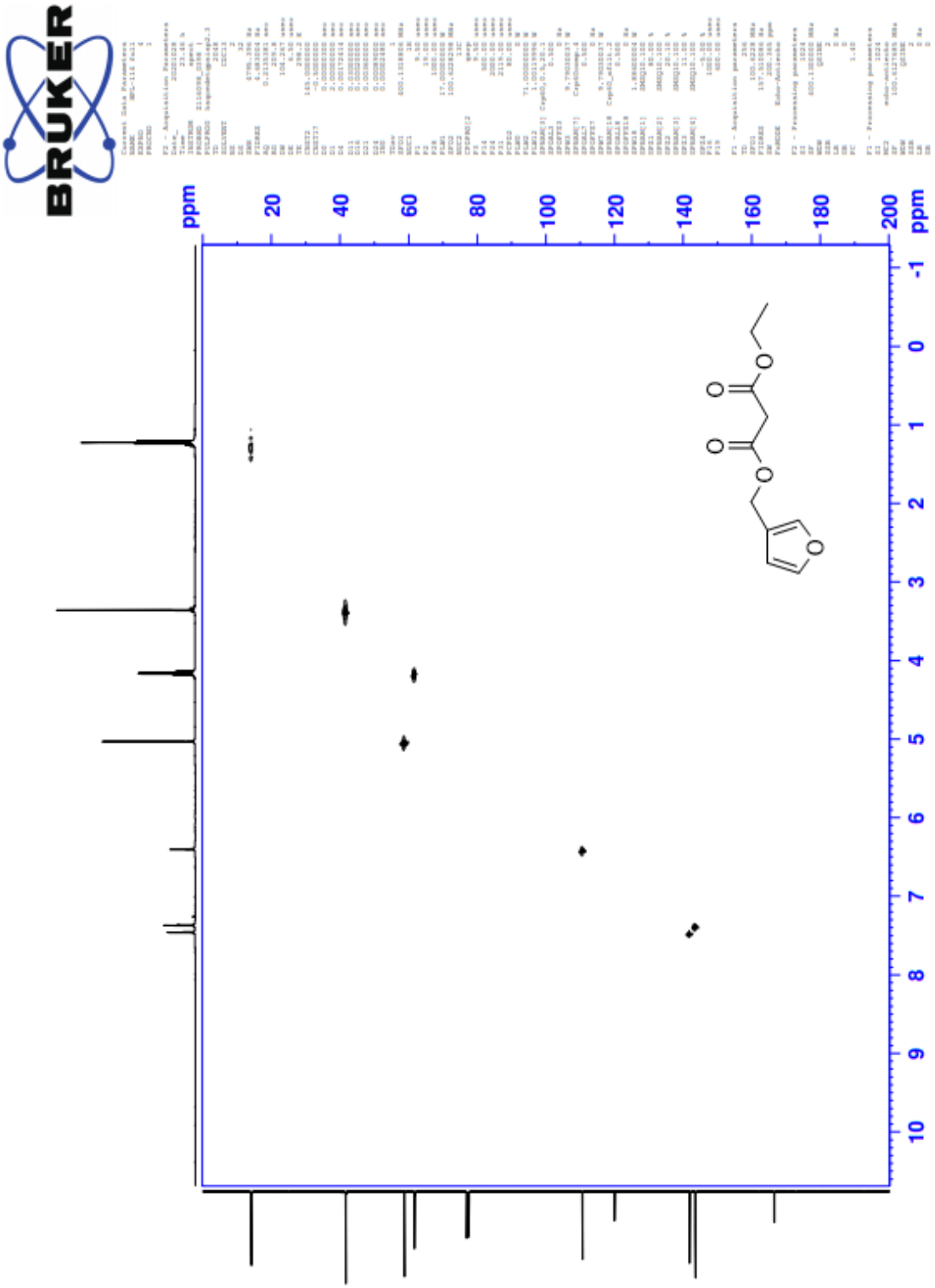

HMBC spectrum of compound 4

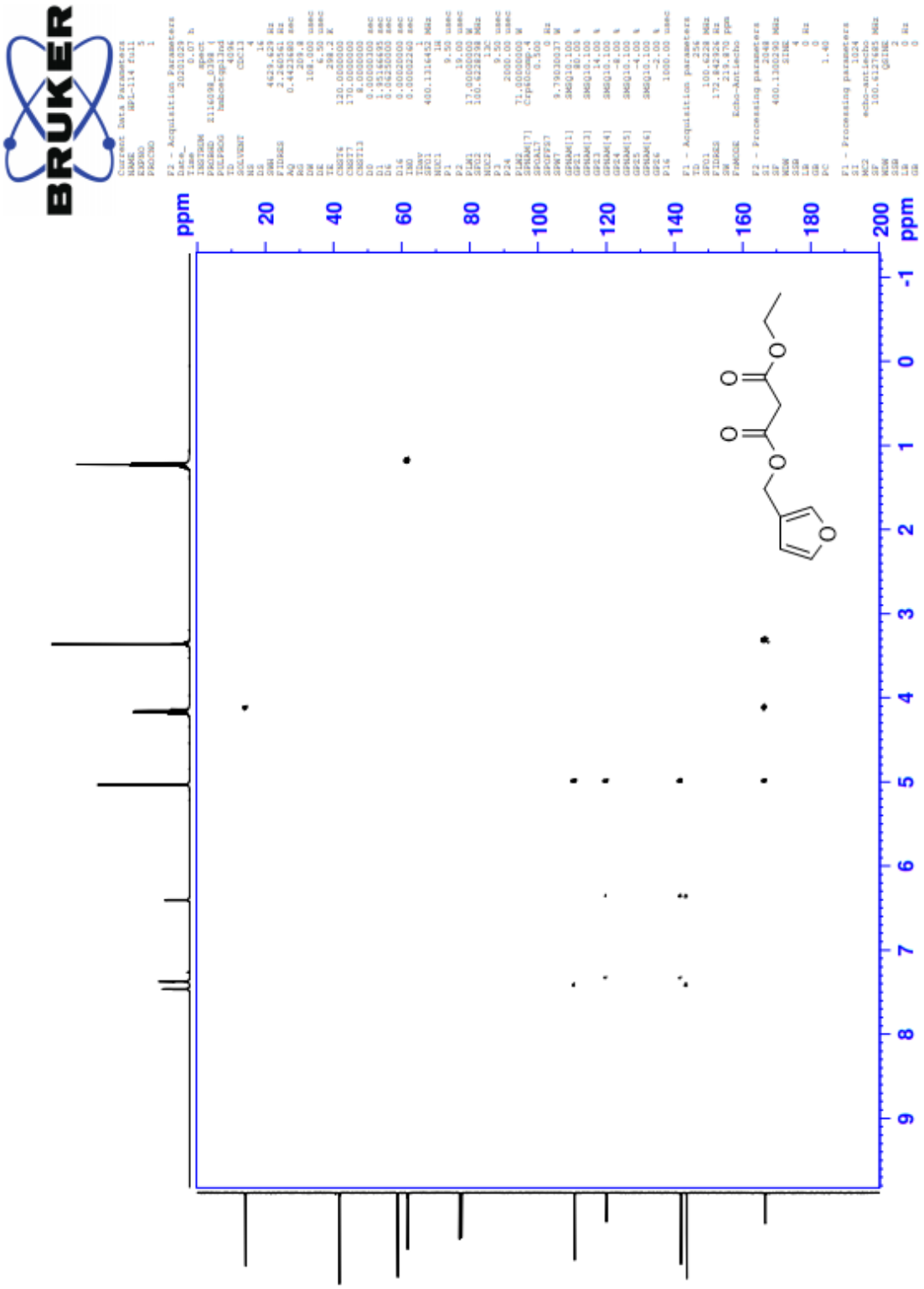

IR spectrum of compound 4

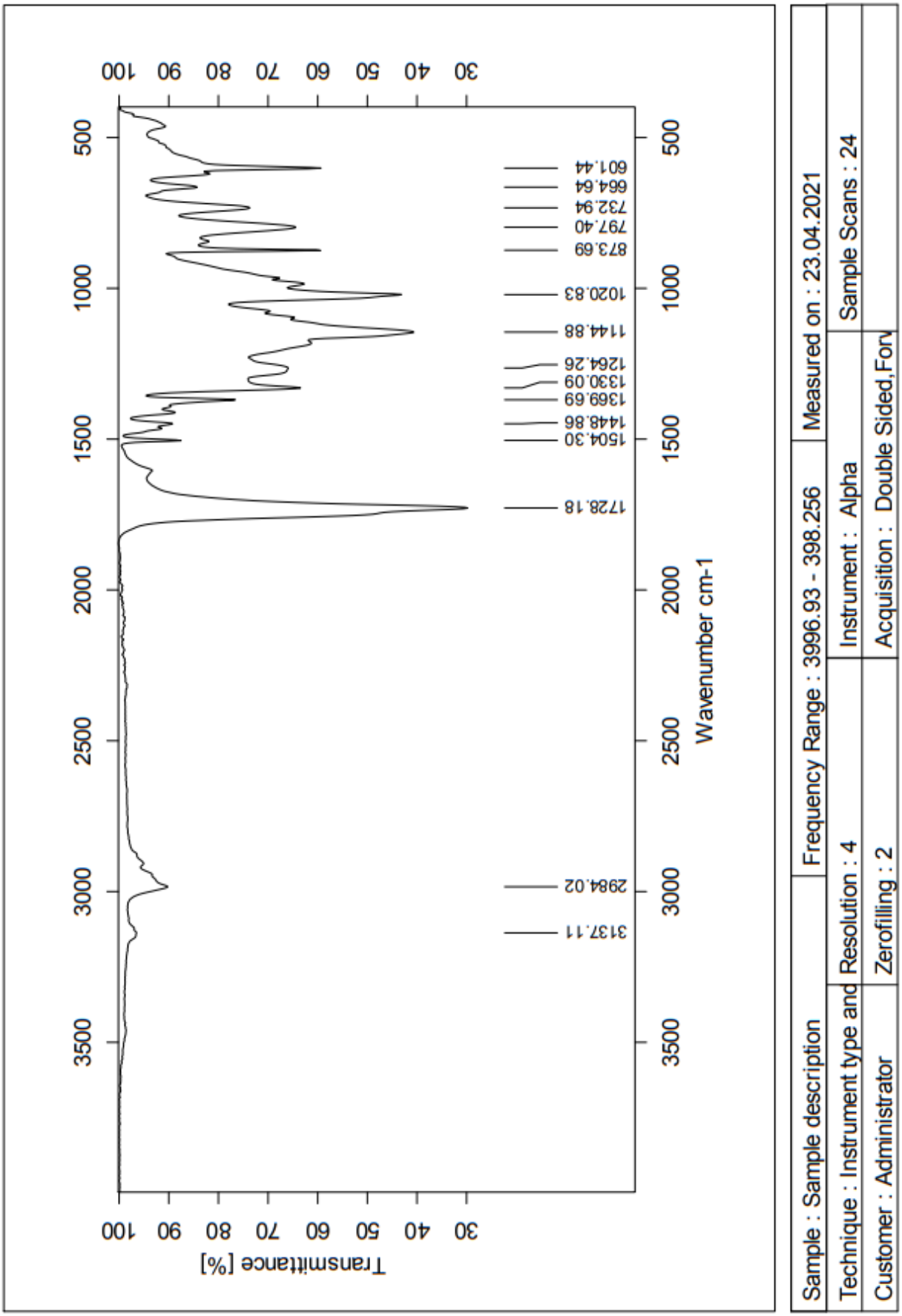

HRMS spectrum of compound 4

Elemental Composition Report **Page 1**

Single Mass Analysis
Tolerance = 2.0 PPM / DBE: min = -1.5, max = 50.0
Element prediction: Off
Number of isotope peaks used for i-FIT = 6

Monoisotopic Mass, Even Electron Ions
567 formula(e) evaluated with 1 results within limits (all results (up to 1000) for each mass)
Elements Used:
C: 0-100 H: 0-100 N: 0-10 O: 0-10 Na: 0-1 I: 0-2

2020_534rerun 69 (0.656) AM2 (Ar,35000.0,0.00,0.00); Cm (67:73)
1: TOF MS ES+

3.40e+005

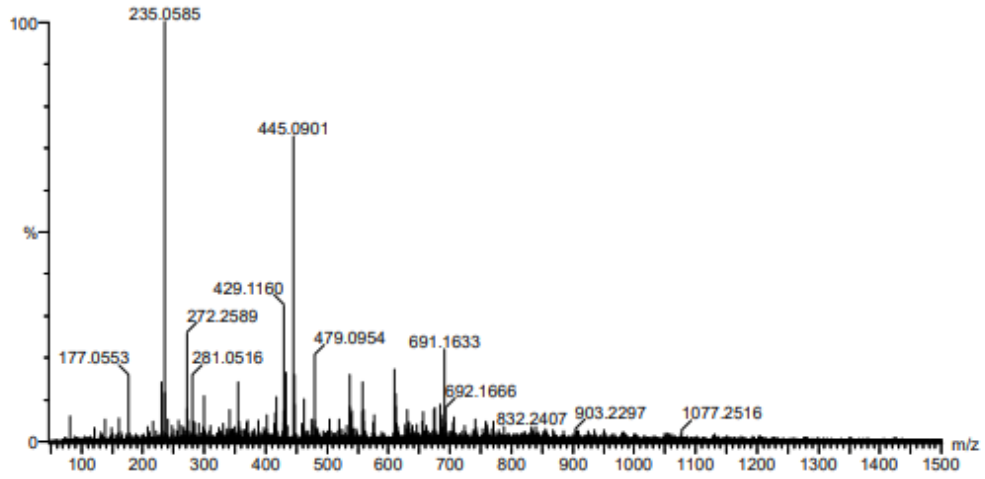

Minimum:				-1.5				
Maximum:		5.0	2.0	50.0				
Mass	Calc. Mass	mDa	PPM	DBE	i-FIT	Norm	Conf(%)	Formula
235.0585	235.0582	0.3	1.3	4.5	2669.8	n/a	n/a	C10 H12 O5 Na

E Spectroscopic data - Exfoliated Graphene 5

MicroRaman spectrum of graphite and graphene (5)

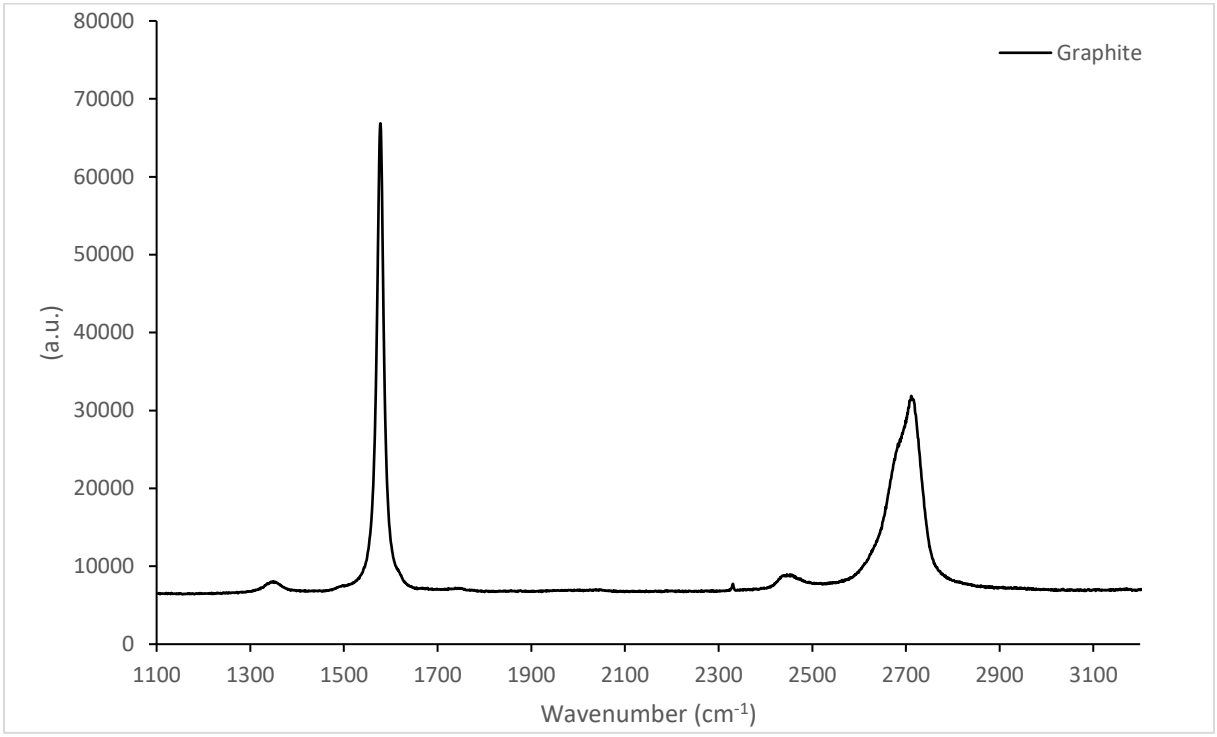

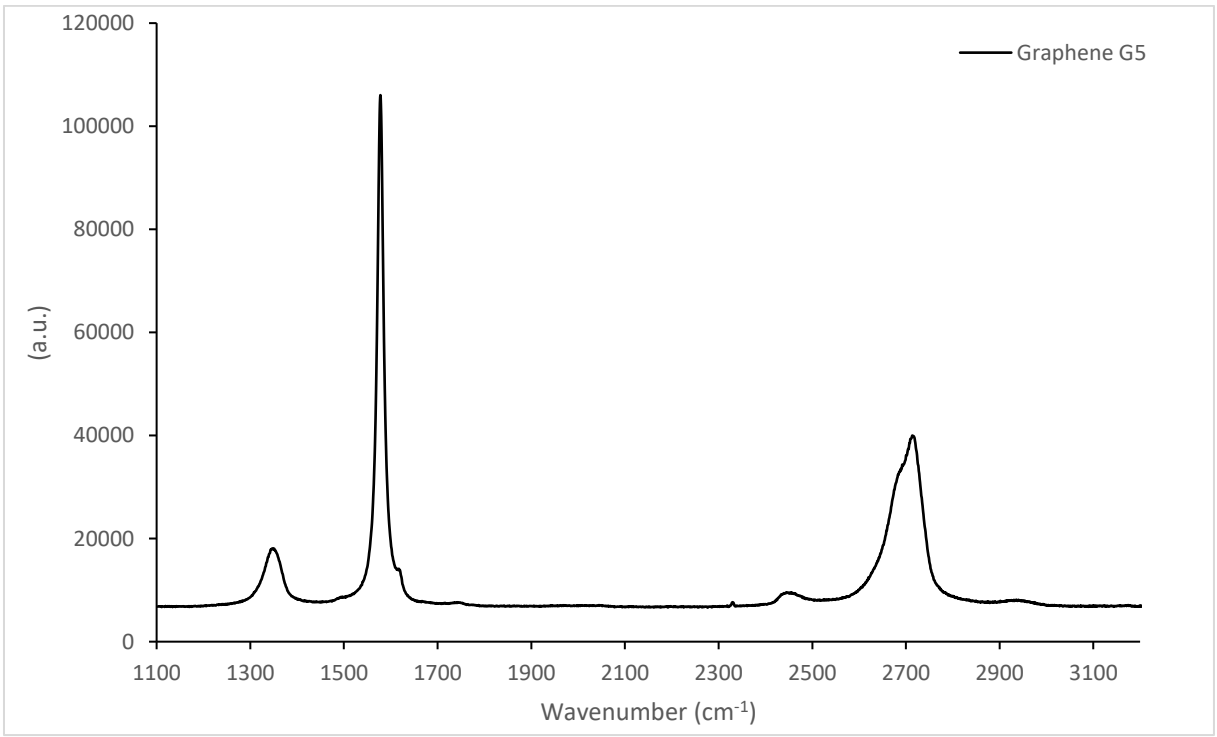

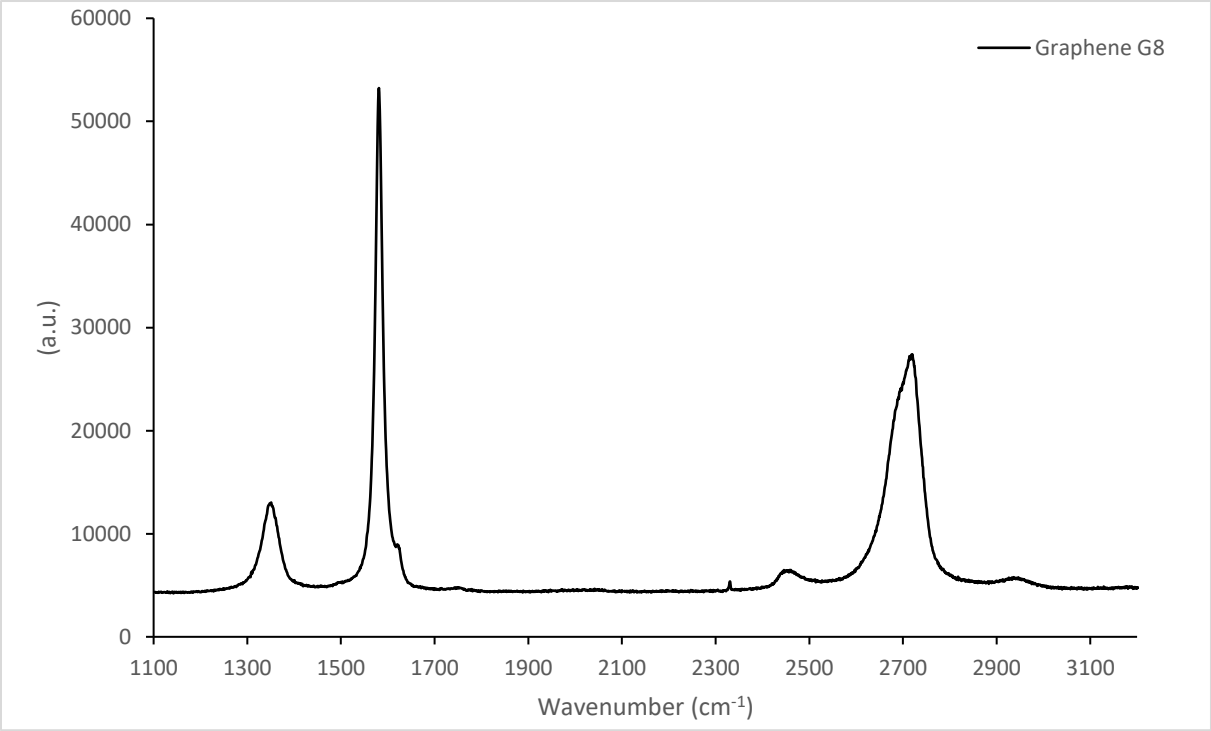
Graphene G8
60000
50000
40000
30000
20000
10000
0
(a.u.)
1100
1300
1500
1700
1900
2100
2300
2500
2700
2900
3100
Wavenumber (cm-1)

F Spectroscopic data - Bingel Graphene 6

MicroRaman spectra of Bingel graphene (6)

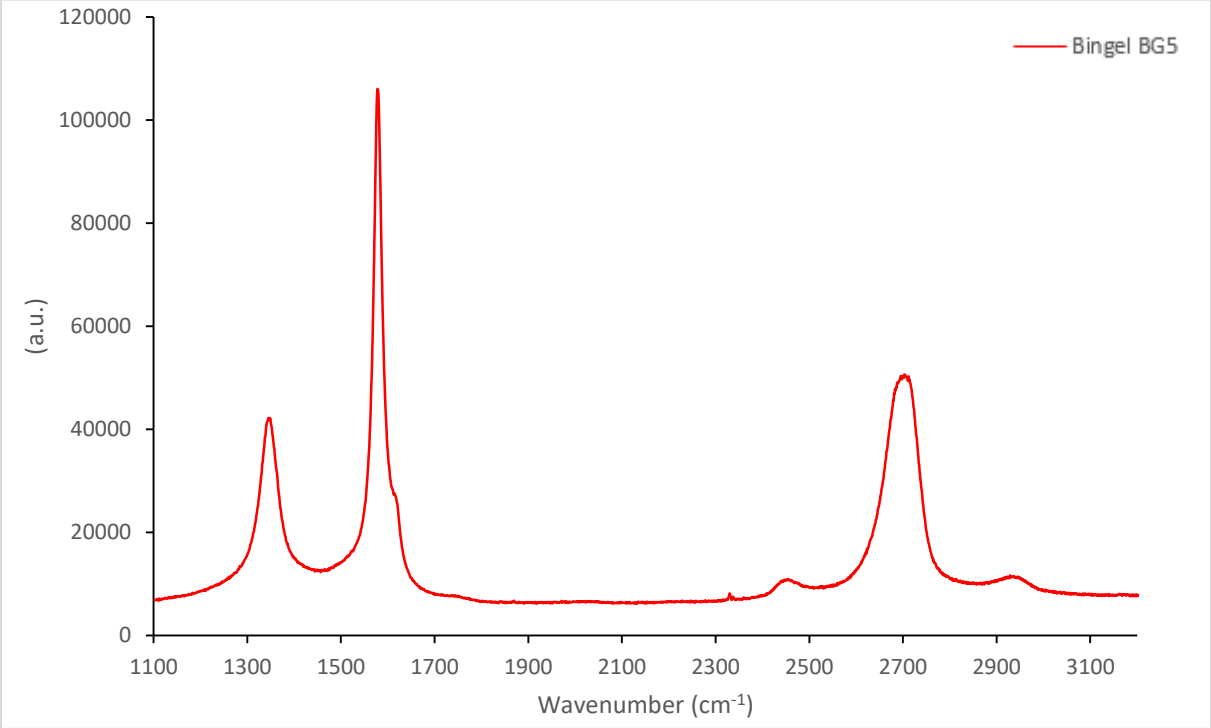

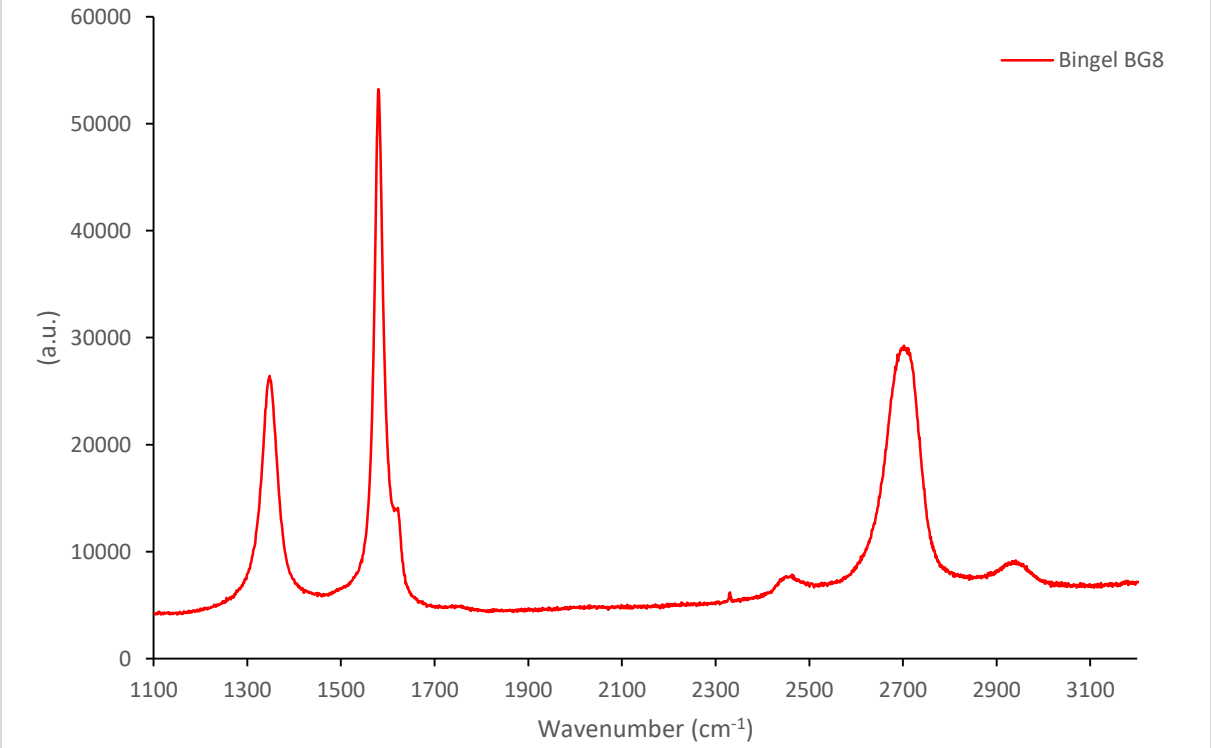

G Spectroscopic data - Compound 7

IR spectrum of compound 7

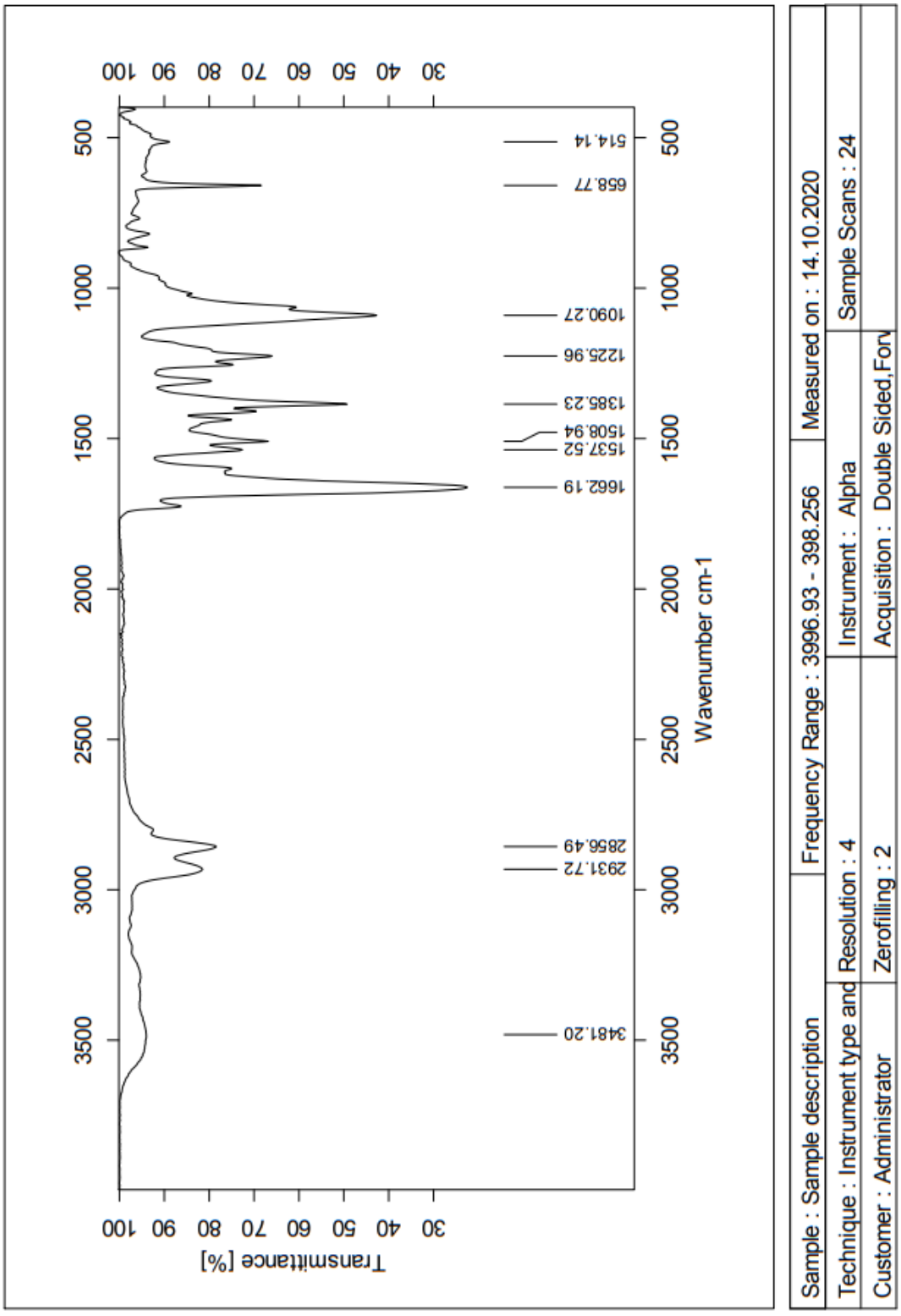

GPC report of compound 7

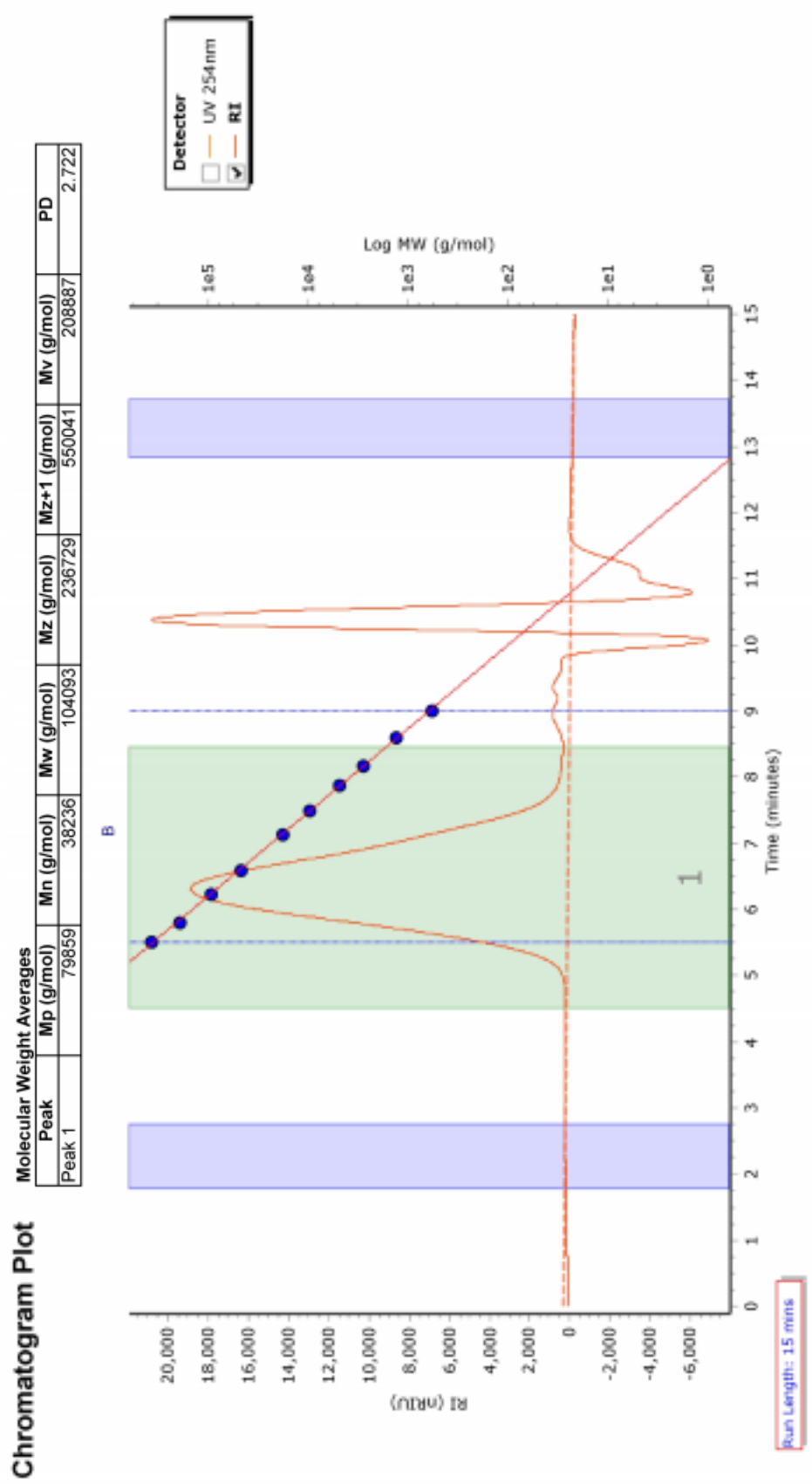

H Spectroscopic data - Compound 8

^{1}H-NMR spectrum of compound 8

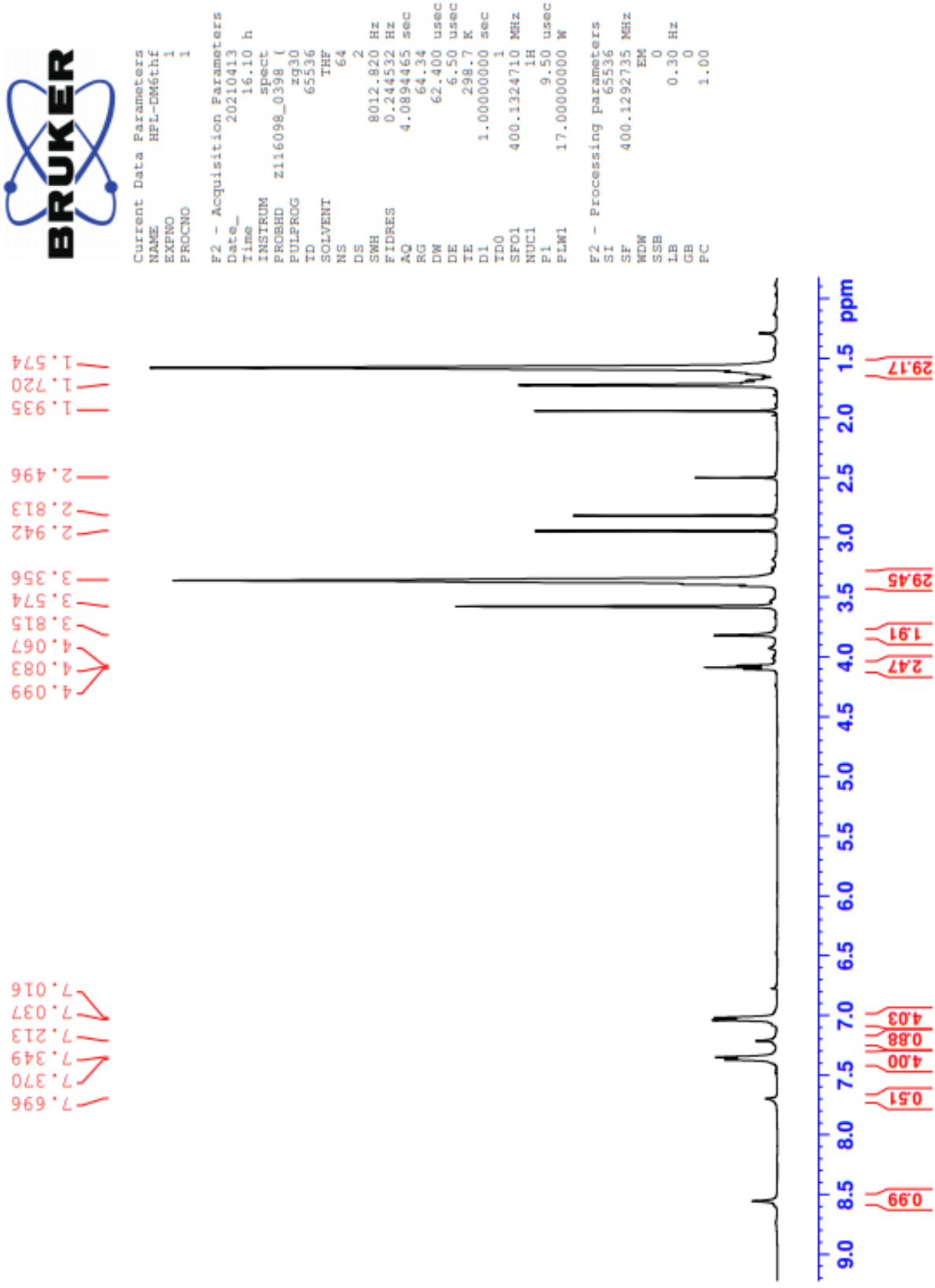

IR spectrum of compound 8

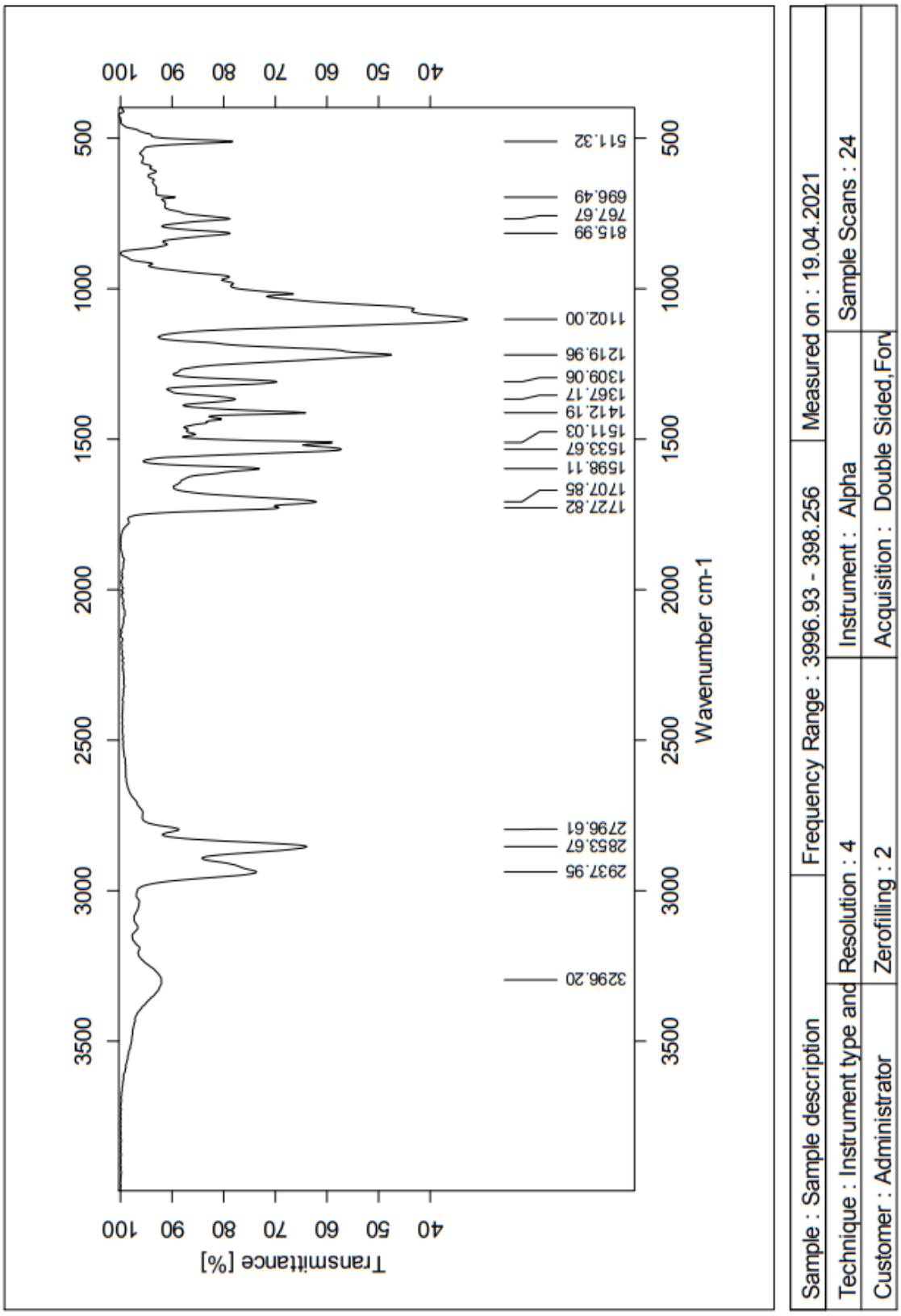

GPC report of compound 8

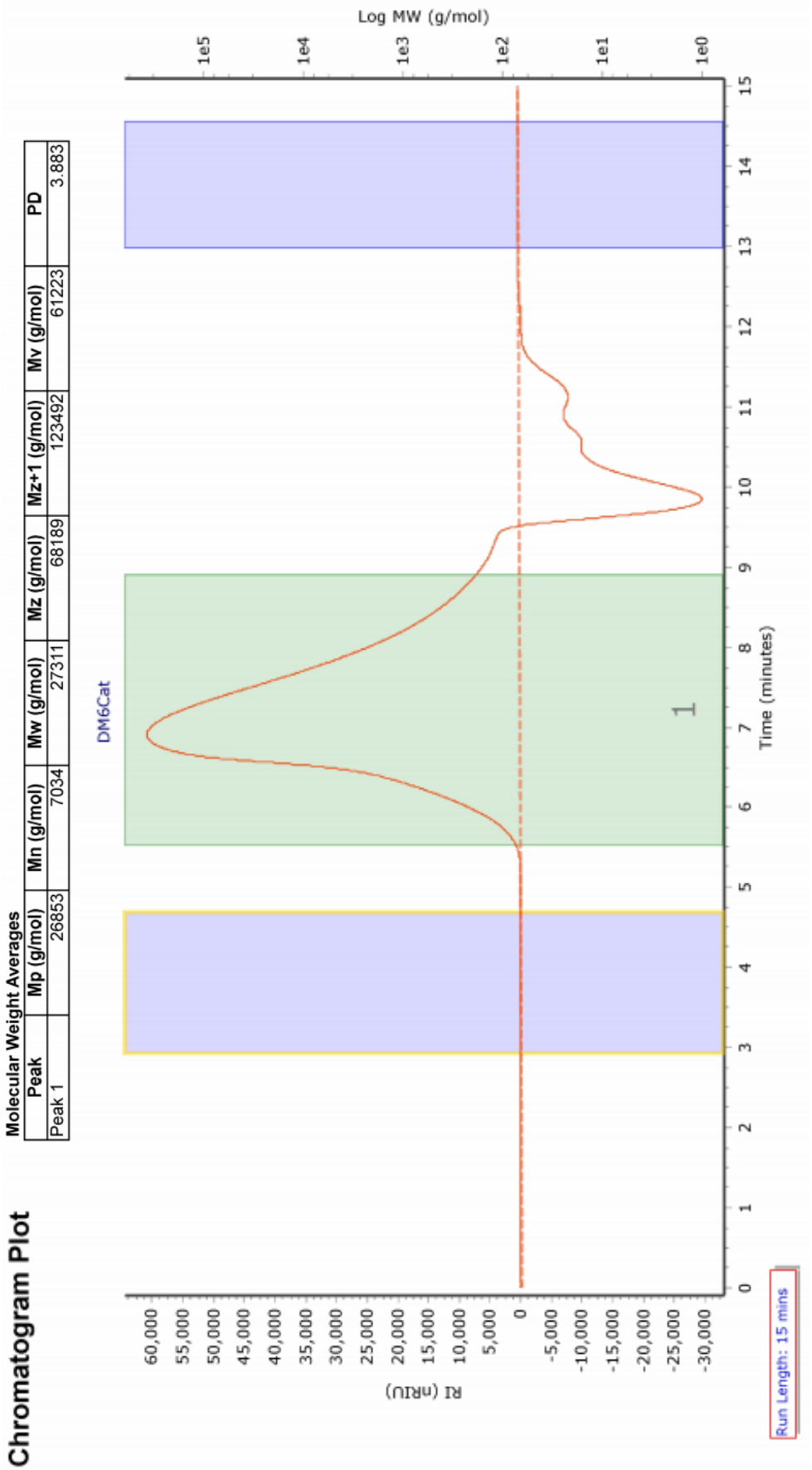

SEM imaging of compound 8

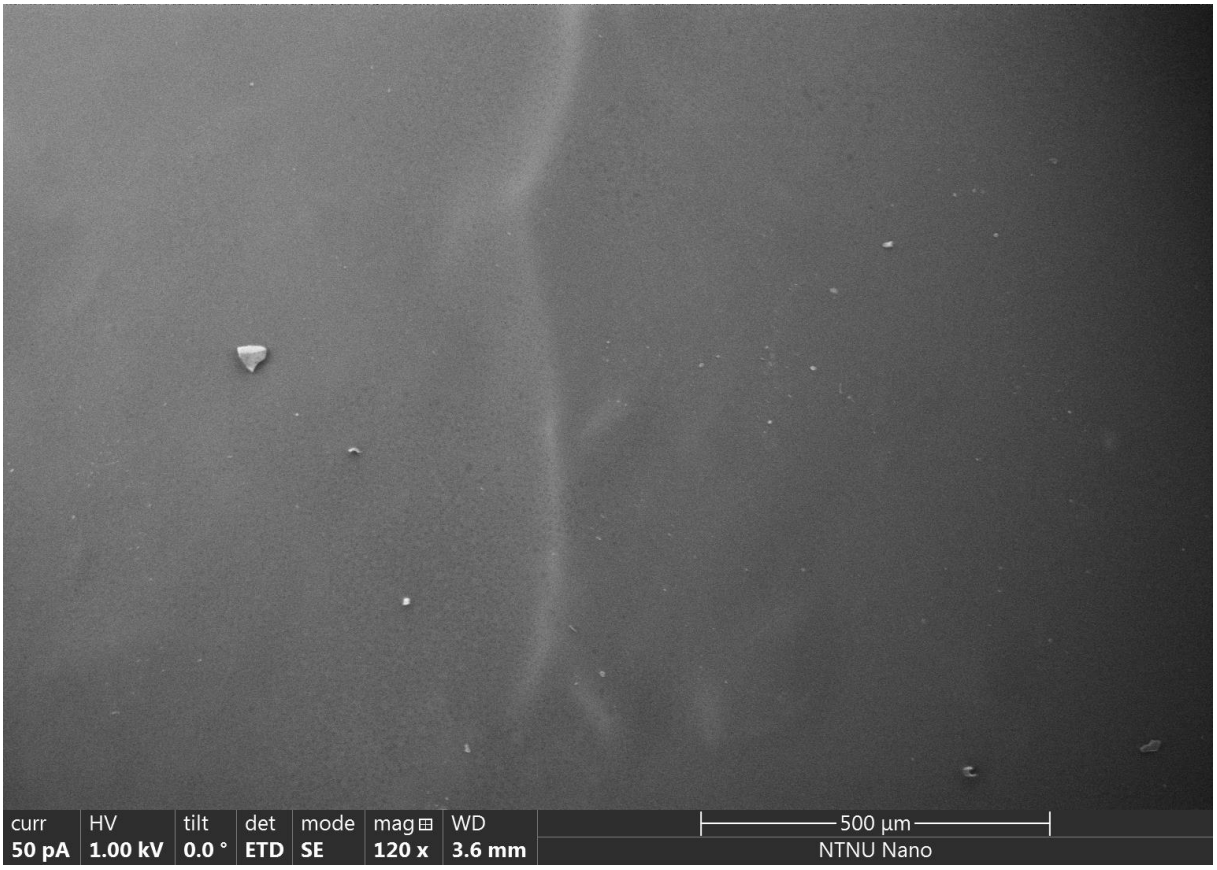

I Parameters for graphene exfoliation and microwave assisted Bingel reaction

Table 1. Parameters for Graphene exfoliation. All runs were processed with NMP as solvent, output power 90% and a sonication for 30 min.

Sample number	Solvent [mL]	Graphite [mg]	Probe	Centrifugation [min]	Centrifugation [RPM(RCF)]
G1	6	102	VS70T	2	3000(704)
G2	20	100	VS70T	2	3000(704)
G3	20	101	VS70T	5	4000(1252)
G4	20	100	VS70T	5	4000(1252)
G5-G8	20	101	VS70T	5	4000(1252)

Table 2. Amounts and settings for microwave assisted Bingel reaction.

Sample number	CBr4 [mg]	Malonate [mg, mmol]	Graphene [mL(source)]	DBU [mL]	Temp [°C]	Power [W]	Time [min]
BG1[a]	503	195	3 (G1)	0.8	130	42	40
BG2[a]	518	210	18 (G2)	0.8	130	42	40
BG3	510	200	3 (G3)	0.8	125	50	30
BG4	500	201	3 (G4)	0.8	125	50	30
BG5	500	200	3 (G5)	0.8	125	50	40
BG6	125	48	20 (G6)	0.8	125	70	40
BG7	125	30	3 (G7)	0.8	125	50	30
BG8A	498	193	3 (G8)	0.8	125[b]	40	40
BG8B	509	223	3 (G8)	0.8	125	50	40

a) Did not reach target temperature.
b) Reached only 115 °C

Hans-Petter Larsen

Synthesis of a self-healing graphene/polyurethane nanocomposite using the Diels-Alder reaction

NTNU
Kunnskap for en bedre verden